THE UNIVERSITY OF MICHIGAN

INDUSTRY PROGRAM OF THE COLLEGE OF ENGINEERING

THE MIXING OF LIQUIDS FLOWING THROUGH BEDS OF PACKED SOLIDS

Earl Albert Ebach

This dissertation was submitted in partial fulfillment of the requirements for the degree of Doctor of Philosophy in the University of Michigan, 1957.

April, 1957

IP-215

.ensm

UMR0991

To My Wife,

Faye

ACKNOWLEDGEMENTS

The author wishes to express his appreciation to all those persons who have aided in this investigation.

In particular, he wishes to acknowledge the interest, guidance and criticism offered by Professor Robert R. White, chairman of the doctoral committee. The interest and suggestions of the members of the doctoral committee, Professors J. T. Banchero, L. E. Brownell, S. W. Churchill, D. L. Katz, J. S. McNown, and G. B. Williams, were also sincerely appreciated.

The author wishes to express his gratitude to Messrs. Ben G. Bray and J. Robert Gellatly for their friendship, interest and aid during the course of this study.

The shop and secretarial personnel of the Chemical and Metallurgical Engineering Department were most cooperative and helpful at all times.

The author is also indebted to the Standard Oil Foundation and the Dow Chemical Company who made this work possible with financial assistance through fellowship grants.

TABLE OF CONTENTS

TABLE OF CONTENTS (CONT'D)

TABLE OF CONTENTS (CONT'D)

LIST OF TABLES

LIST OF FIGURES

LIST OF FIGURES (CONT'D)

STATEMENT OF THE PROBLEM

When a liquid flows through a fixed bed and concentration gradients exist in the liquid, a mass transfer process occurs which tends to decrease the gradients. This mass transfer process is the result of the liquid mixing occurring within the interstices of the bed. Previous studies have concerned the radial mixing of both gases and liquids flowing through fixed beds, and the axial mixing of gases flowing through fixed beds. There are practically no data on axial mixing for liquid systems. The present investigation has resulted in the evaluation of axial eddy diffusivity occurring in liquids flowing through fixed beds of solids. Two groups of factors effecting the axial mixing were investigated: the geometrical properties of the fixed bed and the physical properties of the flowing liquid. The specific variables investigated were particle size and shape, bed length, flow rate and viscosity of the flowing solutions. Continuous photometers were designed and constructed to analyze the color density of the flowing liquid solutions. Several experimental techniques were investigated, with the frequency response and pulse function methods being employed in the research.

I. INTRODUCTION

When a liquid flows through a bed of packed solids and concentration gradients exist in the liquid either because of input composition changes or because of a chemical reaction occurring within the liquid, a mass transfer process is initiated which tends to eliminate the gradient. This mass transfer process is the result of the liquid mixing occurring within the bed. The "back-mixing" in catalytic reactors or adsorption towers tends to decrease the driving forces for chemical reactions or transport processes and thus limits the conversions or separations obtainable. The effectiveness of filtration is often limited by the mixing between the filtrate and the wash liquid. In ion exchange and ion exclusion, the degree of separation produced is a function of the liquid mixing taking place within the beds of resins.

MIXING MECHANISMS

The mixing of liquids flowing through fixed beds may be considered as a mass transfer process. "Molecular diffusion" is the name given to a mass transfer process in which the rate is proportional to the concentration gradient and the proportionality constant is called "diffusivity". In a fluid flowing through a packed bed an additional mixing process occurs which is superimposed on the molecular mechanism of diffusion. The same form of equation as used to describe "molecular diffusion" is still often used to define this overall mass transfer process, but the constant is called "effective diffusivity because of the turbulent flow characteristics which are associated with

the constant's dependence on flow rate and geometry of the system. This model of mixing is described by equation (1).

$$N = - (D_V + \delta_E) \frac{dc}{dy} = -D_T \frac{dc}{dy} \qquad (1)$$

where D_V represents the molecular diffusivity, δ_E the mixing diffusivity and D_T the total effective diffusivity.

The mixing may be rationalized in terms of the following mechanisms. When fluids flow around an object, a surface boundary layer is formed in which the fluid velocity varies from zero at the surface to the main stream velocity at the outer edge of the boundary layer. As the fluid velocity increases, the boundary layer separates from the surface of the object before the rearmost point is reached, curls up on itself, and forms a stationary eddy behind the object. This separation phenomenon occurs at some point in the flow of the boundary layer around the surface because of the adverse pressure gradients which are created, the conversion of mechanical energy to heat and the increase of inertial forces over the shearing forces within the boundary layer. As the rate of flow increases further, the eddies become larger and more complex, and are continuously shed and reformed. Finally the wake behind the object becomes unstable and irregular turbulence occurs. In a packed bed the intersection of the boundary layers and eddies associated with the many particles produces mixing of the fluid in a radial and axial direction even though the flow may not be entirely turbulent.

Several investigators[2,13,36] have discussed the statistical nature of turbulence in flow through packed beds. The "random-walk" theory, explains the contribution of solid particles to the radial mixing process. When a molecular group approaches a particle, the

group divides and moves laterally to pass the object. This side-stepping process is repeated at each layer of particles in the bed. The theory postulates complete mixing in the interstitial space of the several incoming streams. The resulting "random-walk" formula has been proven consistent with experiments concerning radial diffusion[15,26,30]. Recent investigations have shown that effective radial diffusion, represented by D_R, and effective axial diffusion, represented by D_L, are not of the same magnitude[3,26,27,31].

PREVIOUS INVESTIGATIONS

The first measurements of turbulent diffusion in fluids flowing through fixed beds were performed by Bernard and Wilhelm[3,39]. Radial mixing rates in both gaseous and liquid systems were determined using a point-source technique. (The various experimental techniques are explained in the next section.) Baron[3] applied statistical considerations, resulting in the random-walk theory, to radial mixing which predicted results in the experimental range of Bernard and Wilhelm. Latinen[26] extended the radial mixing experiments and the application of the "random-walk" approach. Recent investigations by Fahien and Smith[15] and Plautz and Johnstone[30], concerning heat and mass transfer radially in fixed beds through which gases are flowing, have extended and confirmed the above studies.

Axial mixing, or the mixing in the direction of flow, has been neglected because of experimental and analytical difficulties. Lapidus and Amundson[25] presented a mathematical treatment for adsorption in beds, including axial mixing, which involved the response function of the system to an inlet step function change in concentration.

Danckwerts[11] arrived at similar results and measured a longitudinal diffusivity in water flowing through packed Raschig rings. Employing a frequency response technique (response to a sinusoidally varying input), Kramers and Alberda[24] presented some experimental results for axial diffusion in a system similar to that of Danckwerts'. Deisler and Wilhelm[12] likewise employed the frequency response technique in the study of gaseous diffusion in beds of porous solids. More recently, McHenry[27] employed this method of sinusoidally varying concentrations in the study of axial mixing of binary gas mixtures flowing through a random bed of spheres.

Previous investigations have thus resulted in data concerning the radial mixing of both gases and liquids flowing through fixed beds, and the axial mixing of gases flowing through fixed beds. Although several experimental techniques have been proposed, there are practically no data on axial mixing for liquid systems.

This study was undertaken to investigate the axial mixing of liquids flowing through fixed beds of solids. Two groups of factors were investigated: the geometrical properties of the bed and the physical properties of the liquid. Continuous photometers were designed and constructed to analyze the flowing liquid solutions. Several experimental techniques were investigated, with the frequency response and pulse function methods being employed in the investigation.

II. EXPERIMENTAL

EXPERIMENTAL METHODS

Several different techniques have been employed in the investigations of turbulent mixing in fixed beds. Each method analyzes the response curve resulting from some kind of initial disturbance in a dynamic system.

The point source technique, in which a tracer diffuses from a point source into the fluid flowing through the packed bed, has been used to evaluate the extent of radial mixing[3,15,26,30]. Fluid samples taken at various radial increments are analyzed, as well as samples of the average effluent, resulting in concentration profiles from which radial diffusion coefficients can be determined. The point source method was not used during the present research, but is discussed briefly to present a complete picture of the mixing occurring in fixed beds. The results of several investigations of radial mixing by the point source technique are presented and compared with the data of the present research in the discussion.

The frequency response technique, employed in previous gaseous diffusion measurements[12,27], requires the response to a sinusoidally varying inlet concentration. The longitudinal diffusivities can be computed, as will be shown later, from the ratio of the amplitudes of the sinusoidal concentration wave at the inlet and outlet of the bed. The frequency response method was employed in part of the present research because it presented advantages of simplicity during both the experiments and calculations. However, analytical difficulties were encountered in its applications for low flows because of the length of

the runs and because of the small axial mixing rates. To overcome the analytical problems, other techniques were employed.

A third method involves the response to an inlet step function[11,25]. Experimentally, this could be carried out by flowing a clear solution and a tracer solution successively through a fixed bed and determining exit concentration as a function of time. From this experimental concentration profile the axial diffusion rate can be calculated. However, experimental difficulties are encountered in obtaining a sharp, uniform step function at the inlet to a bed. Several unsuccessful attempts were made to obtain a sharp step function during the present research. In addition, difficulties were encountered in the calculation of the axial diffusivity from the outlet response curve, as explained later.

Yagi and Miyauchi[42] used the pulse wave method in their study of mixing in continuous flow reactors. Danckwerts[11] suggested this method for the investigation of mixing in packed beds. In this method, one determines the exit concentration profile for an experiment in which the tracer is injected over a short period of time, that is, in the form of a unit pulse. From this concentration profile, the axial mixing coefficient can be calculated. The pulse function technique was used during the present research for the low flow rate range.

By making the necessary modifications, the equipment was successfully used for both the frequency response technique and the pulse function method.

EQUIPMENT

Flow System

Figure 1 is a photograph of the experimental equipment employed in the frequency response runs. The flow system for this method is illustrated schematically in Figure 2. The liquid solutions were forced through the system from constant pressure supply tanks. The pressure in these tanks was maintained from the available 90 psig air supply by a Moore Nullimatic pressure regulator. The brass storage tanks, each having a capacity of 10 gallons, contained a clear solution or a dye solution. During a single run the small change in liquid height, resulting in a slight decrease in the tank pressure, did not alter the flow rate within the accuracy of the reading. Hoke needle control valves downstream of the storage tanks regulated the flow from each tank. Copper tubing having an inside diameter of 3/8 inch was used throughout for all liquid flow lines. The clear and dye solutions, alternated by the three-way directional-flow valve and mixed during flow through the pre-bed (a column packed with glass beads) to periodically vary the composition, then flowed through the packed testing section. Analysis of the flowing streams was made at both the inlet and outlet of the testing sections by means of continuous photometers. A third Hoke metering valve following the column added control to the system. The flow rate was measured by three Fisher and Porter flow meters arranged in parallel and covering a flow range from 0.001 gpm to 1.0 gpm. Calibration curves for the flow meters can be found in Appendix III-A.

Essentially the same flow system was employed for the pulse function runs except for a few modifications as shown in Figure 3. A

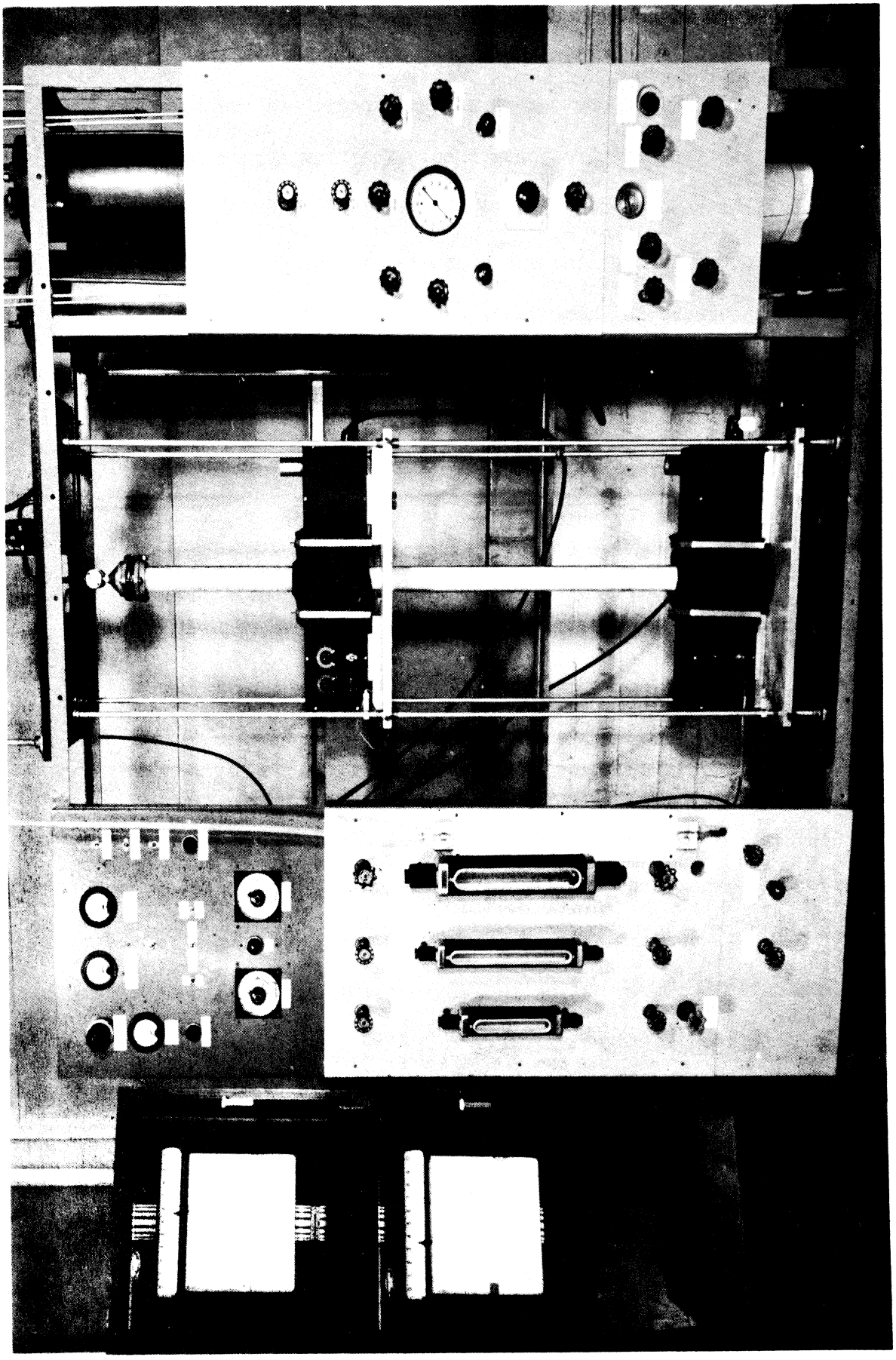

FIGURE 1 - EQUIPMENT ASSEMBLED FOR FREQUENCY RESPONSE EXPERIMENTS

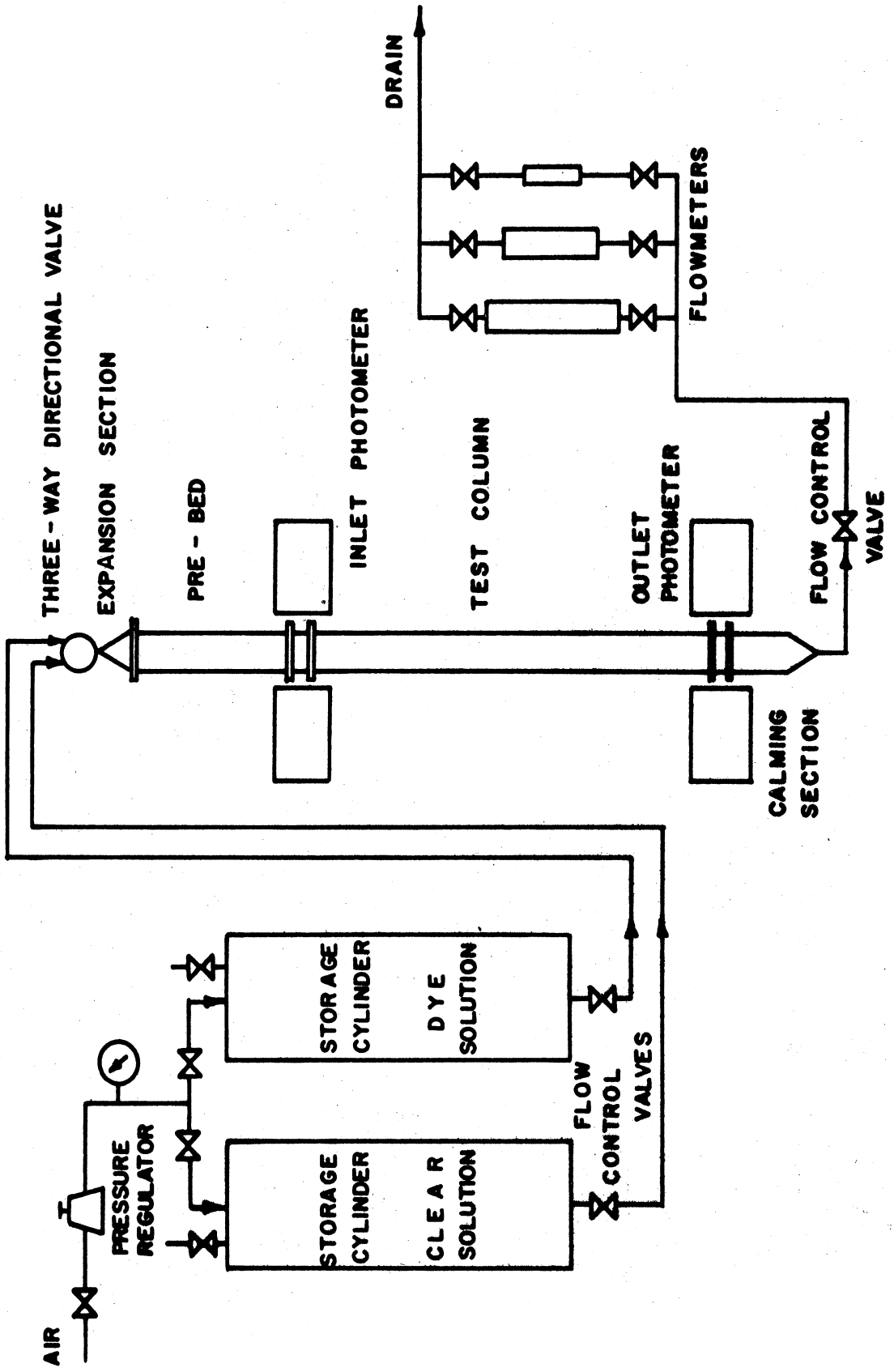

FIGURE 2 - FLOW SYSTEM - FREQUENCY RESPONSE EXPERIMENTS

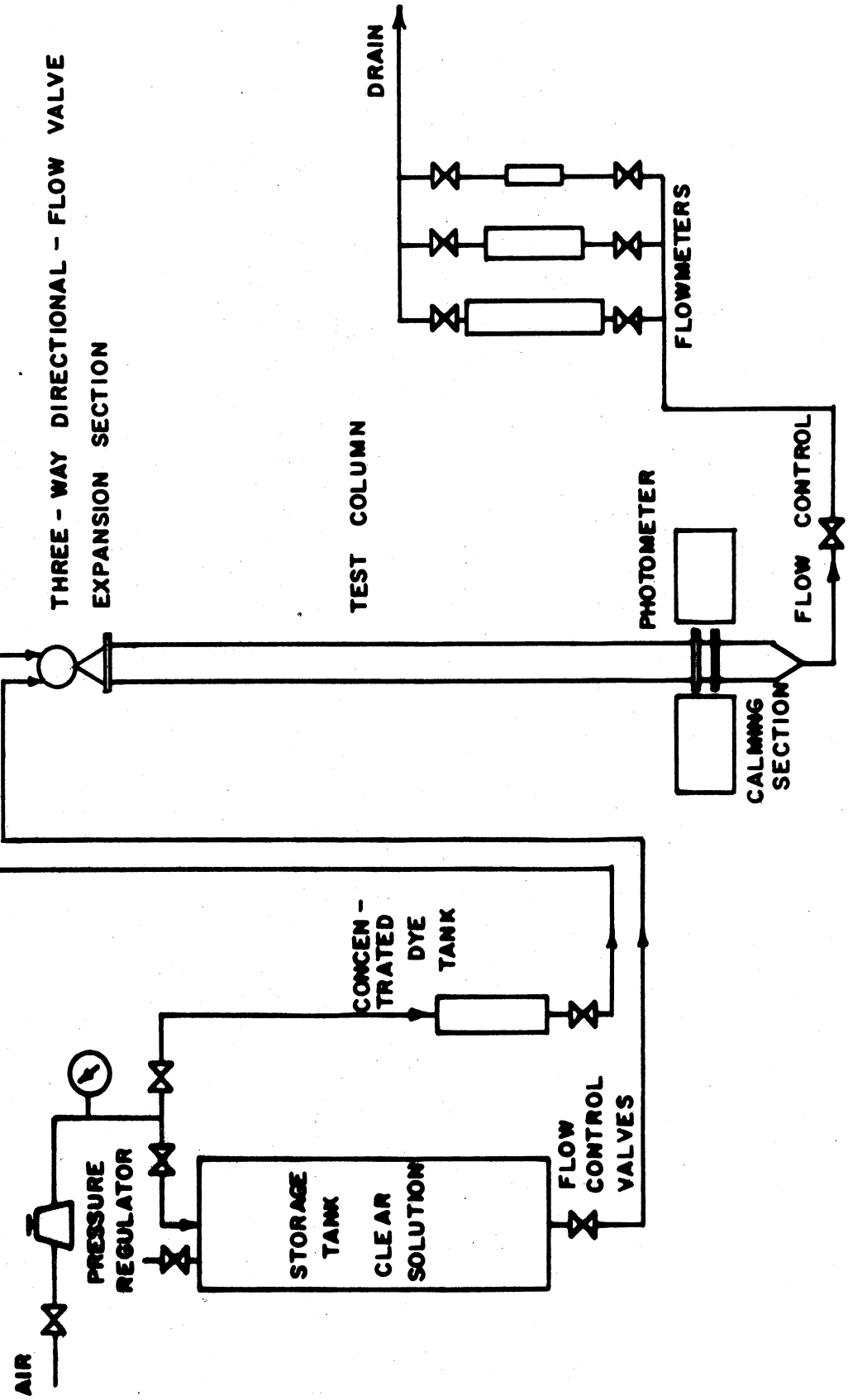

FIGURE 3 - FLOW SYSTEM - PULSE FUNCTION EXPERIMENTS

small 2 liter brass cylinder containing the concentrated tracer solution replaced one of the large storage tanks. Copper tubing having an inside diameter of 1/4 inch was used for the concentrated dye lines. The clear liquid flowed continuously through the system, with a short dye pulse being injected into the flow by means of the three-way directional-flow solenoid valve. The pre-bed was not used, but longer test columns were employed. The liquid flowing through the column was analyzed only at the outlet of the testing section by a continuous photometer.

Features of the systems were: the method of periodically varying the liquid composition, the method of introducing the pulse function, the columns and packings investigated, and the analytical units.

Wave Generator - Frequency Response Method

The inlet stream composition, which varied periodically with time, was obtained by passing alternate volumes of clear and dyed solution through a pre-bed of glass spheres. The feed to the pre-bed, a step-function composition, was formed by an electrically controlled three-way directional-flow Skinner solenoid valve which alternated the flow of the two solutions. The three-way valve could be operated either manually or automatically. In the automatic operation a combination of two Microflex Reset timers, manufactured by Eagle Signal Corporation, were set so that the solenoid was repeatedly on and off for equivalent intervals. The pre-bed consisted of a brass conical expansion section followed normally by a 1-1/2 foot section of 2 inch inside diameter Pyrex glass pipe. The expansion section was filled with 1 mm glass

spheres, while the glass pipe unit was filled with 3 mm glass spheres, separated and supported by a 100 mesh brass screen as shown in Figure 4.

The pre-bed served two purposes. First, it produced at the inlet to the testing section an approximate constant velocity profile. The measurement of point velocities for fluids flowing within packed beds is very difficult, but several investigations indicated the above assumption valid for the pre-bed system. Studies by Schwartz and Smith[35] on gaseous flow distribution in packed beds showed a maximum in the velocity near the wall. However, their studies indicated that for d_p/d_t less than .04 the assumption of uniform velocity distribution is valid. Thatcher[38] arrived at similar conclusions and also found that entrance effects were almost negligible. A velocity profile for aqueous NaCl solution flowing through packed spheres was obtained by Hirai[20]. The shape of this profile does not agree with previous investigations, but indicates that the uniform velocity distribution assumption is valid for liquid flow through packed beds.

The second purpose of the pre-bed was to disperse or mix the interfaces of the alternate solutions so that an approximate sine wave composition would be obtained. The pre-bed, through this mixing process, served as a damping factor, hence removing most of the higher harmonics from the approximate square waves which were introduced by the three-way valve. The mathematical approach to the damping effect of the pre-bed and the calculations for a predicted wave are presented in Appendix I-B-5. The upper portion of Figure 5 compares an experimental outlet wave of the pre-bed with the predicted wave, the calculated values of which are based on the known experimental conditions of pre-bed particle diameter, pre-bed height and liquid velocity and the degree of liquid mixing determined through this research. In the initial runs, the pre-bed was packed with 1 mm glass beads and the resulting wave was not as

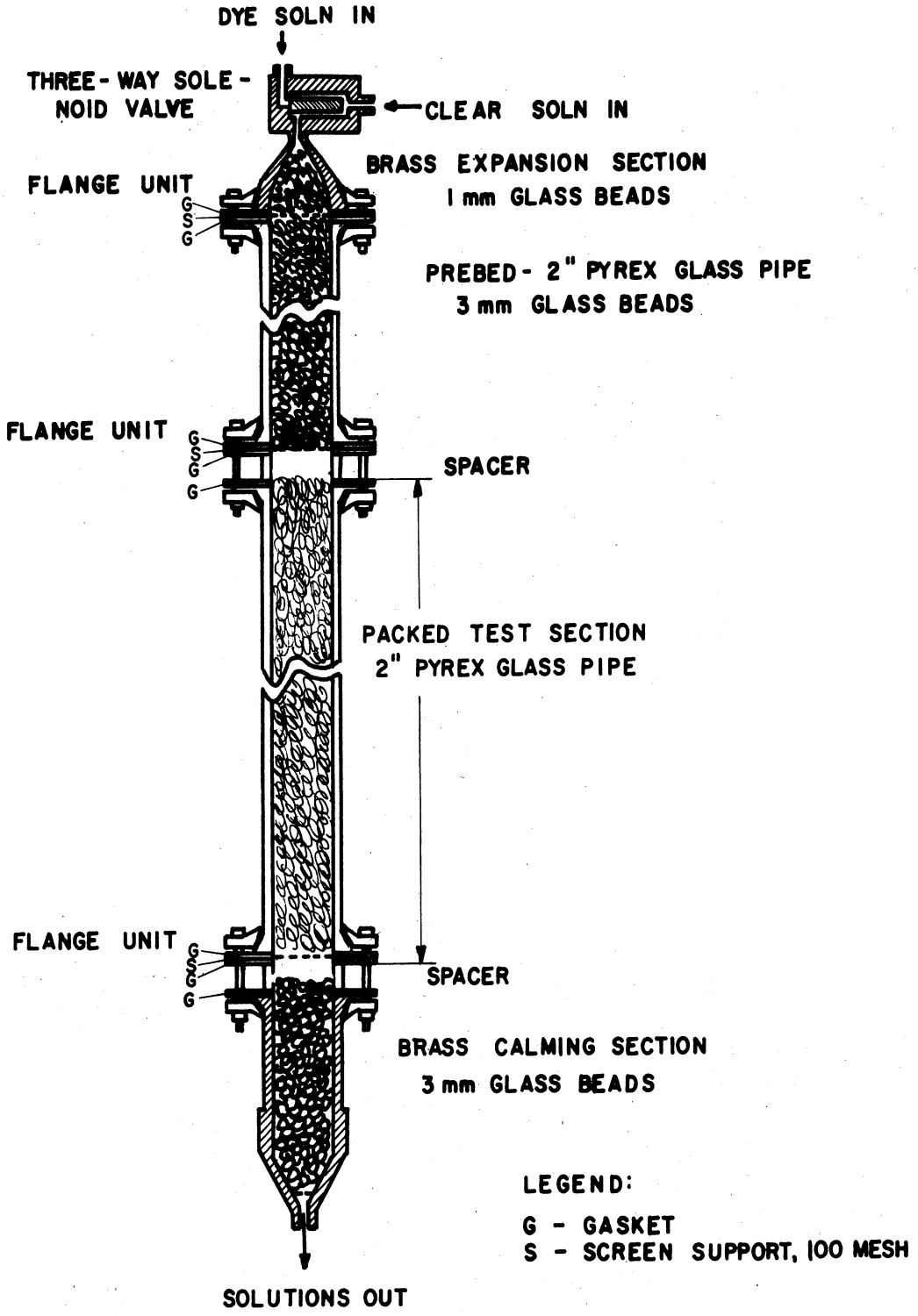

FIGURE 4 - COLUMN DETAIL-FREQUENCY RESPONSE TECHNIQUE

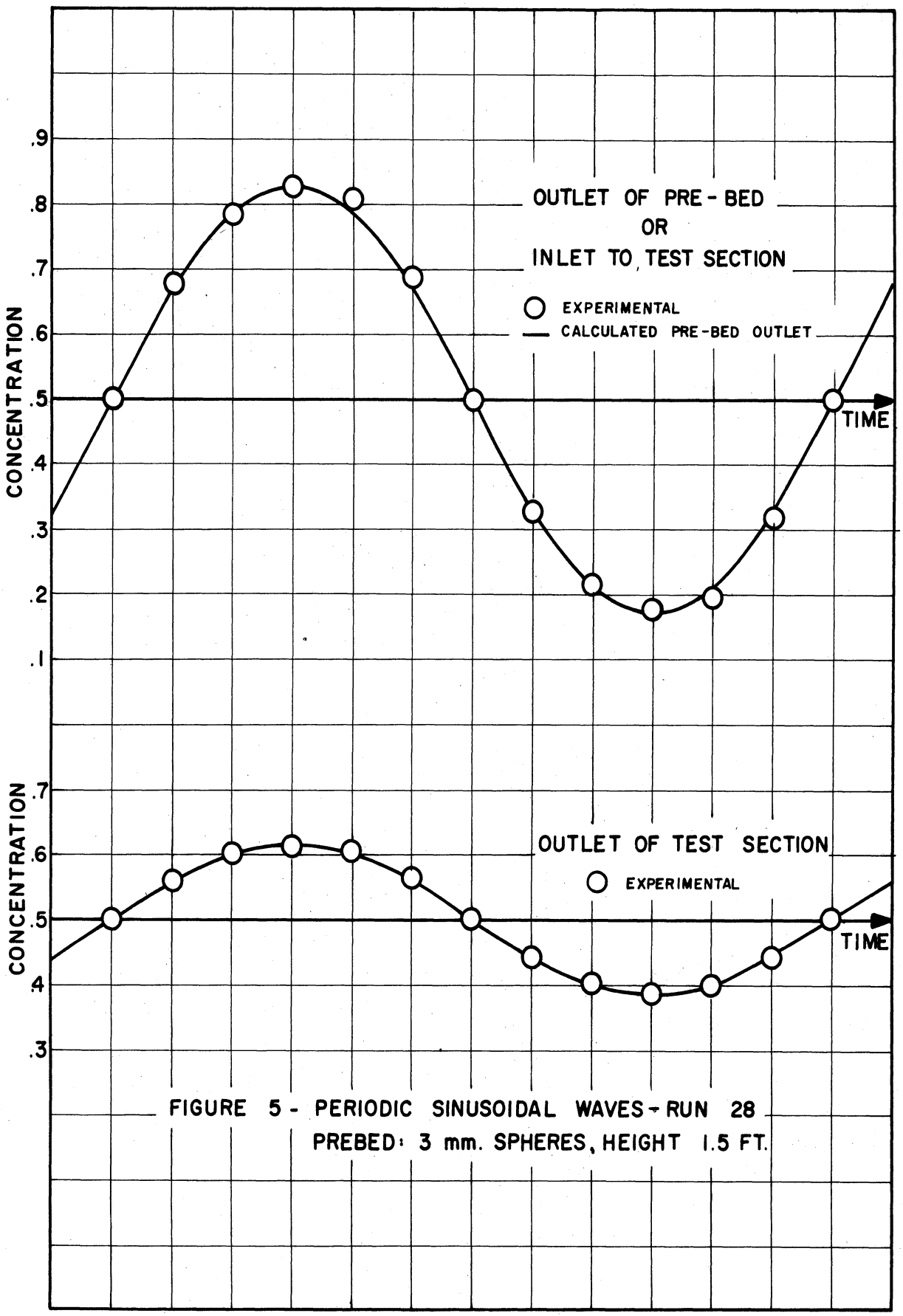

FIGURE 5 - PERIODIC SINUSOIDAL WAVES - RUN 28
PREBED: 3 mm. SPHERES, HEIGHT 1.5 FT.

close an approximation of a true sine wave as desired, but could be represented by a short Fourier series. The pre-bed also damped out the small irregular waves sometimes formed at the interface in the operation of the three-way valve.

Pulse Generator

A unit pulse of concentrated dye solution was injected into the flowing clear solution by means of the three-way Skinner solenoid valve. The length of the pulse was determined by the residence time of the run being made. For short residence times, an instantaneous on-off flick of the manual switch was used; for low flow rate runs with residence times greater than ten minutes, pulse lengths up to four seconds were used.

Test Column

Figure 4 is a section drawing of the main test column showing the several sections flanged together. Two 3/4 inch glass spacers used in the analytical system separated the main test section from the pre-bed and the calming section. Neoprene interface gaskets were used at all joints. All glass sections of the column were 2 inch inside diameter Pyrex glass pipe. The spacers, gaskets and brass calming section were likewise 2 inch inside diameter so as to maintain a smooth wall across the joints. The lengths of the main test section of glass pipe used in the frequency response experiments were 3.0 and 2.0 feet. Column lengths of 3.0 and 5.0 feet were used in the pulse function runs. Glass spheres, Raschig rings, Berl saddles, and Intalox saddles were used as packing. The characteristics of the packings are shown in Table I. The porcelain packings were supplied through the courtesy of the United States Stoneware Company. The fraction voids were

measured each time the column was set up. A 100 mesh brass screen, fastened between two gaskets, supported the packing in both the pre-bed and test sections. No screen was used above the packing in the test section. The same method of packing, i.e., pouring the beads slowly through a funnel at the top of the column and tapping the column

TABLE I. PACKING CHARACTERISTICS

Type	Material	Nominal Size	Equivalent Diameter d_p	d_p/d_t	Bed Porosity ϵ
Spherical	Glass	60/80 mesh	.0083 in.	.0042	.352
Spherical	Glass	1 mm	.039 in.	.020	.340
Spherical	Glass	3 mm	.133 in.	.067	.340
Spherical	Glass	6 mm	.265 in.	.13	.367
Raschig rings	Porcelain	1/4 in.	.22 in.	.11	.632
Berl saddles	Porcelain	1/4 in.	.23 in.	.12	.616
Intalox saddles	Porcelain	1/4 in.	.20 in.	.10	.629

lightly to promote settling, was used each time the column was repacked with spheres. The column and the entire system were backfilled very slowly with water to remove all air.

A wet method was used in loading the longer column with the porcelain shapes for the pulse function runs. The column was filled partially with water, and the rings or saddles were slowly poured through a funnel at the top. The water prevented breakage and provided slow, even settling of the particles. The column was also tapped lightly to promote settling. When the test section contained 6 mm spheres,

Raschig rings, Berl saddles, or Intalox saddles, the expansion section was filled with 1 mm glass beads to remove velocity variations and produce an even pulse distribution at the entrance. Normally, the expansion section was filled with the same size beads as were in the test section. Allowance was made in the calculations for the extra length.

Analytical System

Method of Analysis. In the frequency response technique the inlet and outlet wave compositions located above and below the fixed bed must be determined. The continuous analysis of a liquid flowing through a bed of packed solids is a difficult task. The method of continuous colorimetric analysis was chosen over others investigated, such as conductometry and refractometry. Conductivity measurements were ruled out because of the close temperature control needed, the flow interference caused by the electrodes within the column, and possible erroneous readings caused by the coating of electrodes with the leading liquid. Methods using a refractometer were also ruled out because of the high cost and excessive flow interference. The continuous colorimetric photometers were employed at both the outlet and inlet without causing any flow disturbances and gave an instantaneous measurement of the dye concentration flowing through a horizontal section of the column.

Photometer Design. The two identical photoelectric colorimeters used in the research were constructed in the laboratory because available commercial models would have required extensive modifications. The colorimeters were designed and constructed by trial and error experimentation after an extensive literature survey[23,28,40] and study of

existing instruments. A sectional drawing of one unit is shown in Figure 6. In operation, the instrument employed the basic physical relationships needed to measure color intensity. Light from a tungsten source was collimated by a lens, passed through a filter which selected the desired color of light, and then directed through the flowing liquid. The flowing stream absorbed a certain amount of light, depending on its color intensity. The remaining light was then detected by a sensitive phototube in the receiver, and electrically amplified and recorded. A photograph of a photometer, exposing the light source compartment, is shown in Figure 7. The two units were mounted on vertically adjustable aluminum platforms around the test column as shown in the photographs. The light source compartment and the photocell compartment each moved horizontally on a track, so that once the colorimeter units were aligned, positions were reproducible.

Light Source. The light source was a 100 watt, T-8, double contact, projection bulb mounted in a standard socket which was adjustable both horizontally and vertically. Power to the light source was provided by a 500 watt Sola Constant Voltage Transformer which regulated the output voltage to 115 volts plus or minus 1 percent over the input range of 95-125 volts. Preliminary tests indicated no noticeable variation in light intensity during the length of a run. The lamp was adequately cooled by air blown through the chimney. The life of a lamp was approximately 20 hours; hence, several were used during the experiments. Because the incandescent projection lamp emits light in the range 420-750 millimicrons, selective filters were needed to limit the band of light passing through; this narrowing of the light band increased the sensitivity and stability of the colorimeter.

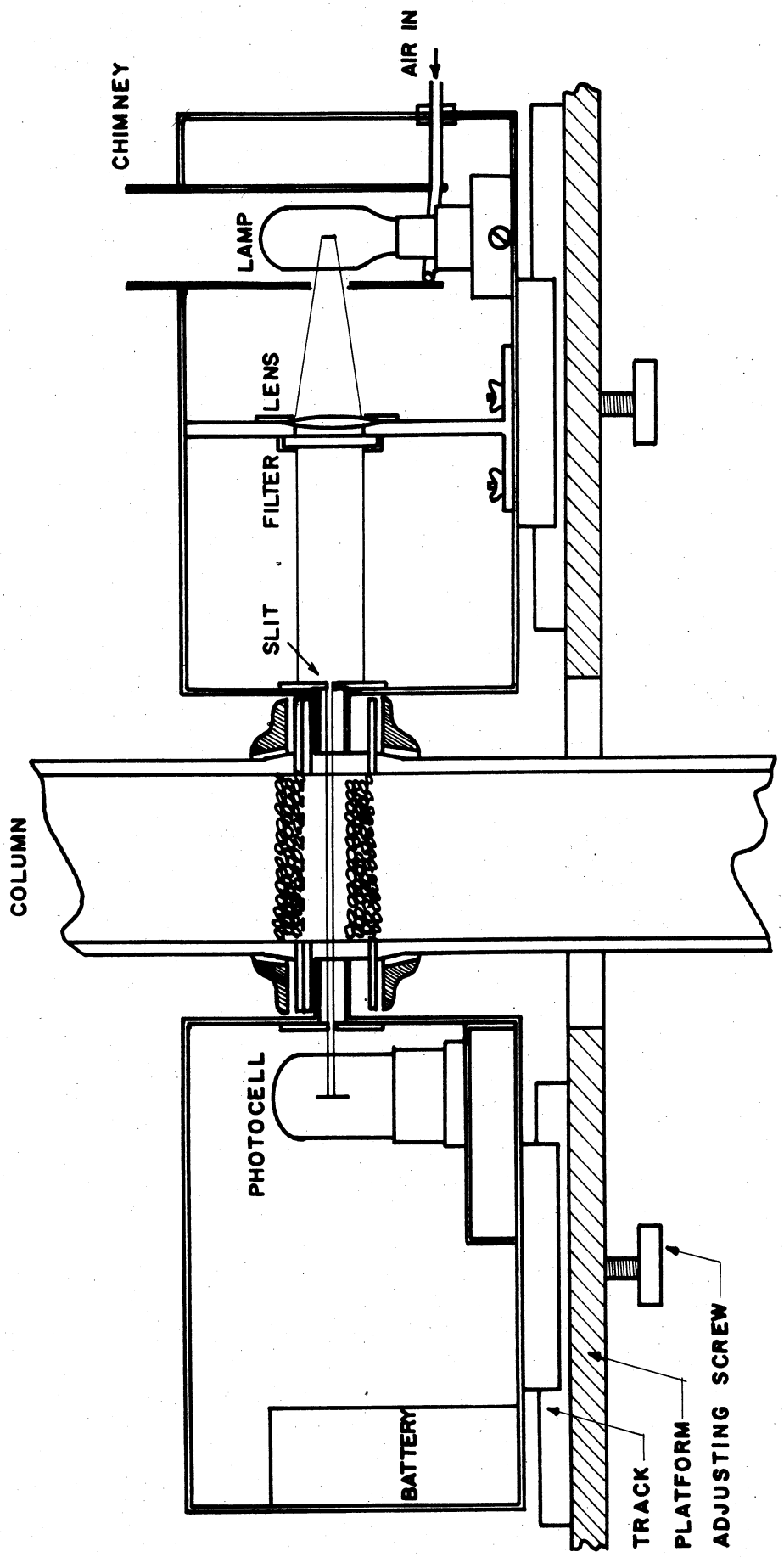

FIG. 6 - SECTIONAL VIEW OF CONTINUOUS PHOTOMETER

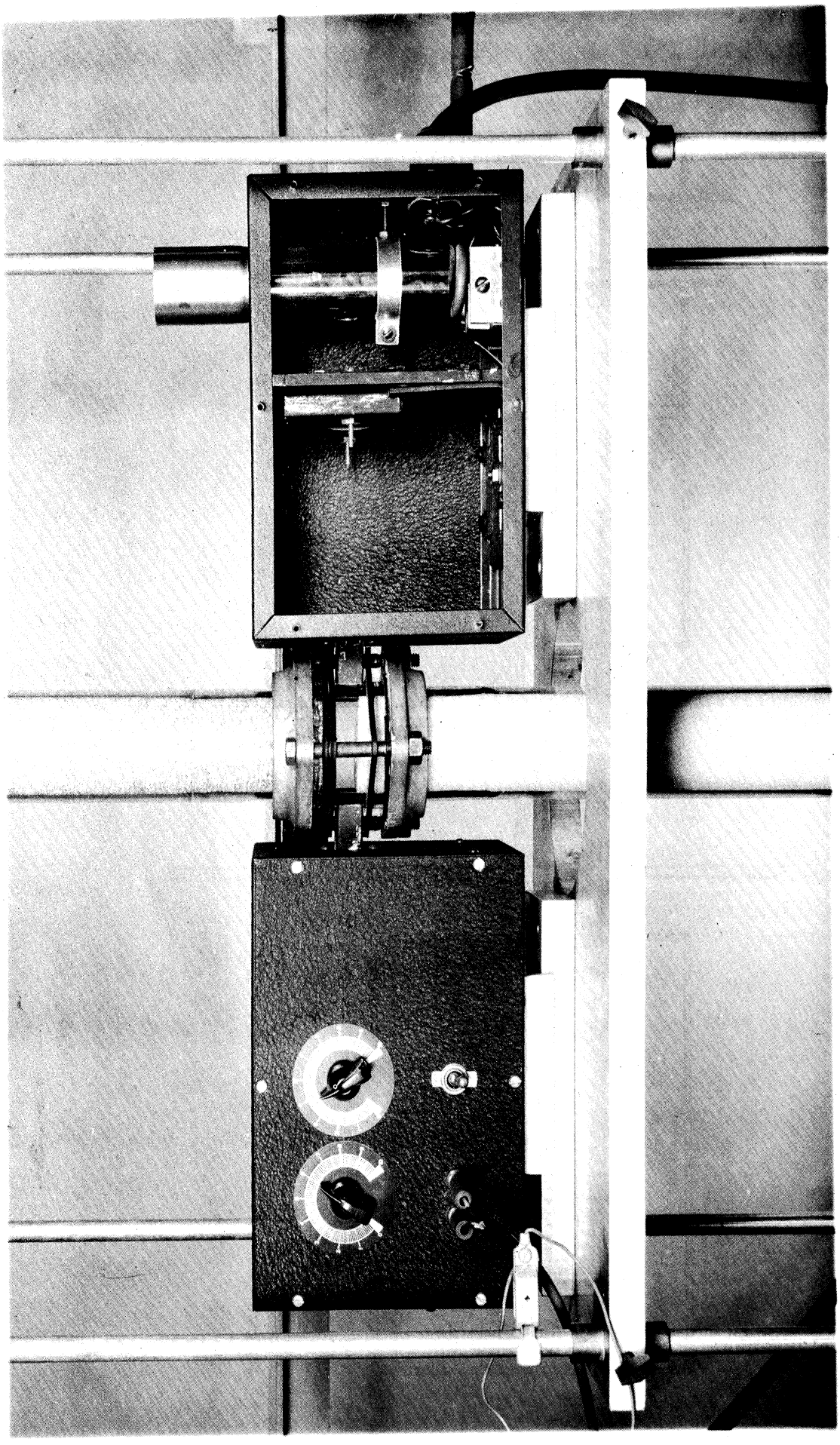

FIGURE 7 - CONTINUOUS PHOTOMETER EXPOSING LIGHT SOURCE COMPARTMENT

Filter and Lens. Since maximum sensitivity was desired, the selections of the filter, dye solution and photocell were all interrelated. The method described by Cooper[8] was employed in choosing the optimum combination of filter and photocell with the desired dye. This method is based primarily on the fact that the variation in transmittancy with concentration is greatest when the incident light is restricted to the spectral region of the solute's greatest absorptance. The photometers were initially designed on the basis that Pontachrome Blue ECR dye would be used as the tracer during the experiments. The resulting optimum combination of dye, photocell and filter is presented in Figure 8 showing the desired relationships between the percent transmittance curve for Pontachrome Blue ECR, the spectral sensitivity characteristic of a phototube having a S-4 photosurface and the transmittance curve for a Cenco B filter. After construction of the photometers, preliminary experiments indicated, as will be explained later, that Pontamine Sky Blue 6BX dye would be a more satisfactory tracer. Hence a Cenco C, 610 millimicron peak, 100 millimicron band pass filter, which has a transmittance curve corresponding to the transmittance curve for Pontamine Sky Blue 6BX as shown in Figure 9, was used in the photometers during the experimental work.

A double convex lens for creating an intense and homogeneous beam of light was mounted with the filter on an adjustable base. The beam of light, further restricted by slits 3/32 inch by 1/4 inch, was directed through the flowing liquid at the glass spacers on a diameter line of the column. The marked spacers were always returned to their identical positions to insure reproducibility.

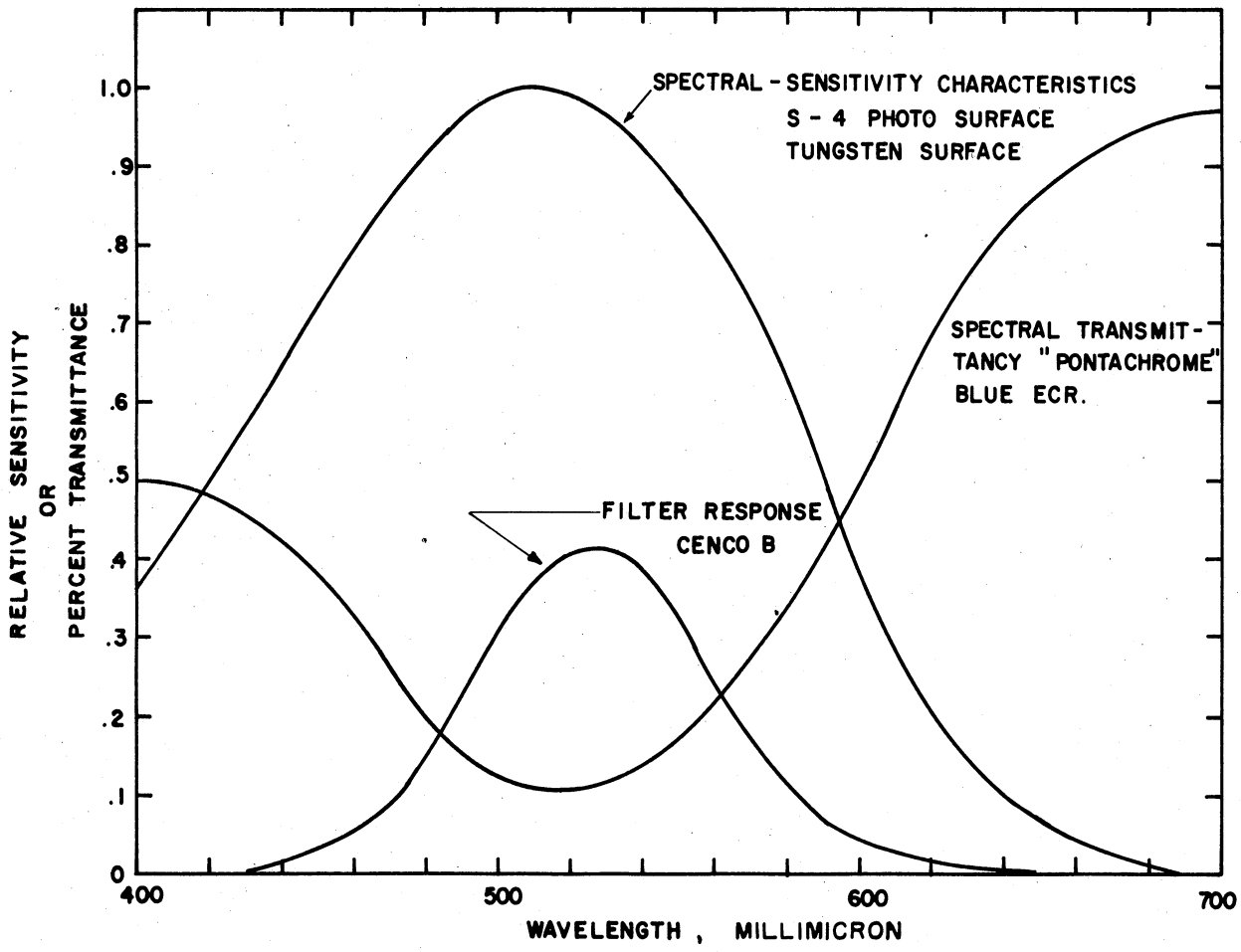

FIGURE 8 - COMPARISON OF FILTER, DYE AND PHOTOCELL IN DESIGN OF PHOTOMETERS

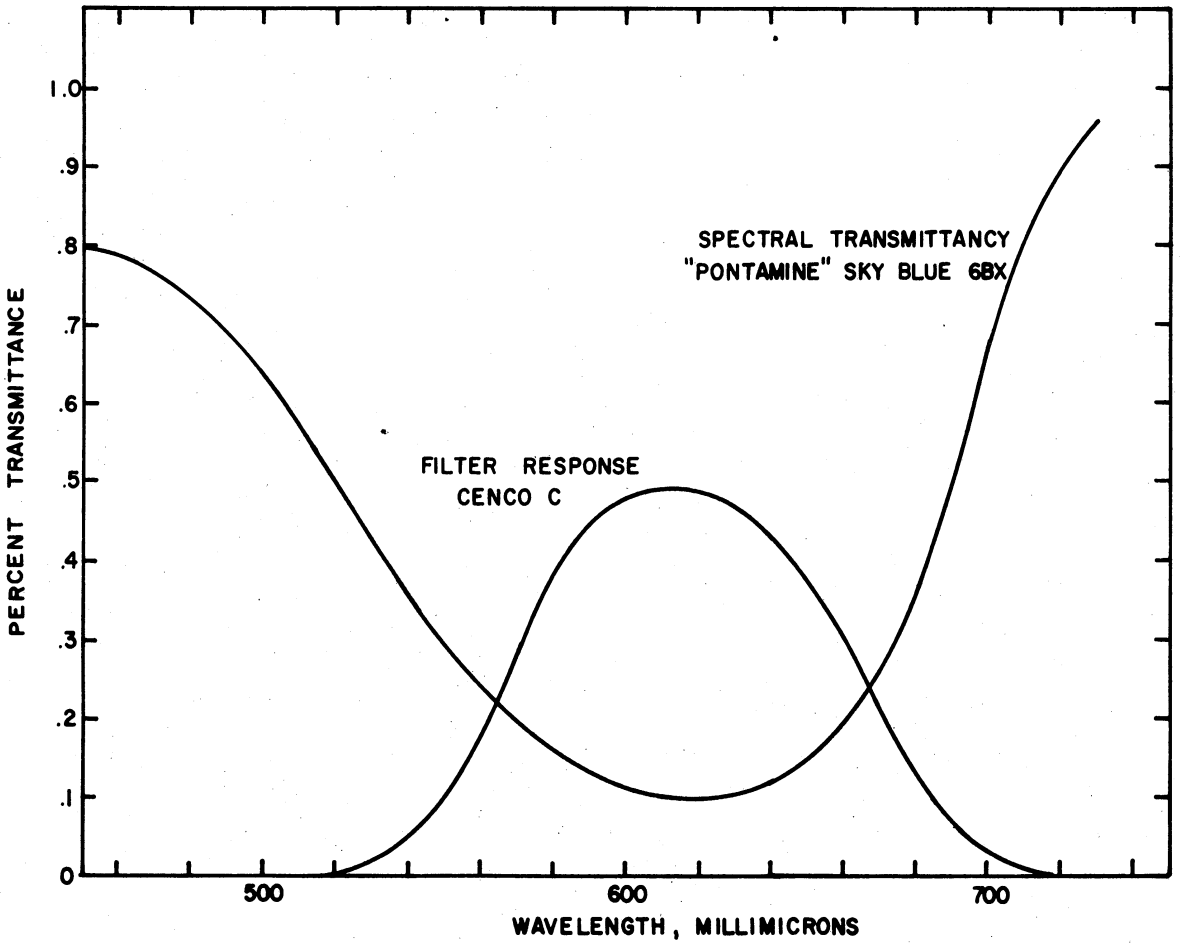

FIGURE 9 - COMPARISON OF SPECTRAL CHARACTERISTICS OF CENCO C FILTER AND PONTAMINE SKY BLUE 6BX DYE

Photocell. The vacuum photocell was chosen over other light measuring cells because of its stability, instantaneous response and high sensitivity[37]. Gas-filled photoemissive cells were not used because of their instability. Multiplier phototubes were not employed because of the extremely constant high voltage supply required and because the incident light exceeded the toleration of the normal cell. Photovoltaic cells were ruled unsatisfactory for a continuous colorimeter because of their response lag or temporary fatigue, great sensitivity to temperature changes and nonlinearity. A high-vacuum phototube, IP39, having a spectral response of S-4 was chosen because of its great sensitivity and excellent operating characteristics[33]. Numerous IP39 tubes were tested until two sets (one for each of the upper and lower photometers, and one for replacement purposes) were obtained having similar sensitivities and characteristics. The phototube was mounted upright in the receiving compartment the surfaces of which were sprayed with light-absorbing black paint. The receiving compartment also housed the power supply to the phototube and the circuitry associated with the measuring system. A schematic wiring diagram of the measuring circuit is given in Figure 10. For the type of phototube used and the experimental conditions encountered, the potentiometer circuit was the most desirable and least expensive[19,37,43]. This basic circuit produced a voltage drop in the series of resistances proportional to the light intensity. The power supply consisted of a 90 volt radio battery, which was periodically checked with a portable potentiometer. No replacement of the battery was necessary during the experimental work. The low anode voltage used 90 volts combined with the

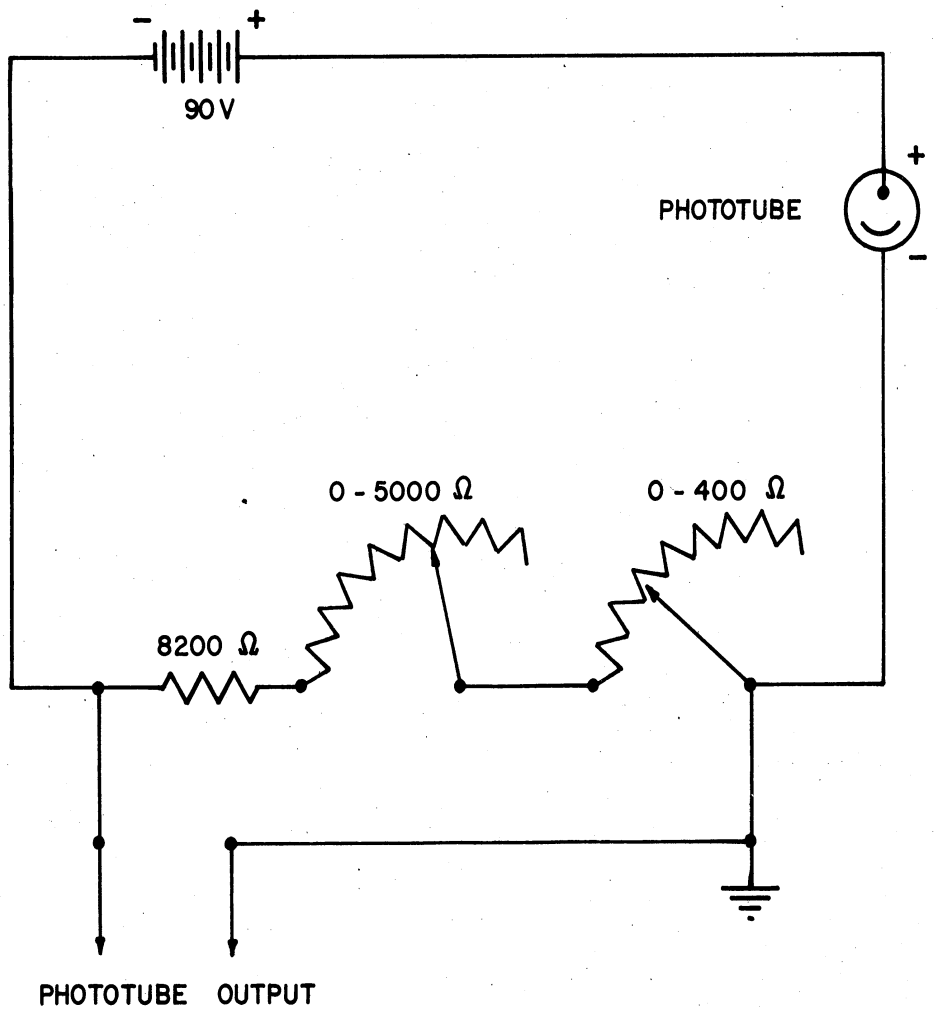

FIGURE 10 - SCHEMATIC WIRING DIAGRAM OF THE MEASURING CIRCUIT

relatively low resistance (maximum: 13,600 ohms) produced a strictly linear response.

Recording Instruments. The output of the phototube circuit, i.e., the voltage drop which is directly proportional to the light intensity, was measured by a Leeds and Northrup Model S Speedomax G Indicating Recorder. Two recorders were required to obtain a continuous record of the inlet and outlet wave compositions in the frequency response method. The balancing system of the Speedomax, supplied with a D-C potentiometer circuit, consisted of a converter-amplifier unit and a two-phase balancing motor. The response of the instrument was one second full scale with a range of 0 to 10 millivolts. The recorder was quite versatile in that chart speeds of 3 in./hr to 2160 in./hr could be easily obtained by changing gears. A separate switch controlled the chart.

Tracer Solution

The dye initially proposed for the tracer and used in the design of the photometers was Pontachrome Blue ECR[23]. However, preliminary tests, using a Fisher Electrophotometer, indicated the spectral transmittancy of the dye was affected by light, by the pH of the tap water, and possibly by contact with the copper used throughout the equipment. Several dyes and indicators were tested intensively to determine the effect of light, pH of solution and reaction with copper. The solution found most satisfactory for the tracer was Pontamine Sky Blue 6BX dye dissolved in distilled water and buffered with potassium acid phthalate[16]. Several dyes, including the two mentioned above, were supplied (with their spectral transmittancy curves as shown in

Figures 8 and 9) through the courtesy of the E. I. DuPont de Nemours and Company.

Solutions of Pontamine Sky Blue 6BX dye were found to conform to Beer's law for the range of concentrations used during the present research. This relationship may be expressed as

$$I = I_o \, 10^{-Kc} \tag{2}$$

or

$$\log_{10}\left(\frac{I}{I_o}\right) = -Kc \tag{2a}$$

where

I_o = intensity of incident light

I = intensity of emergent light

c = concentration of absorbing solution

K = absorption coefficient

Since the tracer solutions conformed to Beer's law, a straight line relationship existed between the logarithm of the transmittancy and the concentration of the solutions.

The chemical composition of the dye used is given in the structural formula below:

Pontamine Sky Blue 6BX (Color Index No. 518)

Chemical name:

Sodium salt of

dimethoxydiphenyldisazo-bis-8-amino-1-napthol-5:7-disulphonic acid

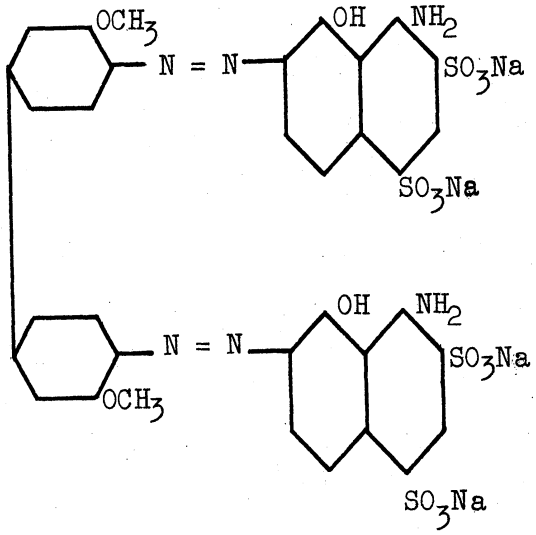

The molecular diffusivity of Pontamine Sky Blue 6BX was found in the literature[1] to be 7.5×10^{-9} ft^2/sec and was therefore considered negligible in the experimental work. The Pontamine Sky Blue 6BX dye was also employed successfully as the tracer in the propylene glycol solutions used to determine the effect of viscosity on the diffusivity.

Pontamine Fast Turquoise 8GLD dye, having similar spectral characteristics, was used for a single run to determine whether a different dye affected the experimental results.

Initial Calibration of Photometers

Both photometers were initially calibrated simultaneously using standard solutions of Pontamine Sky Blue 6BX. The equipment was assembled as if in preparation for a run, with the clear reference solution in one storage cylinder and the standard dye solution in the other cylinder. After an hour warm-up period for the photometers and Speedomax recorders, the clear reference solution was allowed to flow through the system. The photometers were then standardized by varying the resistances in the photocell circuits until the Speedomax recorders

each indicated 9.0 millivolts. The standard dye solution was then allowed to flow through the system, by switching the three-way valve. The resulting change in color density was recorded. This method was followed for each standard solution.

Since the tracer solutions conformed to Beer's law, the calibration curves can be represented by the formula

$$y = A\ 10^{mc} \tag{3}$$

where

y = recorder reading, millivolts

c = concentration, $gms/_{1i}$

A, m = constants of the calibration

A plot of logarithm y as a function of concentration results in a straight line relationship represented by the modification of equation (3) as

$$\log y = \log A + mc \tag{3a}$$

where

$\log A$ = intercept

m = slope

The calibration curves for the inlet and outlet photometers, presented in Appendix III-B, are identical and approximate a straight line. The resulting formula for concentration, with the evaluated calibration constants, is

$$c = \frac{.95424 - \log y}{148.92} \tag{3b}$$

Materials

Distilled water, buffered with 0.0012 molar potassium acid phthalate, was the fluid normally used during the investigation. During the frequency response runs the tracer solution contained approximately 0.0064 grams per liter of Pontamine Sky Blue 6BX. This concentration produced a color density which when analyzed in the photometers resulted in an approximate Speedomax recorder reading of

TABLE II. PROPERTIES OF PROPYLENE GLYCOL-DISTILLED WATER SOLUTIONS

Percent Propylene Glycol	Temperature °C	Density gm/cc	Viscosity Cp
0	20.0	0.998	1.007
50	20.0	1.040	6.205
67	19.5	1.045	11.726
85	18.5	1.043	26.881

1.0 millivolt. The concentrated dye solution used in the pulse function experiments contained approximately 4 grams per liter of Pontamine Sky Blue 6BX. The density of the solutions used were assumed to be identical to that of water since the concentrations were so small. The viscosities of the solutions were determined as a function of temperature and found to be almost identical to that of water as shown in Appendix III-C.

Several runs were made to determine the effect of viscosity on the mixing characteristics. Propylene glycol was used in preparing solutions of high viscosity. It is readily miscible with water in all

proportions, and produces a solution having a relatively constant density for all concentrations. The properties of the propylene glycol-distilled water solutions are shown in Table II. The concentrated dye injected into each of the above solutions contained a similar percentage of propylene glycol.

EXPERIMENTAL PROCEDURE AND DATA

Frequency Response Method

The experimental procedure can be best explained by describing a typical frequency response run. The equipment was assembled, as shown in Figures 1 and 2, and the entire system was filled with distilled water and purged of air. One of the tanks was filled with the clear solution, while the other was filled with the dye solution. The dye solution was mixed before each run from a standard concentrated dye solution. Prior to each run the flow rate, the frequency of the periodic wave, and the chart speeds needed to record the sine waves were determined. The photometers and recorders required an hour to stabilize. Before turning the light sources on it was necessary to start the cooling air. During the warm-up period, the two Microflex timers were set at the desired frequency. Preliminary experiments determined what frequency was required for the pre-bed to produce a satisfactory sine wave. A stop watch was employed during the run to check the timers. The recorder charts were also adjusted to the desired speed by installing the necessary gear arrangements.

After the electrical measuring units were stabilized, the clear reference solution was allowed to flow through the system. Both

photometers were standardized by varying their resistances until the Speedomax recorders indicated 9.0 millivolts. A record of this standardization was made on the chart paper and also on the data sheet. Then the dye solution was allowed to flow through the system and the resulting measurement (approximately 1.0 millivolts) recorded as before. This standardization procedure was followed before each run.

The pressure in the storage tanks was normally set at 50 psig; however, in cases where higher pressure was required to force the solutions through the system, 80 psig was used. After the standardization of the photometers, the Hoke metering valves downstream of the storage tanks were opened a certain number of turns. Then the needle control valve following the column was opened and set at the desired flow rate, allowing the clear solution to flow through the column. The three-way directional-flow solenoid valve in the unenergized position allowed the clear solution to flow. Once the flow rate was stable, the solenoid valve was energized and the dye solution allowed to flow. Then, the metering valve following the dye storage tank was adjusted so that equivalent flow rates were obtained. Repetition of this process assured identical flow rates for both solutions.

The run was begun by switching the three-way valve to the automatic control of the timers, and starting the chart paper in the recorders. A minimum of twenty waves were allowed to pass through the testing section, thus allowing the column to reach equilibrium. During the run the liquid flow rate and temperature of the solutions were recorded. The liquid rates remained steady so that the flowmeters could be accurately read to 0.2 of a division. Following the run, the charts

containing the continuous record of the inlet and outlet wave compositions were marked with the run number and inlet or outlet analysis.

The following is a list of the data which was recorded during a frequency response run:

- Run designation
- Date and time
- Column properties
  - Particle diameter
  - Height
  - Porosity
- Pre-bed properties
  - Particle diameter
  - Height
- Frequency of periodic wave
- Chart speed
- Liquid flow rate
- Liquid temperature
- Recorder traces
  - Colorimeter calibrations
    - Inlet colorimeter: clear and dye solutions
    - Outlet colorimeter: clear and dye solutions
  - Inlet and outlet concentration profiles

Experimental data for the frequency response runs are presented in Table III. Column 1 contains the run designation, and columns 2 and 3 the particle diameter and height of the pre-bed. The corrected flow rate of the liquid solutions is reported in column 4, and the temperatures of the solutions in column 7. Columns 10, 11 and 12 report the physical properties of the test section: column 10 the diameter of the glass spheres, column 11 the porosity of the packed bed, and column 12 the height of the packing. The period of the introduced concentration wave is reported in column 21. The maximum and

TABLE III

EXPERIMENTAL DATA AND CALCULATED RESULTS - FREQUENCY RESPONSE TECHNIQUE

1	2	3	4	5	6	7	8	9	10	11	12	13	14	15	16	17	18	19	20	21	22	23	24	25	26
RUN	PRE-BED		LIQUID FLOW RATE			LIQUID PROPERTIES			BED PROPERTIES			PERIODIC WAVE DATA										AXIAL DIFFUSIVITY		Reynolds Number	Peclet Number
	Particle	Height		Superficial Velocity	Interstitial Velocity							INLET WAVE			OUTLET WAVE					Period	Frequency				
		ft	v gpm	v_o ft/sec	u ft/sec	Temperature °C	Density ρ gms/cc	Viscosity μ cp	Particle Diameter d_p in	Bed Porosity ε	Bed Height z ft	Maximum Concentration	Minimum Concentration	Amplitude A_1	Maximum Concentration	Minimum Concentration	Amplitude A_e	$\frac{A_1}{A_e}$	$\ln\frac{A_1}{A_e}$	sec/cycle	ω rad/sec	$D_L = \frac{u^3 \ln\frac{A_1}{A_e}}{z\omega^2}$ ft²/sec	D_L (Non-sinusoidal method) ft²/sec	$\frac{d_p v_o \rho}{\mu}$	$\frac{d_p u}{D_L}$
A	18/20 Mesh	1.0	.0809	.00780	.0230	21.0	.998	.981	.039	.340	1.50	.832	.168	.664	.779	.221	.558	1.190	.1740	60	.1047	.000128	.000141	2.40	.529
B	18/20 Mesh	1.0	.0809	.00780	.0230	21.0	.998	.981	.039	.340	1.50	.876	.125	.751	.840	.160	.680	1.104	.09894	80	.0785	.000131	.000147	2.40	.508
C	25/30 Mesh	1.5	.707	.07225	.2127	21.0	.998	.981	.039	.340	3.010	.860	.141	.719	.760	.241	.519	1.385	.3255	8	.7847	.00169	.00168	22.20	.412
D	25/30 Mesh	1.5	.844	.08625	.2540	22.5	.998	.947	.039	.340	3.010	.906	.094	.812	.827	.173	.654	1.242	.2167	8	.7847	.00192	.00195	27.45	.423
E	25/30 Mesh	1.5	.842	.08600	.2535	22.5	.998	.947	.039	.340	3.010	.897	.102	.795	.816	.185	.631	1.261	.2320	8	.7847	.00204	.00201	27.40	.410
F	25/30 Mesh	1.5	.724	.07400	.2180	23.0	.998	.936	.039	.340	3.010	.865	.135	.730	.764	.237	.527	1.386	.3262	8	.7847	.00182	.00175	23.82	.405
8	25/30 Mesh	1.5	.0498	.00509	.0150	22.0	.997	.958	.039	.340	3.010	.757	.244	.513	.633	.367	.266	1.930	.6575	80	.0785	.000119	----	1.60	.409
7	25/30 Mesh	1.5	.0502	.00513	.0151	22.0	.998	.958	.039	.340	3.010	.789	.212	.577	.726	.273	.453	1.273	.2415	120	.0519	.000103	.0000950	1.61	.517
6	25/30 Mesh	1.5	.0744	.00760	.0224	21.5	.998	.970	.039	.340	3.010	.808	.192	.616	.734	.267	.467	1.320	.2776	74	.0850	.000144	.000147	2.36	.496
9	25/30 Mesh	1.5	.0745	.00761	.0224	25.5	.997	.886	.039	.340	3.010	.734	.267	.467	.634	.367	.267	1.749	.5590	50	.1257	.000132	.000139	2.58	.551
5	25/30 Mesh	1.5	.1035	.01108	.0326	24.0	.998	.916	.039	.340	3.010	.853	.147	.706	.751	.250	.501	1.410	.3435	50	.1257	.000254	.000277	3.65	.383
4	25/30 Mesh	1.5	.262	.02676	.0788	21.0	.998	.981	.039	.340	3.010	.861	.138	.723	.749	.250	.499	1.448	.3705	20	.3130	.000617	.000591	8.21	.433
3	25/30 Mesh	1.5	.484	.04943	.1456	21.5	.998	.970	.039	.340	3.010	.881	.120	.761	.781	.220	.561	1.357	.3053	12	.5226	.00116	.00122	15.35	.388
2	25/30 Mesh	1.5	.699	.07138	.2103	21.5	.998	.970	.039	.340	3.010	.868	.132	.736	.766	.235	.531	1.387	.3271	8	.7847	.00164	.00168	22.16	.408
1	25/30 Mesh	1.5	.899	.09181	.2704	23.0	.998	.936	.039	.340	3.010	.918	.082	.836	.840	.160	.680	1.230	.2070	8	.7847	.00233	.00244	29.54	.360
35	3 mm	1.5	.0502	.00513	.0138	23.0	.998	.938	.265	.372	2.038	.782	.218	.564	.532	.468	.064	8.834	2.1786	100	.0628	.000709	-------	9.96	.382
34	3 mm	1.5	.108	.01103	.0297	23.0	.998	.938	.265	.372	2.038	.844	.157	.687	.570	.431	.139	4.924	1.5941	50	.1257	.00129	-------	21.43	.451
33	3 mm	1.5	.235	.02400	.0645	22.5	.998	.949	.265	.372	2.038	.812	.187	.625	.569	.431	.138	4.521	1.5087	22	.2866	.00164	-------	46.09	.774
32	3 mm	1.5	.484	.04943	.1329	22.0	.998	.961	.265	.372	2.038	.921	.078	.843	.729	.270	.459	1.836	.6076	14	.4488	.00348	-------	93.74	.752
31	3 mm	1.5	.734	.07496	.2013	21.5	.998	.972	.265	.372	2.038	.889	.112	.777	.674	.325	.349	2.228	.8011	8	.7854	.00520	-------	140.55	.762
30	3 mm	1.5	.860	.08782	.2362	21.5	.998	.972	.265	.372	2.038	.850	.150	.700	.634	.366	.268	2.617	.9620	6	1.0472	.00567	-------	164.67	.819
25	3 mm	1.0	.0223	.00228	.00647	21.0	.998	.984	.0083	.352	3.038	.856	.144	.712	.807	.193	.614	1.159	.1476	150	.0419	.00000750	-------	.15	.597
26	3 mm	1.0	.0422	.00431	.0122	21.0	.998	.984	.0083	.352	3.038	.830	.171	.659	.776	.224	.552	1.196	.1790	80	.0785	.0000175	-------	.28	.483
21	3 mm	1.0	.0665	.00679	.0193	18.5	.999	1.043	.0083	.352	3.038	.876	.124	.752	.825	.175	.650	1.158	.1467	60	.1047	.0000316	-------	.42	.422
22	3 mm	1.0	.101	.01031	.0293	18.5	.999	1.043	.0083	.352	3.038	.876	.124	.752	.820	.180	.640	1.176	.1621	40	.1571	.0000543	-------	.63	.373
23	3 mm	1.0	.217	.02216	.0630	19.0	.998	1.031	.0083	.352	3.038	.887	.113	.774	.835	.166	.669	1.156	.1450	20	.3142	.000121	-------	1.38	.361
20	3 mm	1.0	.235	.02400	.0658	25.5	.997	.886	.0083	.365	2.038	.752	.247	.505	.724	.275	.449	1.123	.1160	20	.3142	.000164	-------	1.88	.301
24	3 mm	1.0	.347	.03544	.1007	20.5	.998	.996	.0083	.352	3.038	.913	.087	.826	.873	.126	.747	1.106	.1008	14	.4488	.000168	-------	2.28	.414
19	3 mm	1.0	.678	.06924	.1897	26.0	.997	.876	.0083	.365	2.038	.797	.203	.594	.772	.228	.544	1.091	.0862	8	.7854	.000468	-------	5.06	.304
10	25/30 Mesh	1.5	.0303	.00309	.00905	26.5	.997	.866	.133	.342	3.038	.767	.232	.534	.550	.450	.100	5.326	1.6793	150	.0419	.000233	-------	3.67	.430
11	25/30 Mesh	1.5	.0495	.00506	.0148	26.5	.997	.866	.133	.342	3.038	.775	.225	.550	.536	.463	.073	7.488	2.0133	80	.0785	.000347	-------	5.99	.472
12	25/30 Mesh	1.5	.0745	.00761	.0223	26.0	.997	.876	.133	.342	3.038	.808	.192	.616	.552	.449	.103	5.938	1.7814	60	.1047	.000589	-------	8.91	.418
13	25/30 Mesh	1.5	.1080	.01103	.0323	26.0	.997	.876	.133	.342	3.038	.809	.192	.617	.550	.450	.100	6.159	1.8179	40	.1571	.000813	-------	12.92	.439
27	3mm	1.5	.1080	.01103	.0321	21.5	.998	.972	.133	.344	3.038	.843	.157	.686	.571	.430	.141	4.862	1.5815	50	.1257	.00109	-------	11.66	.327
14	25/30 Mesh	1.5	.2350	.02400	.0702	25.5	.997	.886	.133	.342	3.038	.820	.180	.640	.571	.429	.142	4.499	1.5039	20	.3142	.00174	-------	27.79	.448
28	3mm	1.5	.235	.02400	.0698	21.5	.998	.972	.133	.344	3.038	.869	.130	.739	.613	.387	.226	3.270	1.1848	24	.2618	.00193	-------	25.36	.400
15	25/30 Mesh	1.5	.484	.04943	.1445	25.5	.997	.886	.133	.342	3.038	.882	.118	.764	.675	.326	.349	2.188	.7830	12	.5236	.00284	-------	57.25	.564
16	25/30 Mesh	1.5	.484	.04943	.1445	25.5	.997	.886	.133	.342	3.038	.883	.117	.766	.678	.323	.355	2.158	.7692	12	.5236	.00279	-------	57.25	.574
17	25/30 Mesh	1.5	.683	.06975	.2039	26.0	.997	.876	.133	.342	3.038	.852	.147	.706	.657	.343	.314	2.249	.8105	8	.7854	.00367	-------	81.70	.616
18	25/30 Mesh	1.5	.840	.08578	.2508	26.0	.997	.876	.133	.342	3.038	.900	.100	.800	.741	.255	.487	1.644	.4971	8	.7854	.00419	-------	100.48	.664
29	3mm	1.5	.835	.08527	.2479	21.5	.998	.972	.133	.344	3.038	.927	.073	.854	.759	.241	.518	1.649	.5002	8	.7854	.00408	-------	90.10	.675

minimum concentration points, averaged for ten inlet periodic waves, are presented in columns 13 and 14, respectively; the maximum and minimum concentration points, averaged for the ten corresponding outlet waves, are presented in columns 16 and 17, respectively. These concentration points are the results of the conversions of the recorder traces (in millivolts) to concentration units on a basis of 0 for the clear solution and 1 for the dye solution. Figure 11 is a reproduction of the actual recorder traces of the inlet and outlet periodic waves of run 28; Figure 5 presents the inlet and outlet waves for run 28 resulting after the conversion to concentration units. The experimental data (recorder trace points in millivolts) for the complete concentration profiles of the inlet and outlet periodic waves of run 6 are presented in Appendix II-B.

Four sets of data, each with a different sized glass sphere as packing, are reported. The first set includes a group of preliminary runs, A-F, which were employed to determine the feasibility of the frequency response method. The 1.5 foot test section was packed with 1 mm glass spheres (d_p = .039 in.) during runs A and B. For the remainder of the first set, runs C-F and 1-9, 1 mm glass spheres in a 3 foot test section were used. In runs 1-9, the velocity, covering a range from 0.05 gpm to 0.90 gpm, was the variable. The second series of runs, 19-26, employed 60/80 mesh glass spheres (d_p = .0083 in.) in either a 2 foot or 3 foot column, with the flow rate varying from 0.02 gpm to 0.68 gpm. In the third group of runs, 10-18 and 27-29, a 3 foot column was packed with 3 mm glass spheres (d_p = .133 in.) and the velocity was varied from 0.03 gpm to 0.84 gpm. The fourth group of runs, 30-35, employing a 2 foot test section packed with 6 mm glass beads (d_p = .265 in.), was

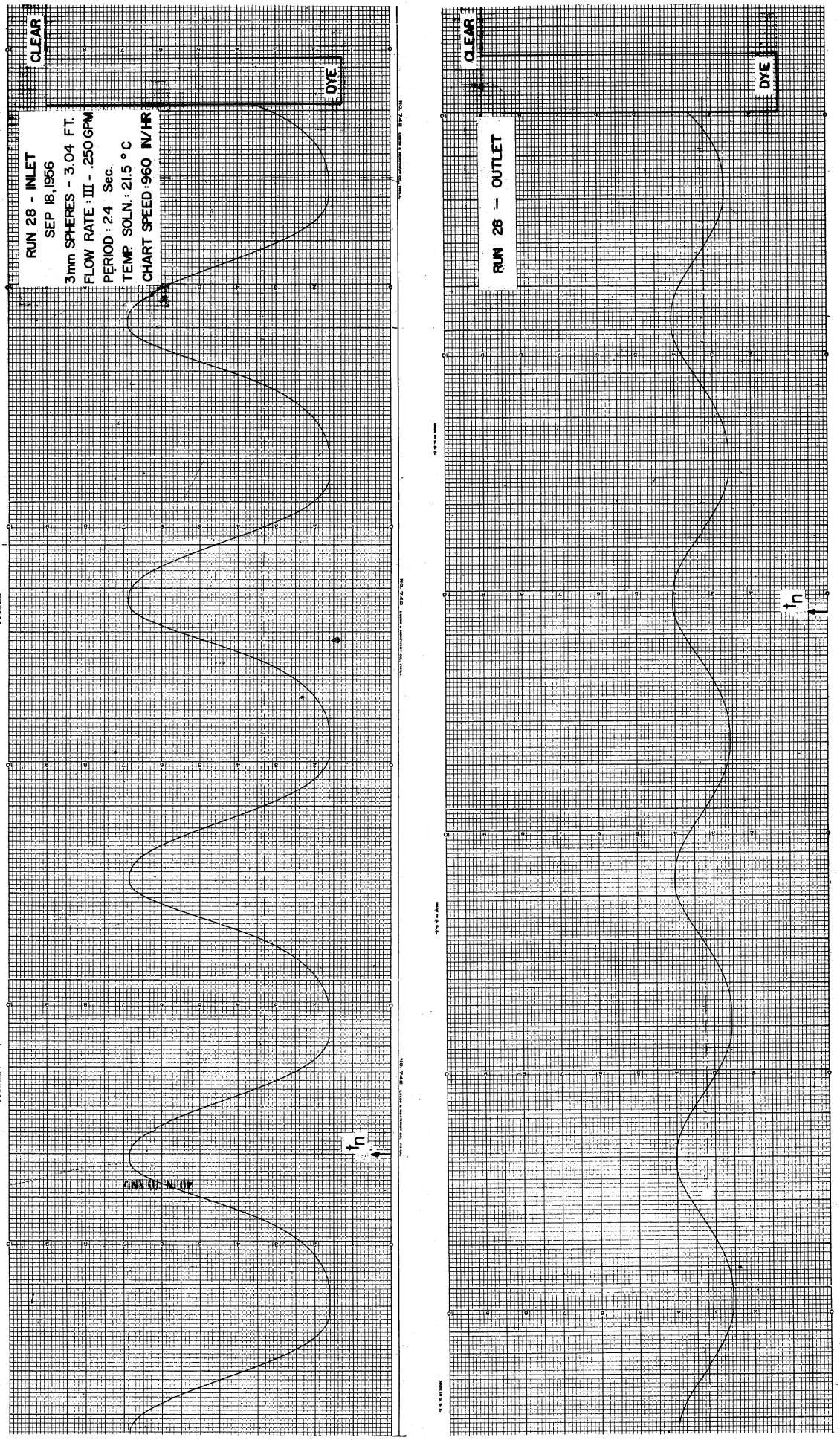

FIGURE 11 - REPRODUCTION OF RECORDER TRACERS, FREQUENCY RESPONSE RUN 28

made to determine the effect of the large d_p/d_t ratio, 0.13, on the diffusivity measurements. The flow in runs 30-35 covered the range from 0.05 gpm to 0.86 gpm.

The reduction of the experimental data and evaluation of axial diffusivity are discussed in the next chapter and in Appendix II.

Pulse Function Method

The equipment for the pulse function runs was assembled as shown in Figure 3. Much of the same procedure as employed in the frequency response runs was followed. Again, the entire system was filled with distilled water and purged of air. Both the large storage cylinder and the small cylinder contained the clear solution. During the necessary warm-up period for the electrical measuring instruments, the gears for the desired chart speed were installed. The flow rates from each cylinder were adjusted as in the frequency response runs. The small cylinder was then drained of clear solution, and filled with concentrated dye solution. The lines from the concentrated dye cylinder were purged of clear solution so that an instantaneous pulse could be introduced. The flow of the clear solution through the system was controlled by the metering valve following the column. The photometer at the exit of the test section was standardized by varying the resistances and setting the recorder at 9.0 millivolts. The concentrated dye pulse was then injected into the flowing stream by instantly energizing and de-energizing the three-way solenoid valve. The injection time was measured with a stop watch. When the pulse approached the exit of the test section, the recorder chart was started. A pip was introduced on the chart through a switch in the photometry circuit, and the time recorded. The pulse function response was continiously recorded by the Speedomax on the chart paper. Figure 12

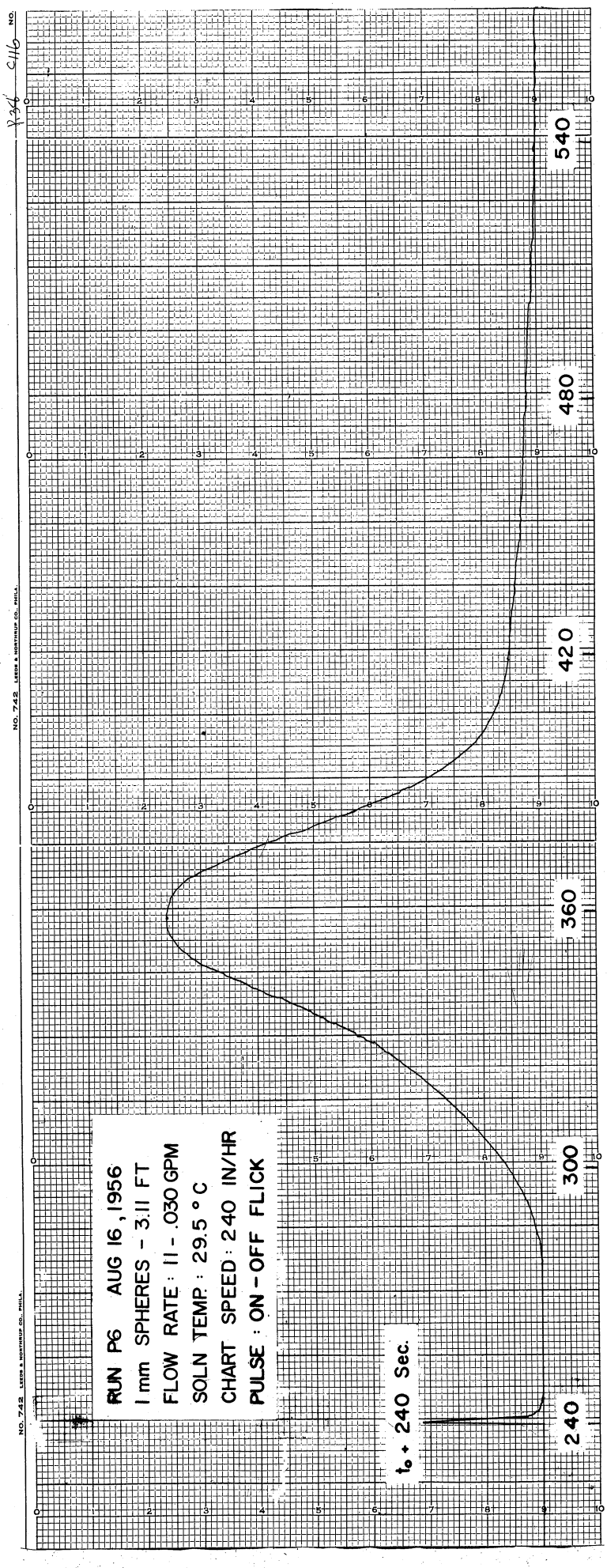

FIGURE 12 - REPRODUCTION OF RECORDER TRACER, PULSE FUNCTION RUN P6

presents a reproduction of the recorder trace for a pulse of run P6. The flow rate and temperature of the solution were checked throughout a run. A series of five pulses, introduced and recorded as described, constituted a run. The pulses were spaced so as not to interfere with each other. A series of runs were made by varying the rate of flow through the column and repeating the above procedure.

The list of data recorded for a pulse function experiment follows:

Run designation

Data and time

Column properties
- Particle diameter and shape
- Height
- Porosity

Chart speed

Liquid flow rate

Liquid temperature

Pulse
- Length of pulse
- Time of pulse injection
- Time of pip on recorder chart

Recorder traces
- Colorimeter calibration
- Outlet concentration

Experimental data for the pulse function runs are presented in Table IV. Column 1 contains the run designation with the prefix "P" referring to the pulse function method. Columns 2, 3, 4, and 5 present the properties of the packing: column 2 the nominal particle size and shape, column 3 the equivalent spherical diameter, column 4 the height of the packing, and column 5 the porosity of the packed bed. Column 6 contains the corrected liquid flow rate, and column 10 the liquid

TABLE IV.

EXPERIMENTAL DATA AND CALCULATED RESULTS - PULSE FUNCTION TECHNIQUE

1	2	3	4	5	6	7	8	9	10	11	12	13	14	15	16	17	18	19	20	21	22	23
	COLUMN PROPERTIES				LIQUID FLOW RATE				LIQUID PROPERTIES			AVERAGE PULSE DATA			RESIDENCE TIME OF PULSE		MAXIMUM CONCENTRATION					
RUN	PACKING		Porosity	Height	v	Interstitial Velocity	Superficial Velocity	Time for Liquid to Pass Through Column	Temperature	Density	Viscosity	Maximum Concentration	Area Under Pulse Profile	Time for Pulse to Pass Through Column	Dimensionless Time Variable	Largest % Deviation of R from Average.	$(\frac{Vc}{Q})_{R=\gamma}$	Largest % Deviation of $(\frac{Vc}{Q})_{R=\gamma}$ from average	S $\frac{1}{4\pi R^2(\frac{Vc}{Q})^2_{R=\gamma}}$	Axial Diffusivity D_L (Suz)	Reynolds Number $\frac{d_p v_o \rho}{\mu}$	Peclet Number $\frac{d_p u}{D_L}$
	Nominal Size and Shape	Diam. d_p in.	ϵ	z ft	gpm	u ft/sec	v_o ft/sec	z/u min	°C	gms/cc	cp	gm/li x 10^2	gm/li x 10^2	min	R					ft^2/sec		
P4	1mm spheres	.039	.340	3.11	.00265	.000271	.000796	65.10	23.0	.998	.938	.402	.0667	77.92	1.197	.9	6.034	1.6	.001526	.00000378	.087	.685
P3	1mm spheres	.039	.340	3.11	.00540	.000551	.00162	31.95	25.0	.997	.896	.507	.0847	34.52	1.081	.1	5.979	.4	.001907	.00000962	.19	.548
P2	1mm spheres	.039	.340	3.11	.00810	.000827	.00243	21.30	28.5	.996	.830	.417	.0650	22.33	1.048	.2	6.401	1.0	.001767	.0000134	.30	.591
P1	1mm spheres	.039	.340	3.11	.0107	.001093	.00322	16.10	26.0	.997	.876	.555	.0852	16.82	1.044	.4	6.522	2.3	.001715	.0000171	.38	.610
P7	1mm spheres	.039	.340	3.11	.0203	.002073	.00610	8.50	30.0	.996	.804	.346	.0515	9.31	1.095	.9	6.709	.7	.001475	.0000280	.78	.709
P6	1mm spheres	.039	.340	3.11	.0303	.003094	.00910	5.69	29.5	.996	.812	.421	.0621	5.96	1.046	.3	6.780	.7	.001581	.0000447	1.15	.661
P5	1mm spheres	.039	.340	3.11	.0512	.005229	.01538	3.37	29.0	.996	.821	.498	.0704	3.55	1.053	.1	7.077	.1	.001434	.0000686	1.91	.729
P9	3mm spheres	.133	.338	3.11	.00265	.000271	.000801	64.72	21.0	.998	.984	.255	.1117	96.80	1.496	.3	2.296	6.7	.006746	.0000168	.28	.528
P14	3mm spheres	.133	.338	3.11	.00532	.000543	.00161	32.24	22.0	.998	.961	.439	.1585	39.58	1.212	2.5	2.772	.3	.007047	.0000352	.58	.506
P13	3mm spheres	.133	.338	3.11	.00801	.000818	.00242	21.41	21.0	.998	.984	.398	.1488	25.31	1.177	.4	2.666	2.8	.008077	.0000608	.85	.441
P12	3mm spheres	.133	.338	3.11	.0108	.001109	.00326	15.91	24.0	.997	.916	.419	.1500	18.13	1.142	.4	2.791	.5	.007849	.0000796	1.24	.454
P11	3mm spheres	.133	.338	3.11	.0203	.002073	.00613	8.45	24.5	.997	.906	.348	.1278	9.87	1.161	.6	2.735	2.3	.007796	.000149	2.35	.457
P10	3mm spheres	.133	.338	3.11	.0303	.003094	.00915	5.66	23.5	.998	.927	.319	.1073	6.36	1.124	.2	2.970	1.4	.007136	.000203	3.43	.499
P8	3mm spheres	.133	.338	3.11	.0512	.005229	.01547	3.35	23.5	.998	.927	.411	.1347	3.77	1.124	.7	3.051	1.8	.006771	.000326	5.79	.526
P24	3mm spheres	.133	.334	5.05	.0203	.002073	.00621	13.77	23.0	.998	.938	.357	.0957	15.97	1.160	.4	3.733	.9	.004243	.000133	2.27	.517
P15	60/80 Mesh spheres	.0083	.353	5.12	.00267	.000273	.000773	110.45	29.0	.996	.821	.391	.0305	149.97	1.353	.2	12.814	.1	.0002646	.00000105	.021	.511
P16	60/80 Mesh spheres	.0083	.353	5.12	.00532	.000543	.00154	54.44	26.0	.997	.876	.539	.0407	64.78	1.163	.1	13.237	.9	.0003361	.00000265	.040	.402
P17	60/80 Mesh spheres	.0083	.353	5.12	.00801	.000818	.00232	36.82	28.0	.996	.839	.400	.0254	41.60	1.130	.1	15.857	.7	.0002479	.00000294	.062	.545
P18	60/80 Mesh spheres	.0083	.353	5.12	.0107	.001093	.00310	27.48	29.0	.996	.821	.543	.0362	29.61	1.076	.3	14.983	.5	.0003062	.00000486	.085	.441
P19	60/80 Mesh spheres	.0083	.353	5.12	.0203	.002073	.00587	14.53	29.0	.996	.821	.439	.0262	15.76	1.065	.3	16.721	.8	.0002419	.00000727	.16	.559
P20	60/80 Mesh spheres	.0083	.353	5.12	.0304	.003104	.00879	9.70	26.5	.997	.866	.562	.0327	10.15	1.047	.2	17.187	.2	.0002459	.0000111	.23	.549
P21	60/80 Mesh spheres	.0083	.353	5.12	.0501	.005116	.01449	5.89	26.5	.997	.866	.632	.0347	6.13	1.041	.2	18.231	1.2	.0002208	.0000164	.38	.612
P22	60/80 Mesh spheres	.0083	.353	5.12	.0745	.007608	.02155	3.96	26.5	.997	.866	.428	.0231	4.09	1.034	.1	18.540	.6	.0002167	.0000239	.56	.623
P23	60/80 Mesh spheres	.0083	.353	5.12	.1090	.011130	.03153	2.71	25.5	.997	.866	.557	.0318	2.76	1.020	.1	17.519	.1	.0002491	.0000402	.82	.543
P25	6mm sphere	.265	.362	5.00	.0203	.00207	.00573	14.73	28.5	.996	.830	.524	.2077	16.40	1.114	.5	2.520	.5	.01010	.000287	4.54	.392
P26	6mm sphere	.265	.362	5.00	.0502	.00513	.01416	5.96	28.5	.996	.830	.520	.1857	6.22	1.044	.1	2.797	.3	.009337	.000656	11.23	.424
P28	6mm sphere	.265	.362	5.00	.108	.01103	.03047	2.77	26.0	.997	.876	.430	.1367	2.82	1.022	.5	3.148	.6	.007695	.00117	22.93	.514
P27	6mm sphere	.265	.362	5.00	.224	.02287	.06318	1.34	26.0	.997	.876	.508	.1495	1.38	1.030	.3	3.398	.3	.006493	.00204	47.53	.609
P32	1/4 in Raschig rings	.22	.632	5.00	.0206	.00210	.00333	25.06	23.0	.998	.938	.455	.1693	26.06	1.040	.7	2.687	1.3	.01019	.000169	3.81	.362
P30	1/4 in Raschig rings	.22	.632	5.00	.0502	.00513	.00811	10.10	23.0	.998	.938	.569	.2009	10.10	1.000	--	2.833	.1	.009912	.000405	9.28	.372
P31	1/4 in Raschig rings	.22	.632	5.00	.108	.01103	.01745	4.72	24.0	.997	.916	.589	.2025	4.72	1.000	--	2.905	.2	.009432	.000830	20.44	.390
P29	1/4 in Raschig rings	.22	.632	5.00	.224	.02287	.03619	2.31	22.0	.998	.961	.372	.1173	2.33	1.011	--	3.170	.3	.007742	.00140	40.43	.475
P36	1/4 in Intalox saddles	.20	.629	5.00	.0205	.00209	.00333	25.07	22.0	.998	.961	.415	.1582	26.25	1.047	.2	2.626	1.4	.01053	.000174	3.36	.318
P35	1/4 in Intalox saddles	.20	.629	5.00	.0502	.00513	.00815	10.24	23.0	.998	.938	.414	.1530	10.24	1.000	--	2.707	.1	.01086	.000440	8.44	.309
P33	1/4 in Intalox saddles	.20	.629	5.00	.108	.01103	.01754	4.67	23.0	.998	.938	.396	.1331	4.67	1.000	--	2.977	.7	.008980	.000799	18.16	.373
P34	1/4 in Intalox saddles	.20	.629	5.00	.234	.02390	.03800	2.20	23.0	.998	.938	.493	.1507	2.20	1.000	--	3.273	.2	.007430	.00141	39.35	.450
P37	1/4 in Berl saddles	.23	.616	5.00	.0203	.00207	.00337	24.80	20.0	.998	1.007	.278	.1140	26.65	1.105	.7	2.431	.1	.01103	.000185	3.66	.350
P38	1/4 in Berl saddles	.23	.616	5.00	.0502	.00513	.00832	9.63	20.0	.998	1.007	.419	.1542	9.63	1.000	--	2.717	.2	.01078	.000465	9.04	.358
P40	1/4 in Berl saddles	.23	.616	5.00	.108	.01103	.01791	4.51	20.0	.998	1.007	.358	.1187	4.51	1.000	--	3.007	.5	.008803	.000811	19.46	.437
P39	1/4 in Berl saddles	.23	.616	5.00	.234	.02390	.03880	2.09	20.0	.998	1.007	.376	.1113	2.09	1.000	--	3.383	.3	.006954	.00138	42.16	.553
P41	1mm sphere	.039	.340	3.09	.00757	.000773	.00227	22.63	22.5	.998	.949	.510	.0731	23.76	1.050	--	6.970	.4	.001486	.0000104	.25	.708
P42	1mm sphere	.039	.340	3.09	.00757	.000773	.00227	22.63	22.5	.998	.949	.468	.0645	23.88	1.056	.2	7.267	.1	.001353	.00000950	.25	.778
P43	1mm sphere	.039	.340	3.09	.00830	.000847	.00249	20.60	20.0	1.040	6.205	.357	.0570	25.29	1.225	.5	6.257	.9	.001355	.0000104	.043	.777
P44	1mm sphere	.039	.340	3.09	.00773	.000795	.00234	22.14	19.5	1.045	11.726	.401	.0616	24.41	1.108	.1	6.511	.8	.001529	.0000110	.021	.689
P45	1mm sphere	.039	.340	3.09	.00750	.000766	.00225	23.00	18.5	1.043	26.881	.496	.0740	25.33	1.109	.2	6.698	.3	.001442	.0000100	.0090	.730

temperature. The data for an exit pulse profile, averaged from the recorder traces of three or more pulse waves, are presented in columns 13, 14, and 15. Column 13 contains the maximum concentration of the pulse wave in units of gms/li x 10^2, column 14 the area under the exit concentration profile of the pulse wave in units of gms/li x 10^2 and column 15 the time (seconds) for the pulse to pass through the test section. Figure 12 is a reproduction of the recorder traces for a pulse wave of experiment P6. The experimental data for the concentration profiles of three pulse waves of run P6 are presented in Table XIV, Appendix II-C.

The first three groups of pulse function runs were to determine the effect of velocity on mixing in the low flow range and hence extend the data of the frequency response experiments. For each group of runs the velocity was varied from 0.003 gpm to 0.05 gpm, approximately. Each group of runs employed a different particle size: 1 mm, 3 mm and 60/80 mesh glass spheres were used for runs P1-P7, P8-P14, and P15-P23, respectively. A longer column, 5 foot, was used for the 60/80 mesh spheres because of the small amount of mixing occurring, while the 3 foot column was used for the other two groups of runs. The effect of particle diameter on mixing is shown in Figure 13 which presents the concentration profiles of two runs, P7 and P11, made under identical conditions except for the diameter of the spherical packing. Run P24, made to determine the effect of bed length, employed a 5 foot test section packed with 3 mm glass beads. The primary purpose of the runs P25-P40 was to determine the effect of particle shape. Runs P25-P28 used 6 mm glass beads, runs P29-P32 used 1/4 in. Raschig rings, runs P33-P36 used 1/4 in. Intalox saddles, and runs P37-P40 used 1/4 in.

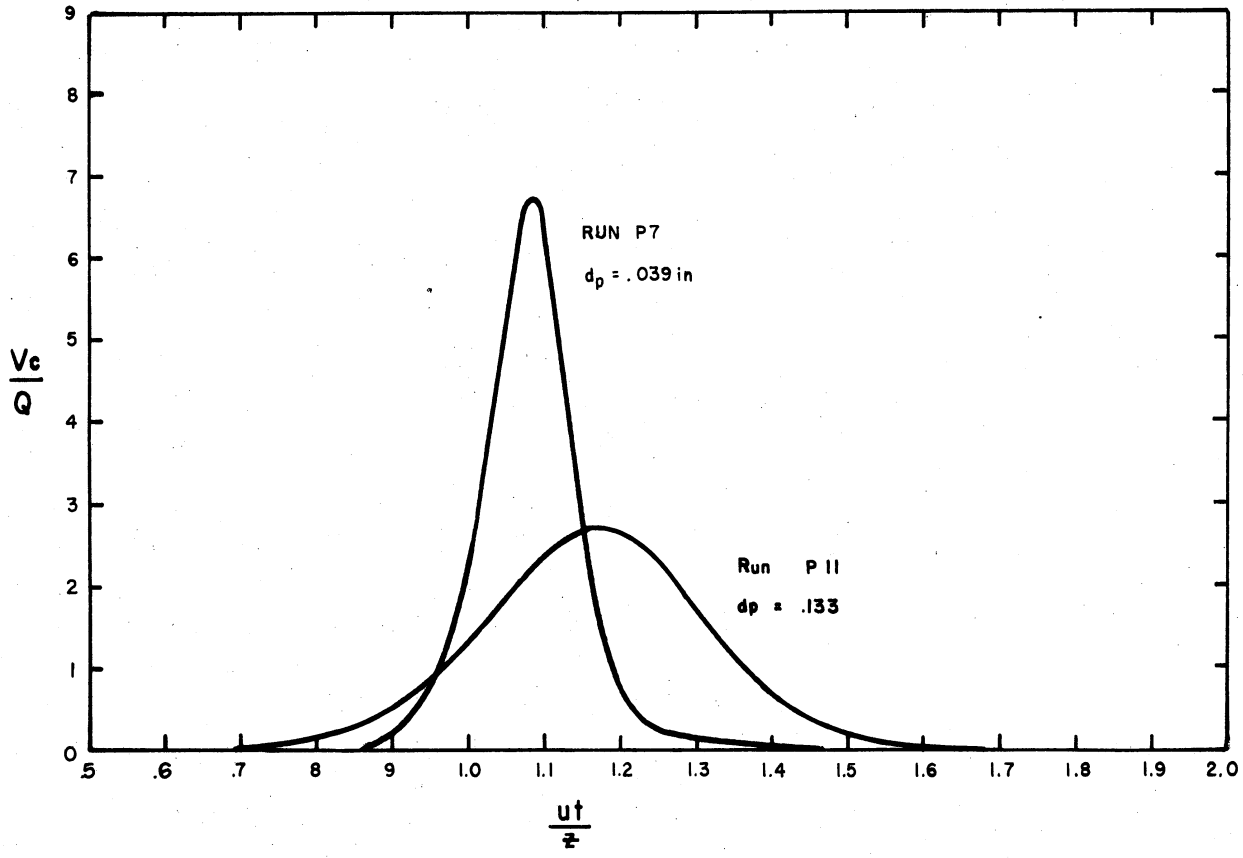

FIGURE 13 - EFFECT OF PARTICLE DIAMETER ON PULSE CONCENTRATION PROFILES

(3 ft. column - Interstitial Velocity .0061 ft/sec)

Berl saddles. The velocity was varied in each set from .02 gpm to .23 gpm. The purpose of runs P41 and P42, employing a 3 foot column packed with 1 mm glass spheres, was to determine if the tracer used had any effect on the measurement of axial diffusion. Pontamine Sky Blue 6BX, the dye used normally, was used in run P41; Pontamine Fast Turquoise 8GLD was used in run P42. Runs P43-P45 were made to determine the viscosity effect; propylene glycol solutions, covering a viscosity range of from 1 to 26 centipoise were used.

Step Function Method

Although experiments by the step function method are not included in the results of this research, several runs were made in an attempt to obtain satisfactory data. The equipment was assembled exactly as in the frequency response method, except for the elimination of the pre-bed. The experimental procedure was exactly as the procedure in the frequency response method up to the time of the introduction of the periodic concentration waves. An approximate step function was then obtained by energizing the three-way directional-flow solenoid valve and allowing the dye solution to follow the clear solution. Several methods of introducing a step function were tried with the above method being the least objectionable. The reverse step function could also be obtained by de-energizing the valve and allowing the clear solution to follow the dye solution. A continuous record of the outlet concentration curve was obtained by the photometer and recorder.

TREATMENT OF EXPERIMENTAL DATA

As a fluid, in which concentration gradients exist, flows through a packed bed eddy diffusion or mixing occurs which can be rationalized as a mass transfer process. This eddy diffusion, superimposed on the molecular mechanism of diffusion, can be described by the equation

$$N = -(D_V + \delta_E)\frac{dc}{dy} = -D_T \frac{dc}{dy} \qquad (1)$$

where

D_V = molecular diffusivity, ft^2/sec

δ_E = mixing diffusivity, ft^2/sec

D_T = total effective diffusivity, ft^2/sec

$-\frac{dc}{dy}$ = concentration gradient, $\frac{moles/ft^3}{ft}$

N = mass transfer rate, $\frac{moles}{sec\text{-}ft^2}$

Experimental data, obtained for fluid flow through beds in which the particle to column ratio was less than .075 and the length to diameter ratio of the column was greater than 10, have verified the rationalization of mixing as a mass transfer process described by equation (1). On the basis of this model, a material balance for an increment of time dt made for a cylindrical element dr in thickness and dz in height results in the equation:

$$D_R\left[\frac{\partial^2 c}{\partial r^2} + \frac{1}{r}\frac{\partial c}{\partial r}\right] + D_L \frac{\partial^2 c}{\partial z^2} - u\frac{\partial c}{\partial z} = \frac{\partial c}{\partial t} \qquad (4)$$

where

D_R = effective radial diffusivity, ft^2/sec

D_L = effective axial diffusivity (in longitudinal direction), ft^2/sec

u = mean velocity, ft/sec

c = concentration of tracer in solution, $moles/ft^3$

r = radial coordinate in cylindrical coordinate system

z = longitudinal coordinate in cylindrical coordinate system

t = time, sec

The derivation of this partial-differential equation, which is representative of the diffusion-convection mixing of a liquid flowing through a fixed bed of particles, can be found in Appendix I-A. The first two terms in equation (4) represent the diffusion of the tracer, the third term the transport of the tracer due to flow and the fourth term represents the accumulation of the tracer.

In theory, determinations of concentration, c, as a function of position, r and z, and time, t, in an experiment where a tracer is fed at a point source into fluid of known composition and flow rate, yield the information required to determine D_R and D_L through the evaluation of the various first and second partial derivatives by numerical differentiation and smoothing. The difficulties of obtaining such data and the large error involved in differentiating the data twice, lead to special experimental conditions for which equation (4) has known mathematical solutions which permit the evaluation of effective diffusivity from specific values of c, r, z, and t. The point-source experiment results in the evaluation of effective radial diffusivity, D_R, while other types of experiments lead to values of effective axial diffusivity, D_L.

FREQUENCY RESPONSE EXPERIMENT

In the frequency response method the concentration at the inlet is varied sinusoidally and the response is obtained at the outlet. Comparison of the amplitudes of the inlet and outlet harmonic functions leads to values of the axial diffusivities.

Mathematical Representation

Sinusoidal Solution. In the mathematical representation of the frequency response experiment, no radial concentration gradients exist and the effective axial diffusivity and velocity are independent of position leading to the modification of equation (4) as follows:

$$D_L \frac{\partial^2 c}{\partial z^2} - u \frac{\partial c}{\partial z} = \frac{\partial c}{\partial t} \tag{5}$$

The two experimental boundary conditions which exist are: first, the inlet concentration is a harmonic function of time; second, at a sufficiently long distance down the bed the amplitude approaches zero. These boundary conditions can be represented as follows:

$$c(z,t)$$

$$c(0,t) = c_m + A(0) \cos \omega t \tag{6}$$

$$c(\infty,t) = c_m$$

$$\text{or } A(z) = 0 \text{ for } z \to \infty$$

where c_m is the mean composition about which the concentration oscillates, $A(0)$ is the amplitude of the inlet concentration wave, and ω is the angular frequency of the oscillations. Danckwerts[11] applied an alternate choice of boundary conditions which resulted in the same approximate solution as equation (10) below. With the introduction of

the above boundary conditions, the periodic steady-state solution resulting is:

$$c(z,t) = c_m + A(0)e^{-B}\cos(\omega t - \varphi) \tag{10}$$

where

$$B = -\frac{zu}{2D_L}\left\{1 - \sqrt{\sqrt{\frac{1}{4} + \left(\frac{2D_L\omega}{u^2}\right)^2} + \frac{1}{2}}\right\} \tag{10a}$$

and

$$\varphi = \frac{zu}{2D_L}\sqrt{\sqrt{\frac{1}{4} + \left(\frac{2D_L\omega}{u^2}\right)^2} - \frac{1}{2}} \tag{10b}$$

The functions B and φ shown in Figure 14 are representative of the decrease in amplitude and the phase shift of the outlet wave, respectively.

Details of two solutions are presented in Appendix I-B. The original solution employs the Laplace transform and requires use of the complex inversion integral for the inverse transformation. The second solution, following the method proposed by other investigators[12,24], is more direct; this method employs complex variables and the principle of superposition. The final solutions are identical.

Approximate Solution. An approximate form of the above solution can be employed when experimental conditions are such that the ratio $4\omega D_L/u^2$, is small. The complex form of the above solution is:

$$c(z,t) = c_m + A(0)\, e^{\left\{\frac{zu}{2D_L}\left[1 - \sqrt{1 + \frac{4\omega D_L}{u^2}\, i}\right] + i\omega t\right\}} \tag{11}$$

Expansion of the radical by means of the Binomial Theorem and rejecting insignificant terms, and then dropping the imaginary part of the solution, leads to the following approximate solution:

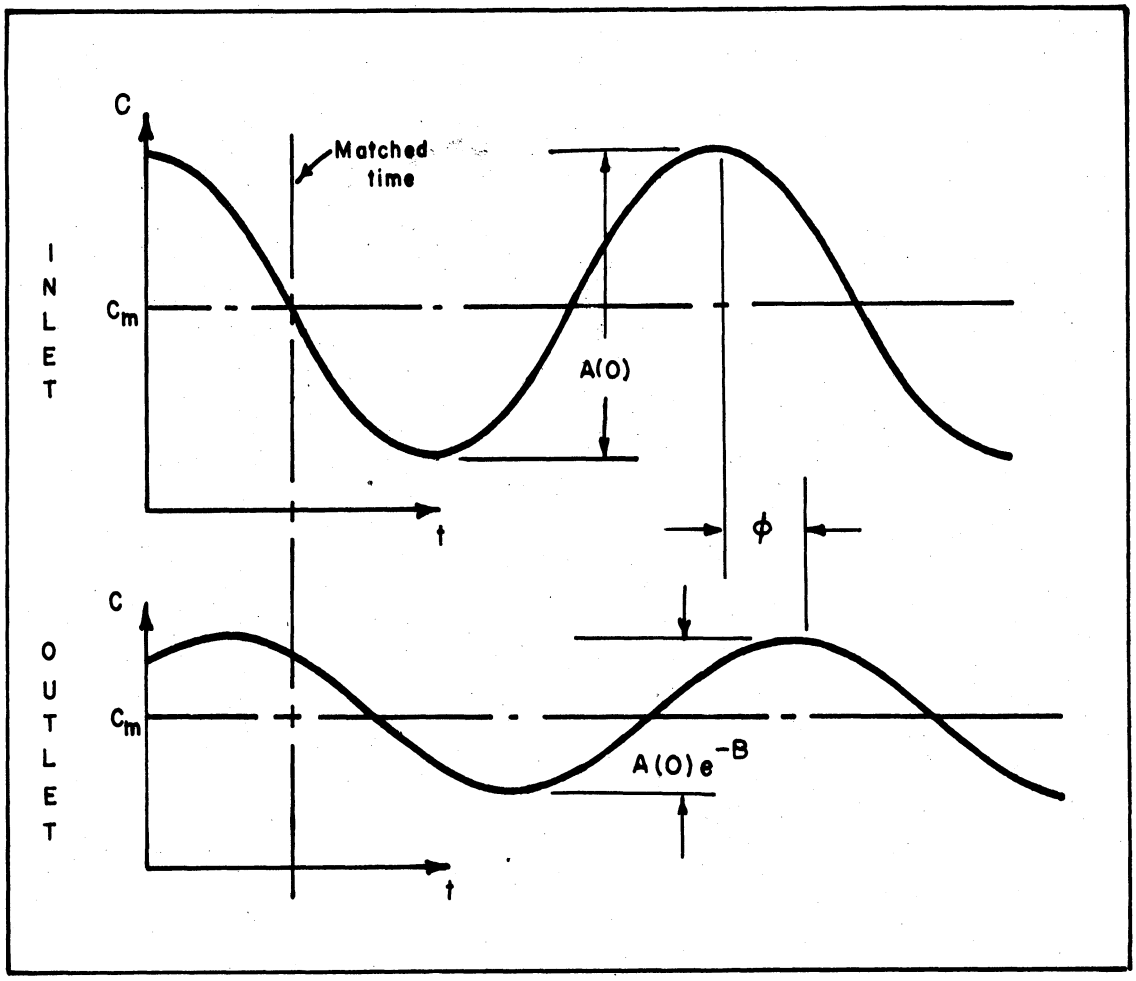

FIGURE 14 - SINUSOIDAL CONCENTRATION WAVES FOR INLET AND OUTLET STREAMS

$$c(z,t) \cong c_m + A(0)\, e^{-\left(\frac{z\omega^2 D_L}{u^3}\right)} \cos\left(\omega t - \frac{z\omega}{u}\right) \qquad (12)$$

in which the value of B is approximated as

$$B \cong \frac{z\omega^2 D_L}{u^3} \qquad (12a)$$

For this approximation, the value of B is in error approximately less than the value of the first term neglected in the binomial expansion, which is the group

$$5\left(\frac{\omega D_L}{u^2}\right)^2 \qquad (12b)$$

For experimental runs in which this approximation produces too large an error, the last term rejected should be included in the expansion of the radical. The approximate solution then resulting is:

$$c(z,t) \cong c_m + A(0)\, e^{-\frac{z\omega^2 D_L}{u^3} + \frac{5z\omega^4 D_L^3}{u^7}} \cos\left(\omega t - \frac{z\omega}{u} + \frac{2z\omega^3 D_L^2}{u^5}\right) \qquad (13)$$

where B is approximated as

$$B \cong \frac{z\omega^2 D_L}{u^3} - \frac{5z\omega^4 D_L^3}{u^7} \qquad (13a)$$

and the maximum error in B is approximately

$$42\left(\frac{\omega D_L}{u^2}\right)^4 \qquad (13b)$$

Assuming the approximate solution of equation (12) is applicable, the ratio of inlet to outlet amplitudes leads to the equation

$$\frac{A_i}{A_e} = \frac{A(0)}{A(0)e^{-B}} = e^{B} = e^{\left[\frac{z\omega^2 D_L}{u^3}\right]} \tag{14}$$

or,

$$\ln \frac{A_i}{A_e} = B \cong \frac{z\omega^2 D_L}{u^3} \tag{14a}$$

from which D_L can be calculated. For experiments in which the first approximation is in excess error, equation (13) can be employed. The ratio of amplitudes then results in the equation

$$\ln \frac{A_i}{A_e} = B \cong \frac{z\omega^2 D_L}{u^3} - \frac{5z\omega^4 D_L^3}{u^7} \tag{15}$$

from which D_L can be calculated by trial and error. The diffusivities were calculated by one of the above approximations so that the maximum error in the value of B caused by the approximation is less than 1.5 percent, which is well within the error of measurement.

Evaluation of axial diffusivity from measurements of the phase angles was not carried out during the present research, since the measurements of amplitude ratios provided a more accurate and reliable means of evaluation. Justification for the elimination of phase angle calculations is apparent in equation (12), since in this approximate solution the phase angle does not contain the diffusivity until higher order terms are included, as indicated in equation (13). Other investigators employing the frequency response technique have arrived at similar conclusions.

Non-Sinusoidal Solution. The outlet wave from the pre-bed, or the inlet wave to the test section, was not always sinusoidal although periodic. Under these conditions, the periodic concentration wave could be represented by a Fourier series having the form

$$c(0,t) = \frac{a_o}{2} + \sum_{n=1}^{\infty} (a_n \cos n\omega t + b_n \sin n\omega t) \tag{16}$$

or the form

$$c(0,t) = \frac{a_o}{2} + \sum_{n=1}^{\infty} A_n(0) \cos (n\omega t - \psi_n) \tag{16a}$$

where

$$A_n(0) = [a_n^2 + b_n^2]^{1/2} \tag{16b}$$

represents the amplitude of the n-th harmonic and

$$\psi_n = \tan^{-1} \frac{b_n}{a_n} \tag{16c}$$

represents the phase lag of the n-th harmonic with reference to a pure cosine wave of the same frequency. Thus, as the above equations indicate, the periodic function is a combination of simple harmonic waves. The term $a_o/2$ represents the neutral position: the terms, $a_1 \cos \omega t + b_1 \sin \omega t$, the fundamental wave; and the other terms, $a_n \cos n\omega t + b_n \sin n\omega t$, the higher harmonics. The outlet concentration wave then also must be represented by a Fourier series in which each harmonic component is dampened and shifted in phase. By the principle of superposition, each harmonic in the outlet corresponds to the outlet expected if the corresponding harmonic in the inlet wave was the only

inlet. Applying the periodic, but non-sinusoidal, inlet wave as a boundary value to the differential equation for the diffusion-convection mixing of a liquid flowing through fixed beds, results in the approximate solution

$$c(z,t) = \frac{a_o}{2} + \sum_{n=1}^{\infty} A_n(0)\, e^{-\left[\frac{zn^2\omega^2 D_L}{u^3}\right]} \cos\left(n\omega t - \psi_n - \frac{nz\omega}{u}\right) \qquad (17)$$

The details of the solution are found in Appendix I-B-4.

This solution confirms the earlier statement that each harmonic component is dampened and shifted in phase. The fact that a periodic function can be resolved into its simple harmonic components, permits the reduction of the inlet wave to its harmonic components, the application of each component to the system, and the construction of the general outlet case by addition of the components. The application of the frequency response method to the periodic concentration waves requires a harmonic analysis of the experimental functions; i.e., a representation of the functions as Fourier series.

Evaluation of Data

The data from the frequency response experiments were analyzed by two methods depending on whether the inlet concentration wave was sinusoidal or non-sinusoidal. An axial diffusion coefficient, Reynolds number, and axial Peclet number were obtained from each set of experimental data. Table III summarizes the important steps and the results of the calculations for each run. Sample calculations for sinusoidal and non-sinusoidal waves are recorded in detail in Appendices II-A, B. The important features of the evaluation of the data and correlations are discussed herewith.

The calculation and correlation of longitudinal diffusivity, regardless of the form of the inlet concentration wave, required, in addition to the recorder traces of the inlet and outlet wave compositions, the following data: flow rate; frequency of periodic wave, ω; liquid properties of density, ρ, and viscosity, μ; bed properties of particle diameter, d_p, porosity, ϵ, bed length, z, and bed diameter, d_t. The densities and viscosities of the solutions, obtained from Figure 32, Appendix III-C, which presents the relationship to solution temperature, are reported in Table III, columns 8 and 9. The superficial velocity, v_o, and the actual mean linear velocity, u, reported in columns 5 and 6, respectively, of Table III, can be calculated from the corrected measured flow rate, the column diameter, and the measured fraction void, ϵ. The length of the wave period in seconds was measured during the runs and, if necessary, was checked by measuring the distance between peaks of two adjacent waves and dividing by the chart speed. From this measured wave period, the angular frequency, reported in column 22, was calculated:

$$\omega = \frac{2\pi}{\tau} \text{ , radians per second}$$

where τ is the period, in seconds.

Reynolds number, defined as $d_p\ v_o\ \rho/\mu$ and presented in column 25, was calculated from the superficial velocity through the unpacked column as converted from the measured flow rate, the known particle diameter, and the density and viscosity corresponding to the temperature of the fluid.

Axial Peclet number, defined as $d_p\ u/D_L$ and reported in column 26 was calculated from the actual mean linear velocity in a packed bed

determined from the measured flow rate, the known particle diameter and the calculated longitudinal diffusivity coefficient.

Sinusoidal Data. For the sinusoidal input concentration waves, the ratio of the inlet and outlet amplitudes was used to calculate the longitudinal diffusivity according to equations (12a) or (13a). The amplitude ratio was determined in the following manner.

Figure 11 is a reproduction of the recorder traces for the inlet and outlet concentrations of run 28. The recorder tracers are not sinusoidal, even with a sinusoidal concentration wave, because the photocell measures only the transmitted light. As shown by Beer's law, it is not the transmittancy, but the logarithm of the transmittancy which is directly proportional to the concentration of the absorbing solution. The concentration wave is therefore obtained by taking the logarithm of the value indicated by the photocell as shown in Figure 15 where a typical recorder trace and its corresponding sinusoidal concentration wave are shown.

Prior to each run, the photometers were calibrated and checked. In this process, recorder traces were obtained for the transmittancies through the clear reference solution and the dye solution. To simplify calculations the dye solution was assumed to have a concentration of 1 and the clear reference solution a concentration of 0. A plot of the logarithm of the transmittancy (recorder units of millivolts) as a function of the concentration is shown in Figure 16, indicating the straight line relationship which exists. As previously shown, the straight line can be represented by the formula

$$\log y = \log A + mc \qquad (3a)$$

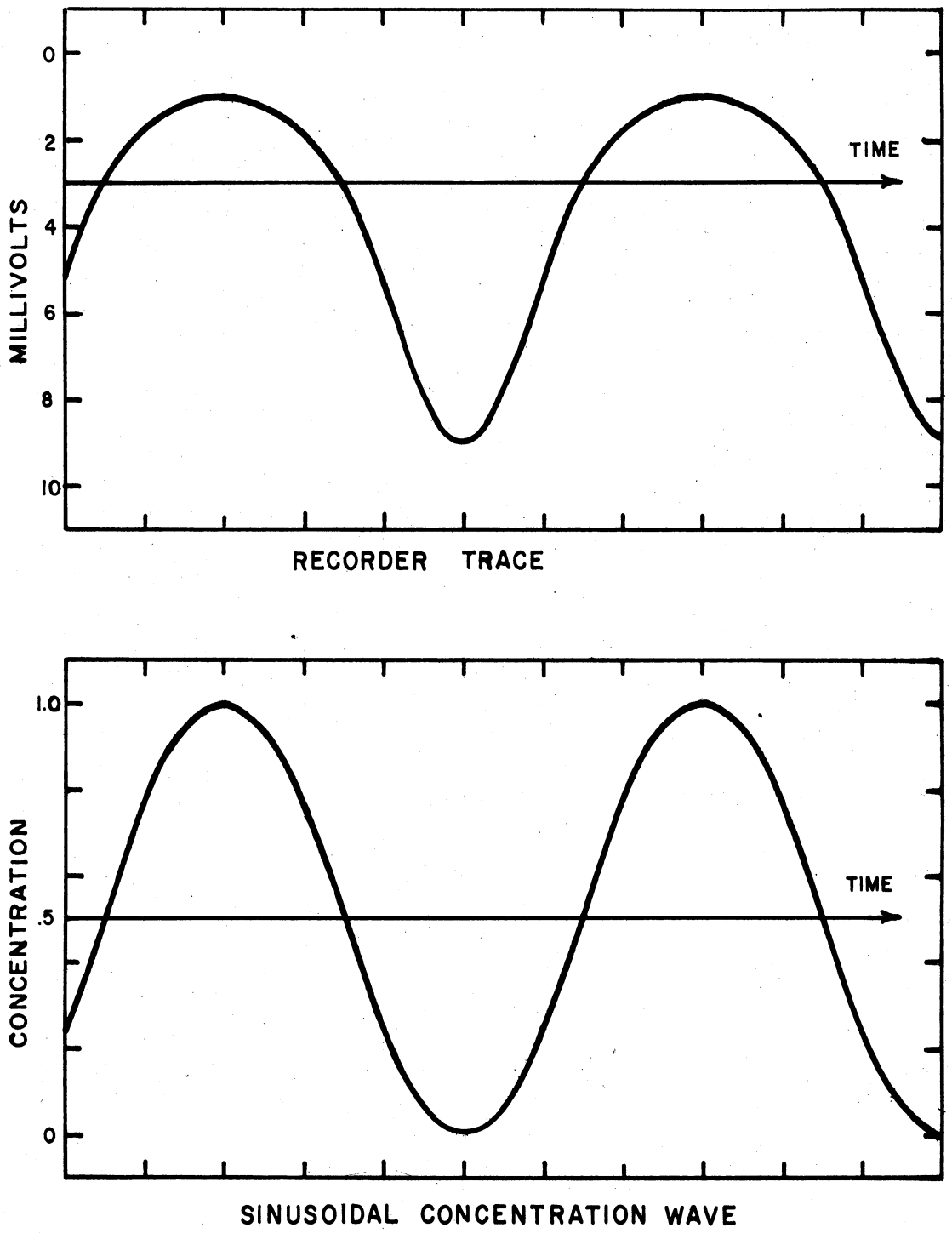

FIGURE 15 - COMPARISON OF RECORDER TRACE AND CORRESPONDING SINUSOIDAL CONCENTRATION WAVE

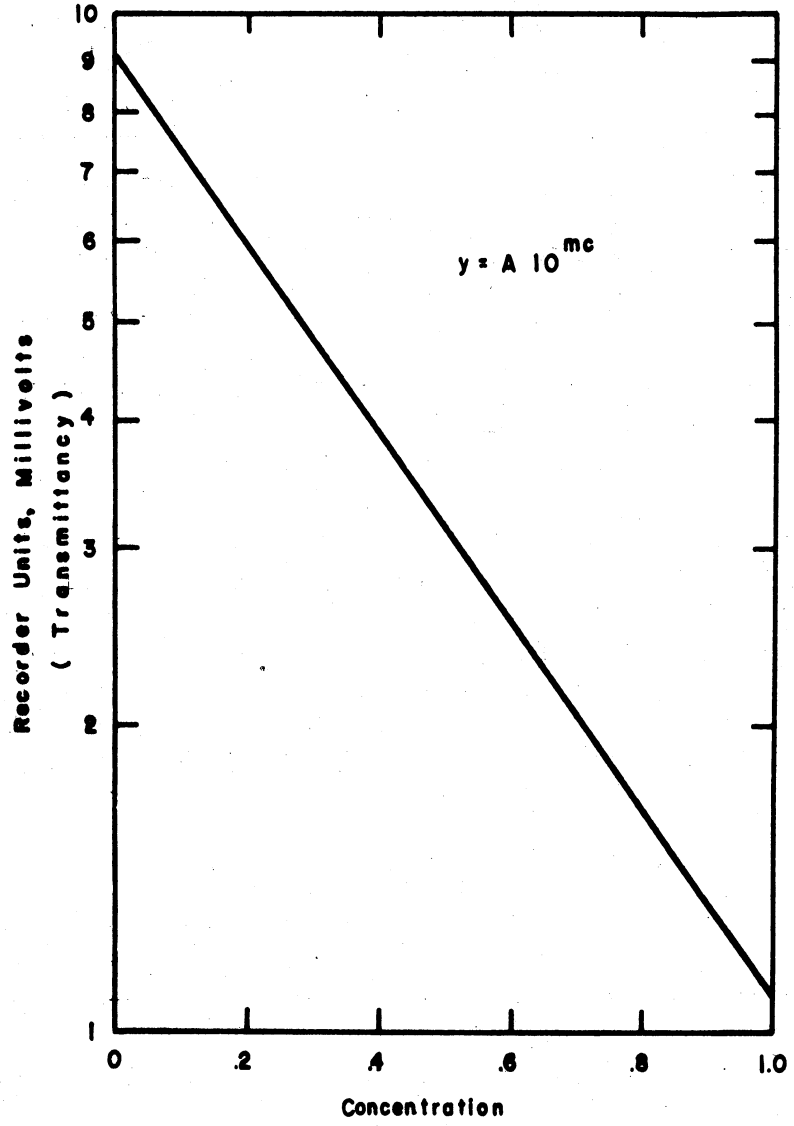

FIGURE 16 - TYPICAL PHOTOMETER CALIBRATION - FREQUENCY RESPONSE EXPERIMENTS

The equation for concentration then has the form:

$$c = \frac{\log A - \log y}{-m}$$

The values of the constants, A and m, were obtained from the calibration data for each frequency response run.

The minimum and maximum readings for ten consecutive inlet sinusoidal waves and their corresponding outlet waves were averaged and the concentrations determined according to the above formula. The minimum and maximum concentrations of the inlet and outlet waves are reported in columns 13, 14 and 16, 17, respectively, of Table III. From these concentrations the amplitudes (columns 15 and 18), and hence the amplitude ratio, A_i/A_e (column 20) into either equation (12a) or (13a) leads to the calculation of the axial diffusivity, D_L, as reported in column 23.

Non-Sinusoidal Data. For non-sinusoidal input waves the experimental inlet composition wave must be converted into a form of the Fourier series. A numerical procedure known as the 12-ordinate scheme of harmonic analysis, discussed in Wylie[41], was used to determine the coefficients in the Fourier series. This numerical procedure is equivalent to the graphical method of approximating the periodic concentration wave by assuming a series of harmonics, whose sum approaches that of the given periodic function. For the numerical harmonic analysis the values of the concentration wave at intervals of one-twelfth of a period were obtained by averaging a series of ten periodic inlet waves. From these concentration values, c_o, c_1, . . ., c_{12}, the values of the Fourier coefficients a_n and b_n are obtained by a series of successive

condensations as shown in an example presented in tabular form in the sample calculations in Appendix II-B. The Fourier series for the inlet wave resulting from the numerical analysis has the form:

$$c(0,t) = \frac{a_o}{2} + a_1 \cos \omega t + b_1 \sin \omega t + \ldots + a_5 \cos 5\omega t + b_5 \sin 5\omega t \tag{18}$$

The corresponding series for the outlet wave must be

$$c(z,t) = \frac{a_o}{2} + a_1 e^{-B} \cos \delta + b_1 e^{-B} \sin \delta + \ldots + a_n e^{-n^2 B} \cos n\delta + b_n e^{-n^2 B} \sin n\delta + \ldots + a_5 e^{-25B} \cos 5\delta + b_5 e^{-25B} \sin 5\delta \tag{19}$$

where

$$\delta = \omega t - \varphi \tag{19a}$$

The equations for B, approximated by the methods previously presented for sinusoidal waves, are:

$$B \cong \frac{z\omega^2 D_L}{u^3} \tag{12a}$$

or

$$B \cong \frac{z\omega^2 D_L}{u^3} - \frac{5z\omega^4 D_L^3}{u^7} \tag{13a}$$

The maximum concentration, $c(z,t)_{max}$, and the corresponding angle, δ, were averaged for ten outlet waves. Substitution of these values, $c(z,t)_{max}$ and δ, and the coefficients a_n and b_n, determined from the harmonic analysis of the inlet wave, into equation 19, results, after a trial and error procedure in a value of B based upon the maximum concentration of the outlet wave. The third and higher terms of the series represented by equation 19 were small, and $e^{-n^2 B}$ approached 0 rapidly, thus simplifying

the calculation of B. This value of B for the peak concentration was then used to compute the entire outlet wave from equation (19). Figure 17 presents the concentration profiles for a typical non-sinusoidal run; the lower portion compares a wave, calculated as described above, with the experimental outlet wave. The comparison indicates that the evaluation of B from equation (19), by substituting the value of the peak and angle of the outlet concentration wave, was valid.

The longitudinal diffusivity was then determined from equation (12a) or (13a), by substituting the value of B, the frequency of the periodic wave, the interstitial flow rate and the column height. Values of axial diffusivity obtained from fifteen experimental runs by this more detailed, non-sinusoidal method are presented in Table III, column 25. These values had an average deviation of approximately 5 percent from values of axial diffusivity obtained by assuming the non-sinusoidal concentration waves to be sinusoidal and comparing the inlet and outlet amplitudes.

STEP FUNCTION EXPERIMENT

Axial mixing of liquids flowing through fixed beds can also be evaluated from the shape of an outlet concentration profile resulting from a step function change in concentration at the inlet. The step function can be obtained experimentally by flowing at a given rate a clear solution and a dye solution successively through a fixed bed of given height.

Mathematical Representation

As before, no radial concentration gradients exist, and effective diffusivity and velocity are independent of position, hence the original diffusion-convection equation reduces to:

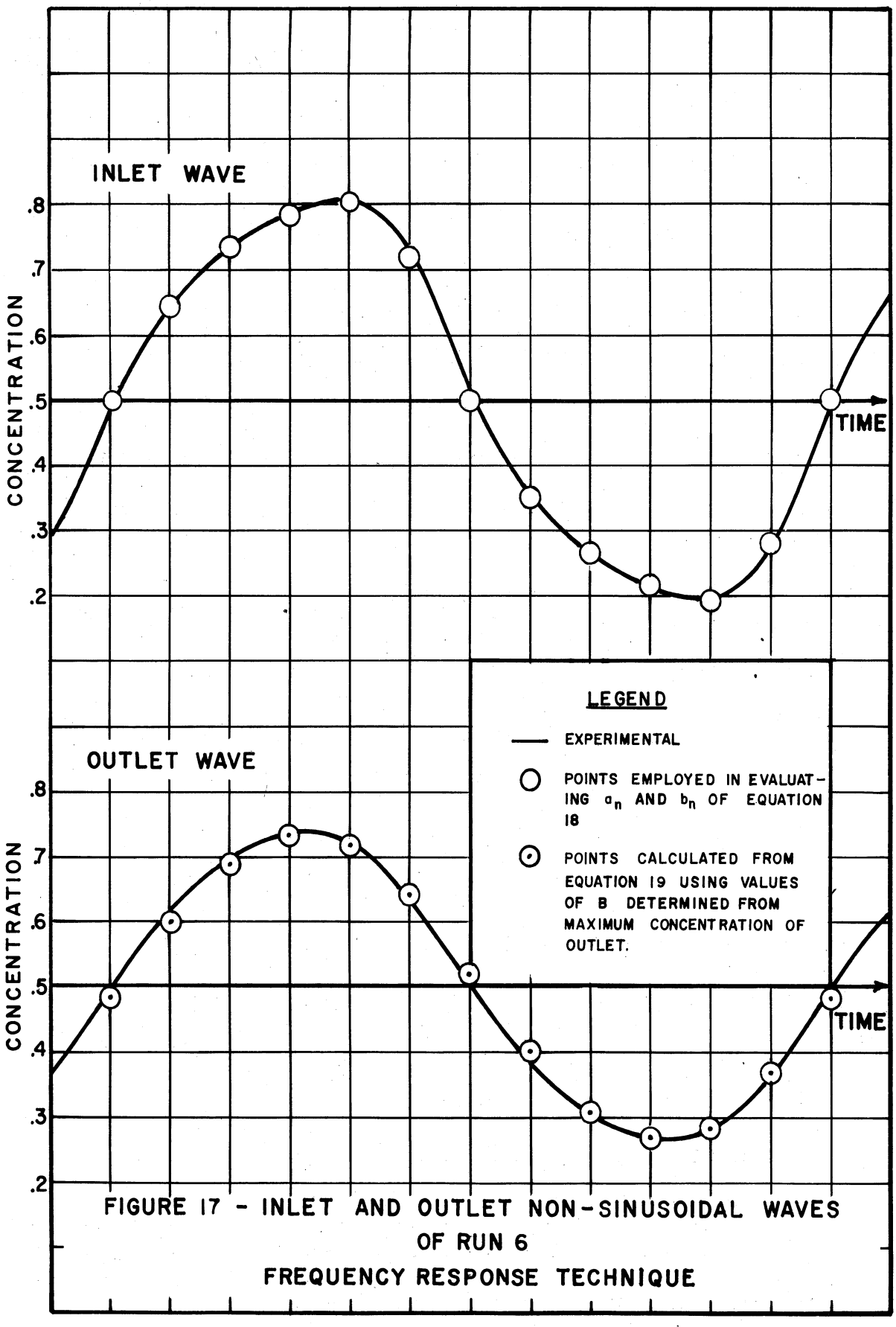

FIGURE 17 - INLET AND OUTLET NON-SINUSOIDAL WAVES OF RUN 6
FREQUENCY RESPONSE TECHNIQUE

$$D_L \frac{\partial^2 c}{\partial z^2} - u \frac{\partial c}{\partial z} = \frac{\partial c}{\partial t} \qquad (10)$$

The sudden change in composition of the feed stream can be represented by boundary conditions:

$c(z,t)$

$$\left.\begin{aligned} c(z,0) &= 1 \qquad z > 0 \\ c(z,0) &= 0 \qquad z < 0 \end{aligned}\right\} \text{ Step function} \qquad (20a)$$

$$c(0,t) = 0 \qquad t < 0 \qquad (20b)$$

c bounded

which then lead to the solution:

$$\frac{c}{c_o} = \frac{1}{2}\left\{ \operatorname{erfc}\left(\frac{R-1}{2\sqrt{RS}}\right) - e^{\frac{1}{S}} \operatorname{erfc}\left(\frac{R+1}{2\sqrt{RS}}\right)\right\} \qquad (21)$$

where

$$R = \frac{ut}{z}, \qquad S = \frac{D_L}{zu} \qquad (21a), (21b)$$

Details of the solution, as well as the mathematics concerning several following statements, are found in Appendix II-C. Lapidus and Amundson[25] employed this solution in their discussion of adsorption in packed beds combined with longitudinal diffusion. Danckwerts[11], having chosen different boundary conditions, arrived at similar solutions.

Experimental Results

The longitudinal diffusivity can be evaluated from the shape of the outlet concentration profile resulting from a step function input. Any value of concentration and time on the outlet concentration profile when substituted in equation (21) gives a value for longitudinal diffusivity. In order to avoid the problem of selecting a

particular point, or averaging the results of many points, it is convenient to use the slope of the concentration profile at R = 1 as shown in Figure 18 to evaluate the axial mixing. Differentiating equation (21) with respect to R, and setting R = 1, results in the equation for the slope of the concentration profile at R = 1:

$$\left(\frac{dc}{dR}\right)_{R=1} = \frac{1}{2\sqrt{S}} = \sqrt{\frac{zu}{4D_L}} \qquad (22)$$

The value of D_L can then be calculated by substituting the slope of the outlet concentration profile, the interstitial velocity and the

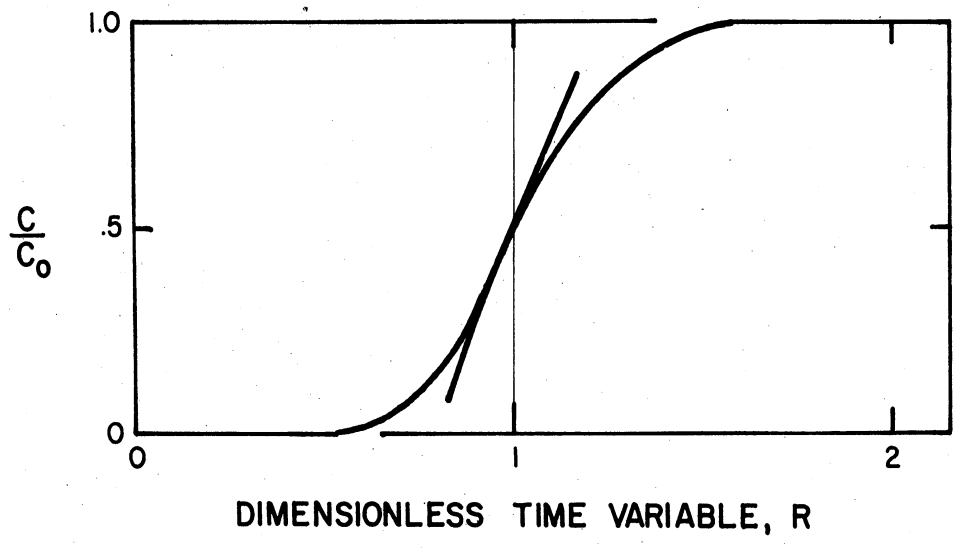

FIGURE 18 - STEP FUNCTION EXPERIMENT - OUTLET CONCENTRATION PROFILE

column length. Danckwerts[11] employed this procedure in determining the longitudinal diffusivity in water flowing through packed Raschig rings.

During the experimental runs it was observed that when the tracer solution followed the clear solution through the packed bed, some form of holdup of the tracer occurred. This phenomenon apparently results from the adsorption of the tracer substance on the surface of the particles. The adsorption hypothesis is substantiated by the fact that the holdup became more apparent in beds operated at low flow rates. The mathematics of longitudinal diffusion combined with adsorption on fluids flowing through packed beds have been discussed by Lapidus and Amundson[25]. The diffusion-convection equation can be modified to include the adsorption effect as follows:

$$D_L \frac{\partial^2 c}{\partial z^2} - u \frac{\partial c}{\partial z} = \frac{\partial c}{\partial t} + \frac{1}{\epsilon} \frac{\partial \eta}{\partial t} \qquad (23)$$

where

η = amount of tracer adsorbed on particle surface

ϵ = fractional void volume in the bed

In addition to the boundary conditions previously assumed (equations (20a), (20b)), it is necessary to make an assumption concerning the mechanism of adsorption. The simplest mechanism assumes that equilibrium is established at each point in the bed according to the relationship:

$$\eta = k_1 c + k_2 \qquad (24)$$

The solution to the problem with the above boundary conditions is:

$$\frac{c}{c_o} = \frac{1}{2}\left\{ \operatorname{erfc}\left(\frac{R-\gamma}{\sqrt{4R\gamma S}}\right) - e^{\frac{1}{S}} \operatorname{erfc}\left(\frac{R+\gamma}{\sqrt{4R\gamma S}}\right)\right\} \quad (25)$$

where

$$\gamma = 1 + \frac{k_1}{\epsilon} \quad (25a)$$

Plots of the above equation in which the two unknowns, S and γ, are obtained by trial and error, compared fairly well with experimental concentration profiles. As shown in Figure 19, values of γ were found

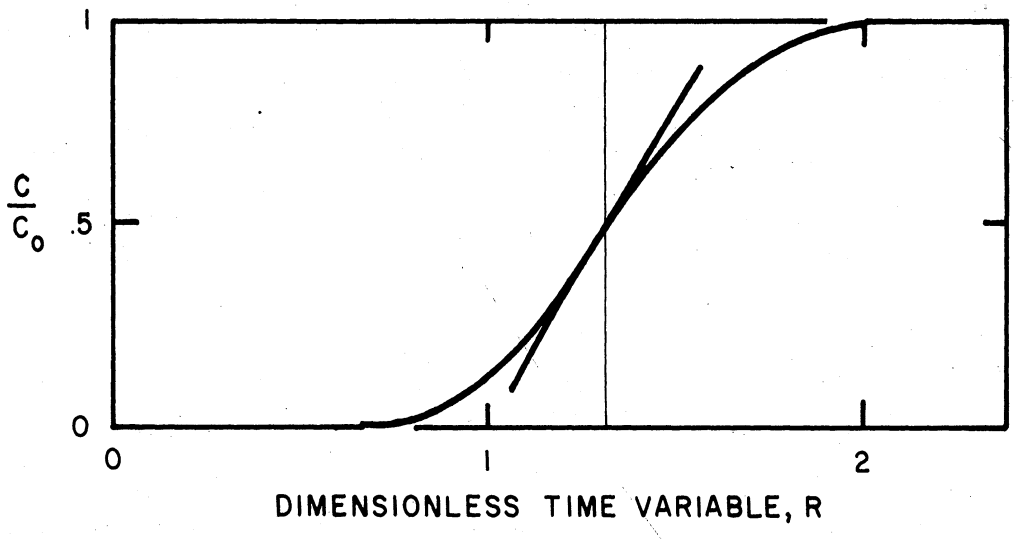

FIGURE 19 - STEP FUNCTION EXPERIMENT - OUTLET CONCENTRATION PROFILE RESULTING FROM ADSORPTION OF TRACER

equal to the value of R where c/c_o equals 0.5. Therefore, as before, D_L can be most conveniently calculated by determining the slope of the concentration profile at the concentration midpoint, which is where $R = \gamma$. Hence by differentiating equation (25) with respect to R, and setting $R = \gamma$, there results:

$$\left(\frac{\partial c}{\partial R}\right)_{R=\gamma} = \frac{1}{2R\sqrt{\pi S}} = \sqrt{\frac{zu}{4\pi R^2 D_L}} \qquad (26)$$

from which D_L can be calculated.

Several preliminary experimental runs employing the step function principle were made to obtain data in the low flow range. Two primary difficulties arose during the preliminary experiments. First, experimental difficulties were encountered in obtaining a true step function concentration change in a flowing liquid at the inlet of the column. The calculation of longitudinal diffusivity from an experimental exit concentration profile by means of equation (25) is only possible when a sharp, uniform change in concentration is produced at the inlet to the column. No experimental method was found to produce a completely satisfactory step function at the inlet to the test column. The second difficulty arose in the calculation of the diffusivity coefficient from the experimental data. The value of D_L determined through equation (26) is very sensitive to errors in the value of the slope of the concentration profile. The slope at the midpoint was difficult to determine accurately from the experimental data, hence the diffusivity coefficients obtained were very unreliable. Data obtained and calculated by this method failed to give reproducible results. The experimental difficulty and the lack of reproducibility of the

preliminary step function experiments led to the consideration and use of another approach.

PULSE FUNCTION EXPERIMENT

Several investigators have proposed the pulse function method to investigate the characteristics of mixing in reactors or packed beds. Danckwerts[11] presented the mathematics of introducing a pulse into a reactor for the detection of mixing characteristics. Yagi and Miyauchi[42] employed the pulse wave method in their study of mixing in continuous flow reactors.

Mathematical Representation

Mathematically, this method is an extension of the step function approach. The inlet boundary conditions are obtained by injecting into the flowing stream a concentrated tracer solution for a short period of time; i.e., in the form of a unit pulse. The concentration profile for this unit pulse is determined at the outlet of the test section. Danckwerts shows that the exit distribution function, which is the equation for the exit concentration profile, for a unit pulse is the derivative of the distribution function for a step function. A physical interpretation of the pulse function derivation as well as details of the differentiation, are shown in Appendix I-D. The formula for the concentration profile for the unit pulse, resulting from the differentiation of the step function distribution function, equation (25), is:

$$\frac{Vc}{Q} = \frac{1}{4\sqrt{\pi}} \left\{ \frac{R+\gamma}{\sqrt{R^3 S\gamma}} \, e^{-\left(\frac{R-\gamma}{\sqrt{4RS\gamma}}\right)^2} - \frac{R-\gamma}{\sqrt{R^3 S\gamma}} \, e^{\left[\frac{1}{S} - \left(\frac{R+\gamma}{\sqrt{4RS\gamma}}\right)^2\right]} \right\} \quad (27)$$

where Q is the quantity of tracer injected into the feed stream at time 0 and V is the void volume of the bed. The values of S and γ can be determined so that a calculated distribution curve will approximately duplicate an experimental concentration profile.

It can also be shown (Appendix I-D) that the area under the exit concentration curve of the unit pulse function is equal to unity; hence

$$\int_0^\infty \left(\frac{Vc}{Q}\right) dR = 1 \qquad (28)$$

This fact becomes of value in the evaluation of the axial diffusivity from the experimental data.

Evaluation of Data

During this research, the pulse function method was employed for runs made at low liquid flow rates, and also for runs using non-spherical particles. As before, the modified Reynolds number and modified Peclet number were obtained from each set of experimental data. Sample calculations for a typical pulse function run are presented in Appendix II-C.

The important steps and the results of the pulse function calculations are summarized in Table IV. The superficial velocity, v_o, and the interstitial velocity, u, calculated from the corrected measured flow rate, the column diameter and the measured porosity are presented in columns 7 and 8, respectively. Column 9 contains the time required for the liquid to pass through the column (residence time, R, equals one) as calculated from the column length and the interstitial velocity. Columns 11 and 12 present the densities and viscosities of the solutions as obtained from Figure 32, Appendix III-C.

The longitudinal diffusivity for each run was determined from the exit pulse distribution function recorded on the chart paper. After several trial and error calculations on a series of runs in which S and γ were approximated in order to duplicate an experimental pulse wave, it was found that under the experimental conditions used, the peak of the concentration profile occurred at $R = \gamma$. The value of Vc/Q at the peak, determined by setting $\gamma = R$ in equation (27), is:

$$\left(\frac{Vc}{Q}\right)_{R=\gamma} = \frac{1}{2R\sqrt{\pi S}} = \sqrt{\frac{zu}{4\pi R^2 D_L}} \qquad (29)$$

from which D_L can be calculated. The feasibility of using the maximum point on the pulse function to calculate the value of D_L is shown in Figure 20, in which a typical experimental pulse profile duplicates fairly well its calculated counterpart. The experimental concentration profile was obtained from the recorder traces by converting the photometer readings in millivolts to concentration units by means of the formula

$$c = \frac{\log A - \log y}{-m} = \frac{.95424 - \log y}{148.92} \text{ gm/li} \qquad (3b)$$

where A and m are constants of the original photometer calibration, and y is the recorder reading in millivolts. Values of concentration were determined at regular increments of time. The time abscissa was converted to values of residence times, R, which is a dimensionless ratio representative of time. The area under the concentration curve was obtained by numerical integration. Because the ordinate was concentration and not Vc/Q, the value of the integrated area was not one as indicated by equation (28). However, by multiplying each of the

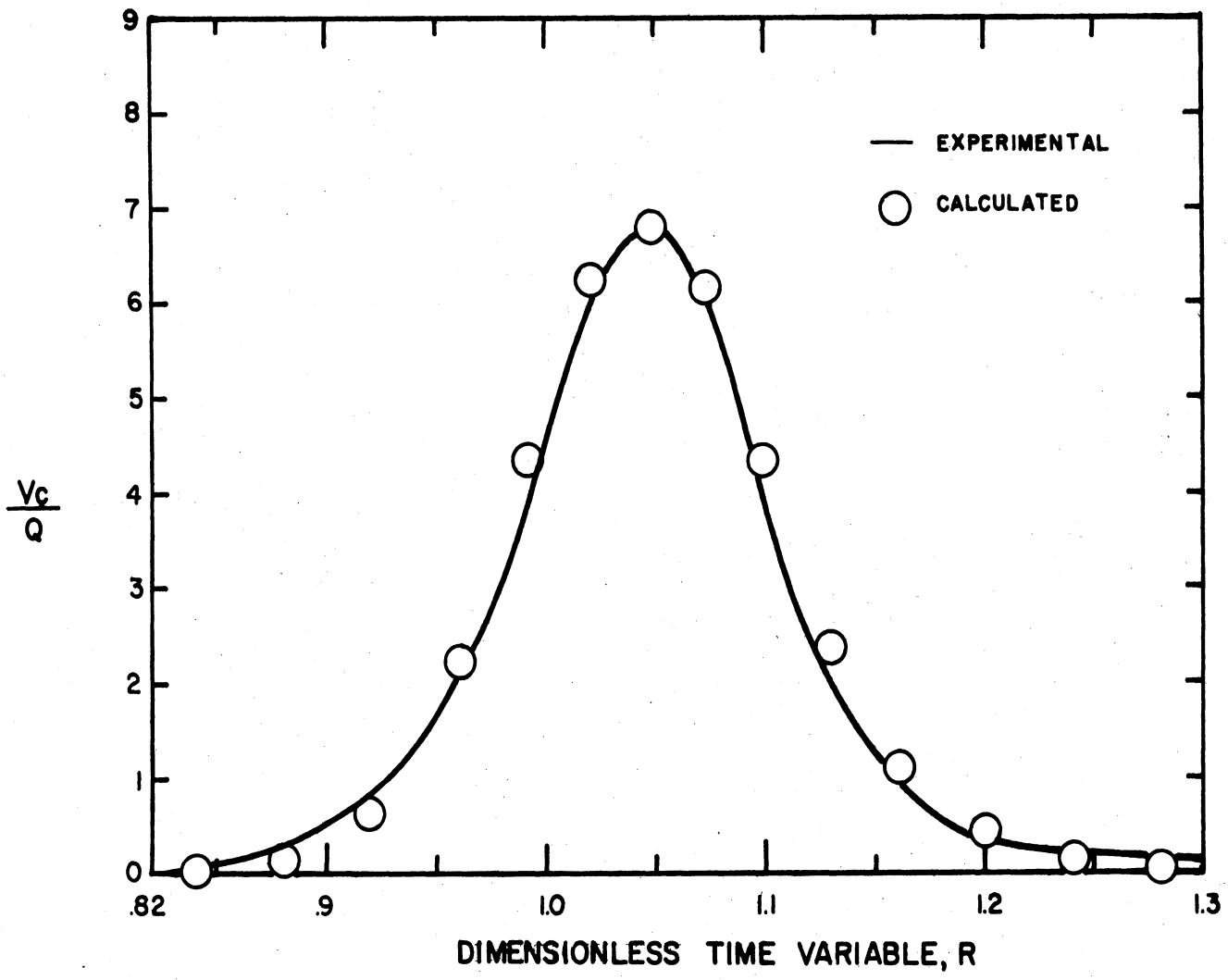

FIGURE 20 - PULSE FUNCTION EXPERIMENT - CONCENTRATION PROFILE - RUN P6

concentration points by the reciprocal of the area calculated, a distribution function for a pulse wave with Vc/Q as ordinate and R as abscissa is obtained. The integrated area of this curve then equals unity. The values, averaged from three pulse waves per run, of the maximum concentration of the pulse wave, of the area under the concentration profile of the pulse wave and of the time required for the pulse to pass through the column are presented in Table IV, columns 13, 14, and 15, respectively. The value of the maximum concentration of the pulse, in terms of the dimensionless ratio, Vc/Q, is calculated by dividing the maximum pulse concentration (column 13) by the area under the concentration profile of the pulse (column 14). These values of Vc/Q and the values of the largest experimental percentage deviation from the reported Vc/Q, are presented in columns 16 and 17, respectively. The values of the dimensionless time ratio, R, and the largest experimental percentage deviation from the reported R, are reported in columns 18 and 19, respectively. The values of R were calculated by dividing the time required for the pulse to pass through the bed (column 15) by the time required for the liquid to pass through the column (column 9). The value of R is usually greater, but never less, than one because of the adsorption of tracer on the particle surface. Column 20 contains the values of S calculated from equation (28).

$$S = \frac{1}{4\pi R^2 \left(\frac{Vc}{Q}\right)^2_{R=\gamma}} = \frac{D_L}{zu} \qquad (29a)$$

The axial diffusivity, presented in column 21, was then calculated from the values of S, column length and interstitial velocity. The

calculations are completed by the evaluation of Reynolds number (column 22) and axial Peclet number (column 23).

RESULTS AND DISCUSSION

The variables affecting axial mixing which were investigated were liquid velocity, particle size, particle shape and liquid viscosity. Several variables resulting from the experimental technique were also investigated; these included the effect of frequency and amplitude of the periodic function in the frequency response experiments, the length of the packed column, and the type of dye solution used as tracer. The column diameter was held constant in all experiments.

LIQUID VELOCITY

A series of experiments were made for each of four particle sizes in which the interstitial velocity was varied from 0.0008 ft/sec to 0.3 ft/sec. A plot of the logarithm of axial diffusivity, D_L, as a function of the logarithm of interstitial velocity, u, with particle size, d_p, as parameter is presented in Figure 21. Data from the two experimental techniques, the frequency response method, covering the high flow range from 0.01 ft/sec to 0.3 ft/sec, and the pulse function method, covering the low flow rate range from 0.0008 ft/sec to 0.02 ft/sec, are presented in the figure. The data from both techniques for a single particle size result in a straight line relationship between the logarithm of D_L and the logarithm of u. The excellent correlation of data obtained by both methods indicated the axial diffusion measurements were quite accurate and not dependent upon the experimental technique employed.

Since the plot of the logarithm of D_L versus logarithm of u approximates a straight line for a particular particle diameter, the relationship

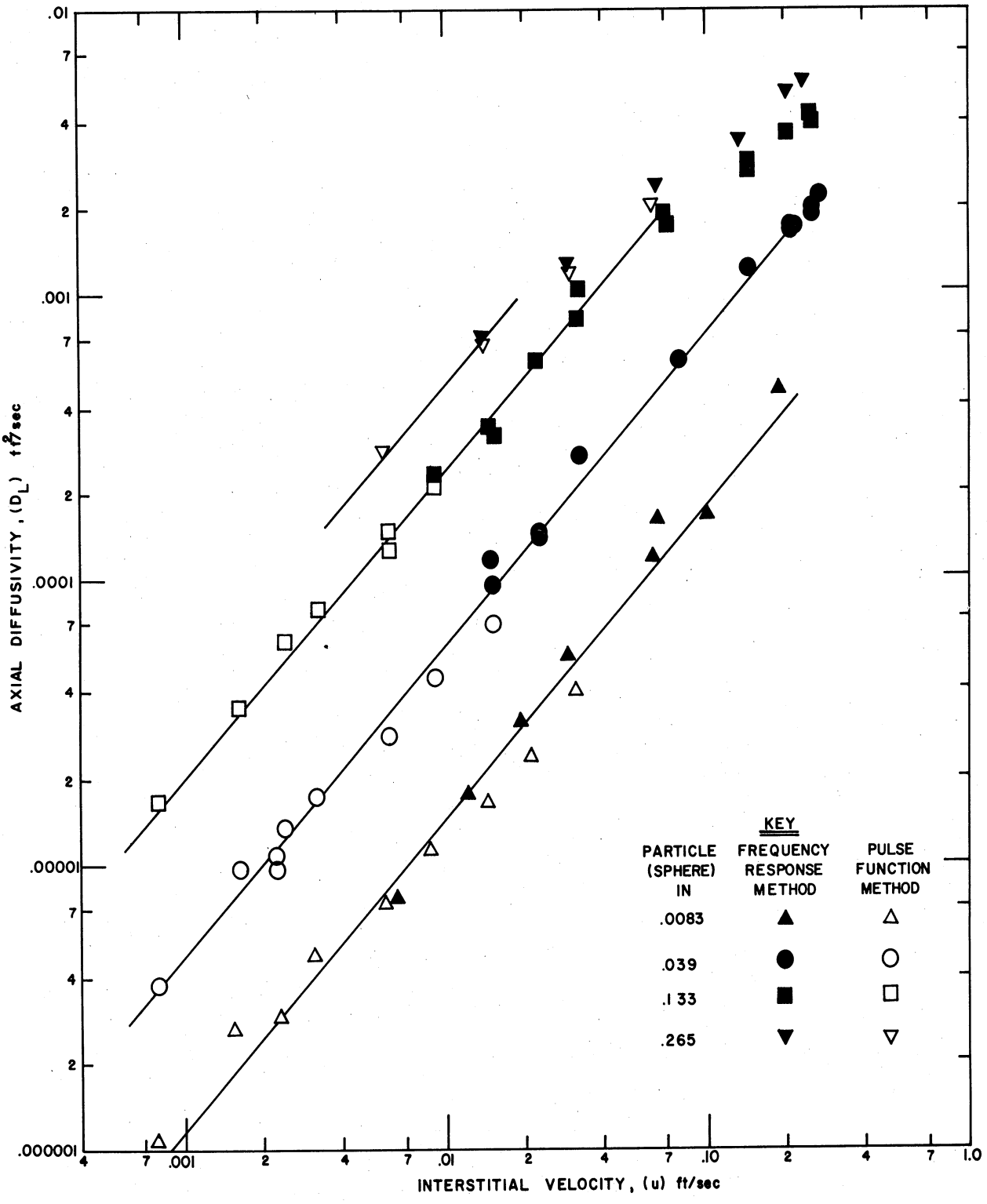

FIG. 21 AXIAL DIFFUSIVITY VS INTERSTITIAL VELOCITY WITH PARAMETERS OF PARTICLE DIAMETER

between axial diffusivity and interstitial velocity may be represented by the equation

$$\log D_L = \log C_1 + b \log u \qquad (30)$$

where $\log C_1$ is the intercept and b is the slope of the straight line. Equation (30) may also be written in the form

$$D_L = C_1 u^b \qquad (30a)$$

The values of the coefficients, $\log C_1$ and b, are determined for the

TABLE V. COMPARISON OF REGRESSION COEFFICIENTS AND THEIR STANDARD DEVIATIONS FOR RELATIONSHIP $D_L = C_1 u^b$

Particle Diameter (inches)	Separate Least Squares Slope b	Simultaneous Least Squares				
		Slope		Intercept		Constant
		b	Standard Deviation	$\log_{10} C_1$	Standard Deviation	C_1
.0083	1.0875	1.0867	±0.0165	-2.6575	±0.0312	0.002200
.039	1.1053	1.0867	±0.0165	-2.0452	±0.0299	0.009011
.133	1.0521	1.0867	±0.0165	-1.4388	±0.0334	0.03641
.265	1.0610	1.0867	±0.0165	-1.1356	±0.0342	0.07318

best straight line through a set of experimental points by the method of least squares. The family of straight lines in Figure 21 all have equal slopes. The separate slopes of each set of data, obtained by least squares, and the common slope, determined by a simultaneous least squares method[14,34], are presented in Table V. Statistical tests indi-

cate that the differences between the individual slopes and the common slope might reasonably be caused by sampling variation; i.e., the common slope does not differ significantly from the individual slopes. The value of the common slope is 1.0867 and its standard deviation is ± 0.0165. Statistical tests also indicated that a common theoretical slope of 1.000, which would result if the axial diffusivity were directly proportional to the interstitial velocity, differs significantly from the slopes obtained from the experimental data.

A fourth series of runs with 0.265 inch spherical particles was made in which the interstitial velocity ranged from 0.006 ft/sec to 0.23 ft/sec. As shown in Figure 21, the straight line relationship does not exist for this particle size for interstitial velocities greater than 0.02 ft/sec. In this range the axial diffusivity does not increase as rapidly with the interstitial velocity as in the lower range. This phenomenon is also observed in the 0.133 inch spherical particles for interstitial velocity greater than 0.06 ft/sec.

PARTICLE SIZE

The axial diffusivity increases as the particle diameter becomes larger, as shown in Figure 21. The relationship between axial diffusivity and the particle diameter can be determined by evaluating the relationship between the constants, C_1, calculated for each particle size, and the particle diameter. A plot of the logarithm of C_1 as a function of the logarithm of d_p approximates a straight line as shown in Figure 22. This relationship can again be represented by the straight line formula

$$\log C_1 = \log C + a \log d_p \qquad (31)$$

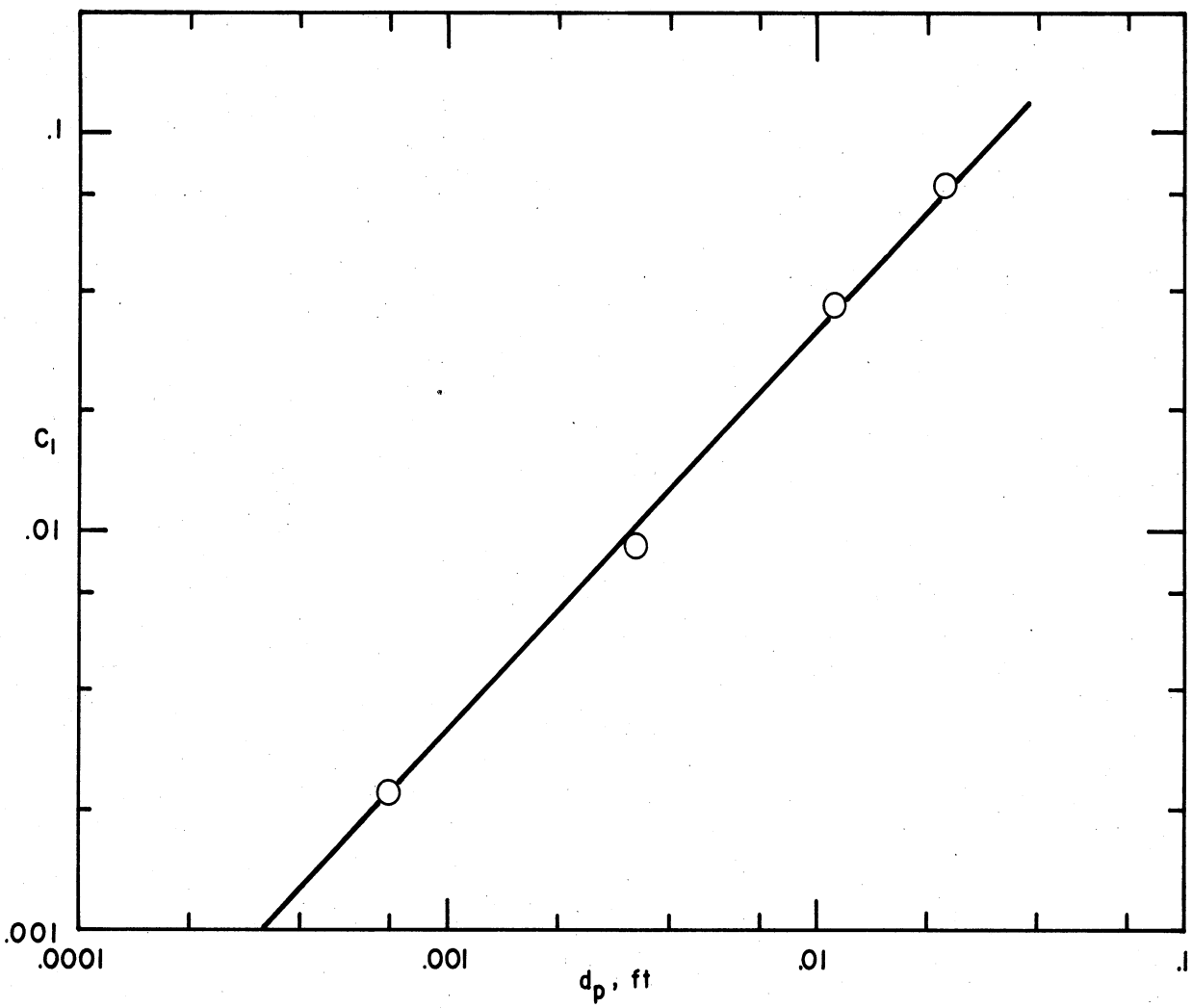

FIGURE 22 - DEPENDENCY OF AXIAL DIFFUSIVITY ON PARTICLE DIAMETER - PLOT OF $C_l = Cd_p^a$ WHERE $D_L = Cd_p^a u^b = C_l u^b$

which may also be written

$$C_1 = C\, d_p^{\,a} \tag{31a}$$

The values of the coefficients, log C and a, are determined by the method of least squares. The slope, a, of the straight line has the value of one; therefore, the constant C_1 is directly proportional to particle diameter, d_p. The proportionality constant C has the value 3.245 and its standard deviation is $\pm$ 0.121.

A combination of equations (30a) and (31a), whose forms were obtained from experimental data, describes the axial diffusivity as a function of particle diameter and interstitial velocity:

$$D_L = C\, d_p\, u^b \tag{32}$$

The coefficients evaluated from the experimental data are

$$C = 3.25 \pm 0.12$$

$$b = 1.09 \pm 0.02$$

where

$$d_p\, u < 5.5 \times 10^{-4}\ \text{ft}^2/\text{sec}.$$

As indicated, this relationship is valid only in the region where the product of particle diameter and linear velocity is less than 5.5×10^{-4} ft^2/sec, since the straight line approximations of the experimental data exist only in this region.

The ratios of particle diameter to tube diameter, d_p/d_t, covered during the experiments are presented in Table VI following. The investigation of Schwartz and Smith[35] indicates that velocity

variations exist in gaseous flow through packed beds for $d_p/d_t > 0.04$. Hence the use of 6 mm glass spheres, or particles of equivalent diameter, in a 2 inch diameter column probably leads to velocity variations due to the increase in voids near the wall. However, the agreement of the experimental data as shown in Figures 21 and 22 indicate

TABLE VI. RATIOS OF PARTICLE DIAMETER TO TUBE DIAMETER, d_p/d_t

Particle Diameter		Tube Diameter Inches	d_p/d_t
Nominal Size	Inches		
60/80 mesh spheres	.0083	2.0	.0042
1 mm spheres	.039	2.0	.020
3 mm spheres	.133	2.0	.067
6 mm spheres	.265	2.0	.13

no detrimental effect in the evaluation of axial diffusivity due to the increase in the ratio, d_p/d_t.

PARTICLE SHAPE

Various types of packing were investigated to determine the effect of particle shape on the mixing of liquids flowing through a packed bed. The smallest available Raschig rings, Berl saddles, and Intalox saddles, each having a nominal size of 1/4 inch, were used. To obtain a comparison with spherical particles having an approximate equivalent diameter, 6 mm glass beads were also investigated. The properties of the various packings are presented in Table I. The data for the above packings are plotted in Figure 23 which shows the relationship between axial diffusivity and interstitial velocity. Both

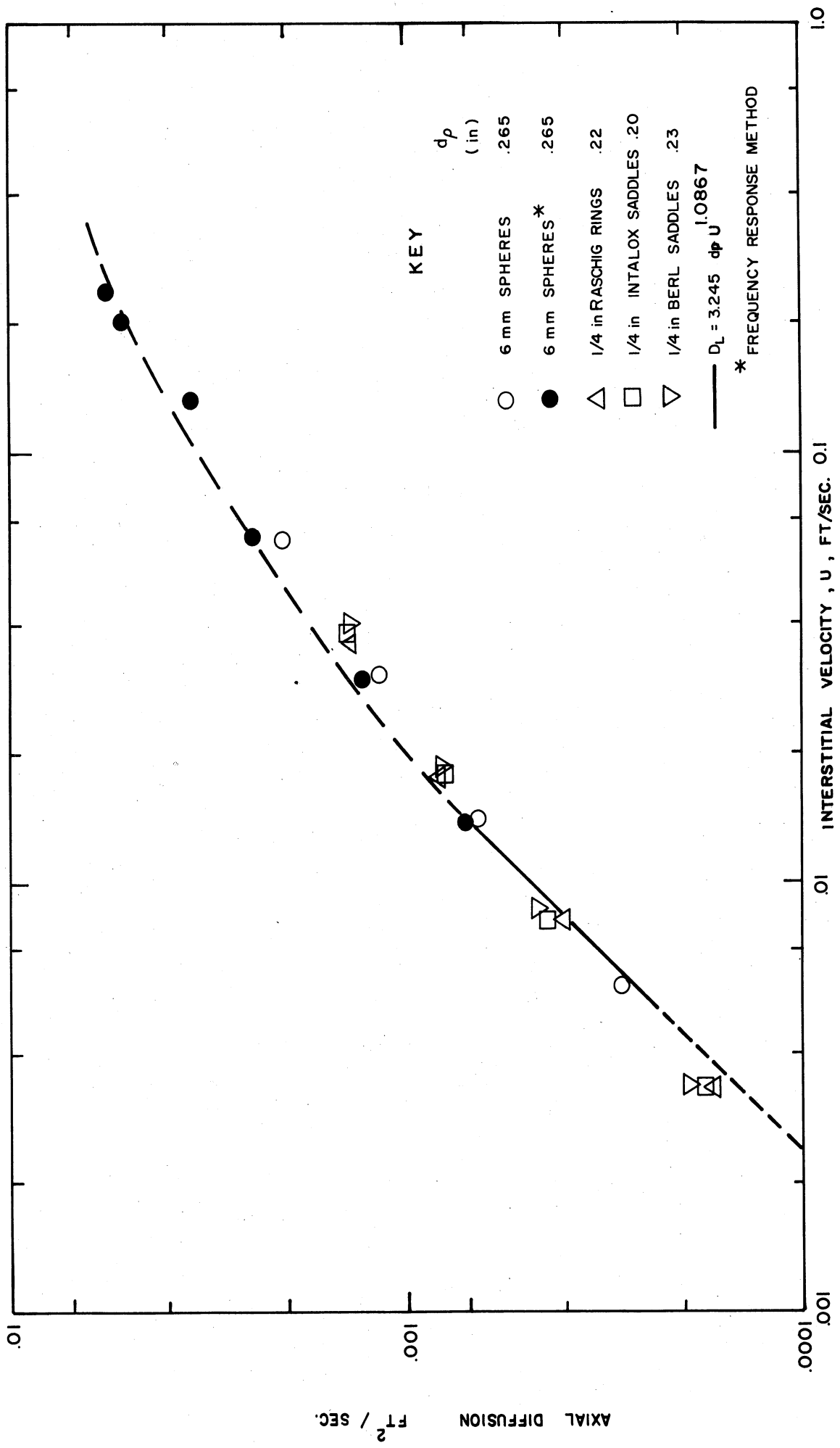

FIGURE 23 - EFFECT OF PARTICLE SHAPE

experimental procedures, the frequency response method and the pulse function method, were used in obtaining data for the 6 mm glass beads to establish the reproducibility of the techniques for the large d_p/d_t ratio. The axial diffusivities for the other packings were obtained by pulse function experiments. The data for all packings studied, having an equivalent diameter in the range 0.20 - 0.26 inches, fall approximately

TABLE VII. EFFECT OF VISCOSITY ON AXIAL DIFFUSION

Run	Solution % Propylene Glycol	Viscosity μ cp	Velocity u ft/sec	Axial Diffusivity D_L ft^2/sec
41	0	0.95	.00227	.0000104
42	0	0.95	.00227	.0000095
43	50	6.21	.00249	.0000104
44	67	11.73	.00234	.0000110
45	85	26.88	.00225	.0000100

along the same curve indicating that axial mixing is dependent upon the size of the particle and not the shape of the particle in so far as it has been investigated.

LIQUID VISCOSITY

The series of runs made to determine the effect of viscosity are summarized in Table VII. Aqueous solutions containing various percentages of propylene glycol were used to vary the viscosity. During these experiments the particle diameter (.039 inches) and the linear

velocity (approximately 0.0023 ft/sec) were held constant, with the viscosity being the only variable. Figure 24 shows that over the viscosity range covered, 1-26 centipoises, there was limited variation in axial diffusivity.

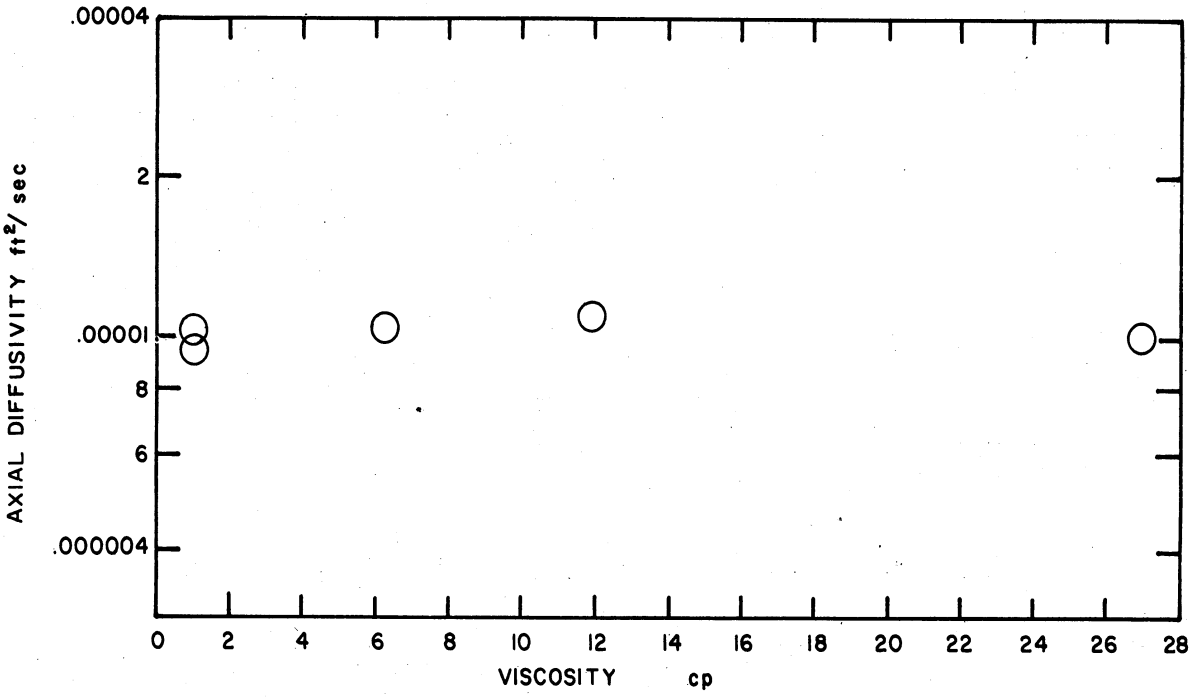

FIGURE 24 - VARIATION OF AXIAL DIFFUSIVITY WITH VISCOSITY AT CONSTANT VELOCITY (u ≅ .0023 ft/sec) AND CONSTANT PARTICLE DIAMETER (d_p = .039 in)

EXPERIMENTAL VARIABLES

Variables of Frequency Response Method

In the frequency response technique, the axial diffusivity was normally calculated from the formula

$$\ln \frac{A_i}{A_e} = \frac{z\omega^2 D_L}{u^3}$$

in which the values $\ln \frac{A_i}{A_e}$, z, ω, and u were obtained experimentally. The axial diffusivity is dependent on the linear velocity, but should not be a function of the amplitude ratio, length of column, or frequency of the periodic composition wave. Hence, a plot of $\ln \frac{A_i}{A_e}$ as a function of $z\omega^2$ should approximate a straight line. Figure 25 shows the relationship between experimental values of $\ln \frac{A_i}{A_e}$ and $z\omega^2$ obtained from runs described in Table VIII in which the linear velocity, u, was held constant. Since the data approximates a straight line, the axial diffusivity is not dependent upon the experimental variables of the frequency response technique. In most cases, individual axial diffusivity coefficients were obtained from a run made at a certain frequency and not from a series of runs at several frequencies.

TABLE VIII. EXPERIMENTAL VARIABLES OF FREQUENCY RESPONSE METHOD

d_p = .039 in.						
Run	Velocity u (ft/sec)	Height z (ft)	Frequency ω (rad/sec)	$\ln \frac{A_i}{A_e}$	$z\omega^2$	Axial Diffusivity D_L (ft^2/sec)
A	.02296	1.50	.1047	.174	.0164	.000141
B	.02296	1.50	.0785	.0989	.00924	.000147
6	.02235	3.01	.0850	.278	.0218	.000147
9	.02238	3.01	.1256	.559	.0474	.000139

A comparison of the diffusivity coefficients determined from the non-sinusoidal input waves with diffusivity coefficients evaluated on the assumption that the input waves were sinusoidal is given in Table IX for a series of runs. The percentage deviation of the assumed

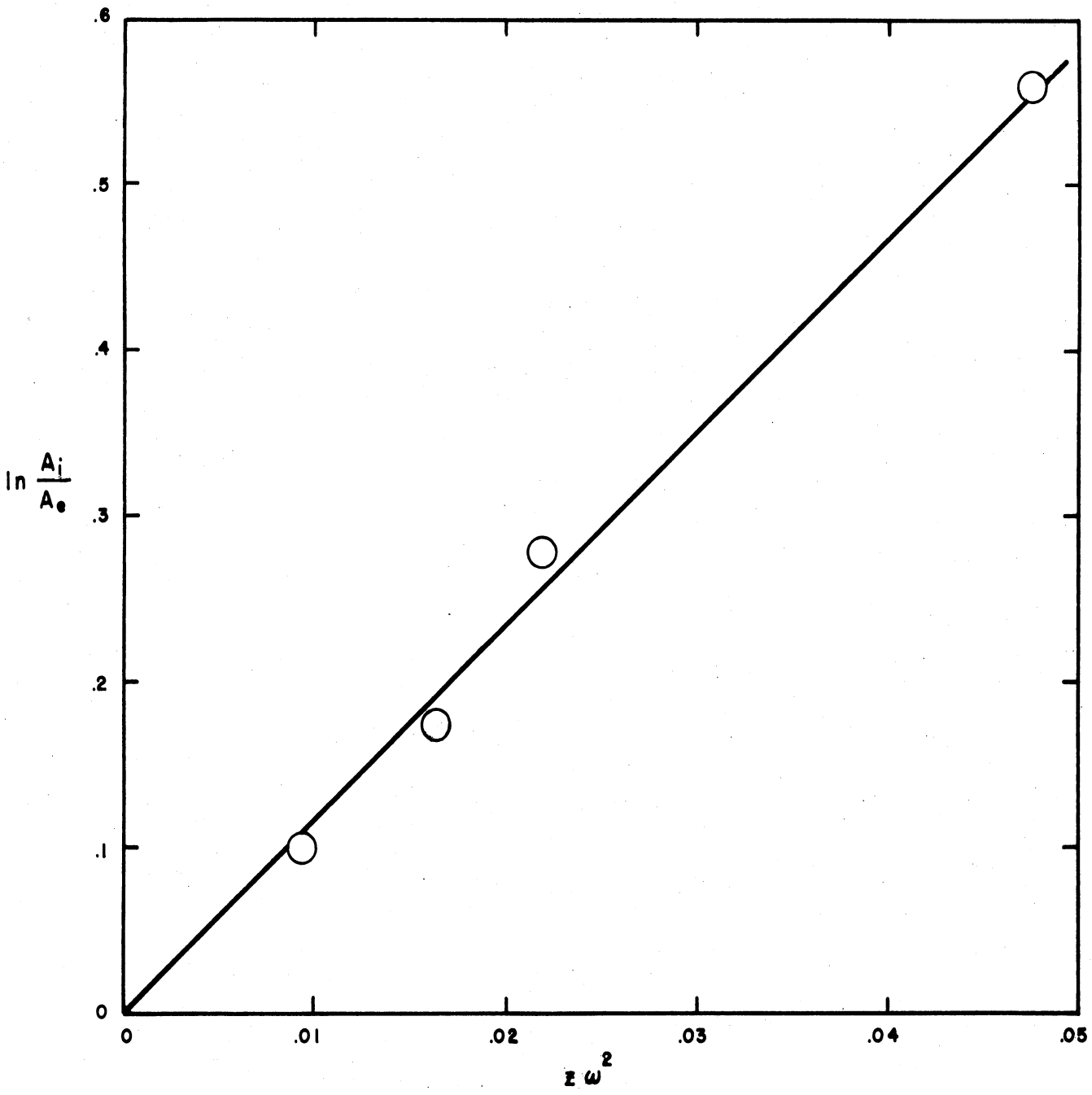

FIGURE 25 - EFFECT OF EXPERIMENTAL VARIABLES OF FREQUENCY RESPONSE METHOD

TABLE IX. COMPARISON NON-SINUSOIDAL CALCULATIONS AND ASSUMED SINUSOIDAL CALCULATIONS OF AXIAL DIFFUSIVITY

Particle diameter: .039 inch				
		Axial Diffusivity		
Run	Velocity u ft/sec	Non-Sinusoidal Calculations ft^2/sec	Assumed Sinusoidal Calculations ft^2/sec	Percent Deviation
7	.0151	.0000950	.000103	+ 8.4
6	.0224	.000147	.000144	- 2.0
9	.0224	.000139	.000132	- 5.0
A	.0230	.000141	.000128	- 9.2
B	.0230	.000147	.000132	-10.2
5	.0326	.000277	.000254	- 8.3
4	.0788	.000591	.000617	+ 4.4
3	.1456	.00122	.00116	- 4.9
2	.210	.00168	.00164	- 2.4
C	.213	.00168	.00169	- 0.6
F	.218	.00175	.00182	+ 4.0
D	.254	.00195	.00192	- 1.5
E	.254	.00201	.00204	+ 1.5
1	.270	.00244	.00233	- 4.5

sinusoidal calculations from the non-sinusoidal calculations is within the experimental error, and indicates that the more complicated non-sinusoidal calculations are not necessary for the evaluation of axial diffusivity.

Effect of Bed Length

Table X summarizes data obtained by the frequency response method and the pulse function method in which the only variable for each set is the bed length. The calculated diffusivity coefficients for both techniques indicate no effect of bed length.

TABLE X. EFFECT OF BED LENGTH

Run	Method	Particle Diameter d_p in.	Column Height z ft.	Velocity u ft/sec	Axial Diffusivity D_L ft^2/sec
6	Frequency Response	.039	3.01	.0224	.000147
A	Frequency Response	.039	1.50	.0230	.000141
P 11	Pulse Function	.133	3.11	.00613	.000149
P 24	Pulse Function	.133	5.05	.00621	.000133

In the frequency response experiments, the amplitude ratios were determined by analyzing the color density of the solution flowing through unpacked sections upstream and downstream to the test section. These unpacked spaces, in which conditions both as to flow and mixing were undoubtedly different from that of the packed bed, could conceivably affect the evaluation of the mixing occurring within the test section. However, the duplicate axial diffusivities obtained for both

the short and long test sections indicated the effect of the unpacked space was negligible. Similar conclusions resulted for the pulse function experiments. Normally, the long columns were used in both methods to evaluate the axial diffusivity.

Effect of Tracer

Table XI shows the results of two experiments designed to determine the effect of the dye used as tracer. The dye normally used, Pontamine Sky Blue 6BX, was compared with a second dye, Pontamine Fast Turquoise 8GLD, which has similar spectral characteristics. The two

TABLE XI. EFFECT OF TRACER

(Pulse Function Experiments)

Run	Tracer	Particle Diameter d_p in.	Column Height z ft.	Velocity u ft/sec	Axial Diffusivity D_L ft^2/sec
41	Pontamine Sky Blue 6BX	.039	3.09	.00227	.0000104
42	Pontamine Fast Turquoise 8GLD	.039	3.09	.00227	.0000095

experiments, in which all conditions were identical except for the tracer used, resulted in similar axial diffusivities indicating the measured coefficients were not dependent upon the tracer.

PECLET NUMBER, REYNOLDS NUMBER CORRELATION

The axial mixing data are correlated in a plot of modified Peclet number as a function of Reynolds number as shown in Figure 26. The ordinate is a modified Peclet number having the form

$$Pe = \frac{d_p u}{D_L}$$

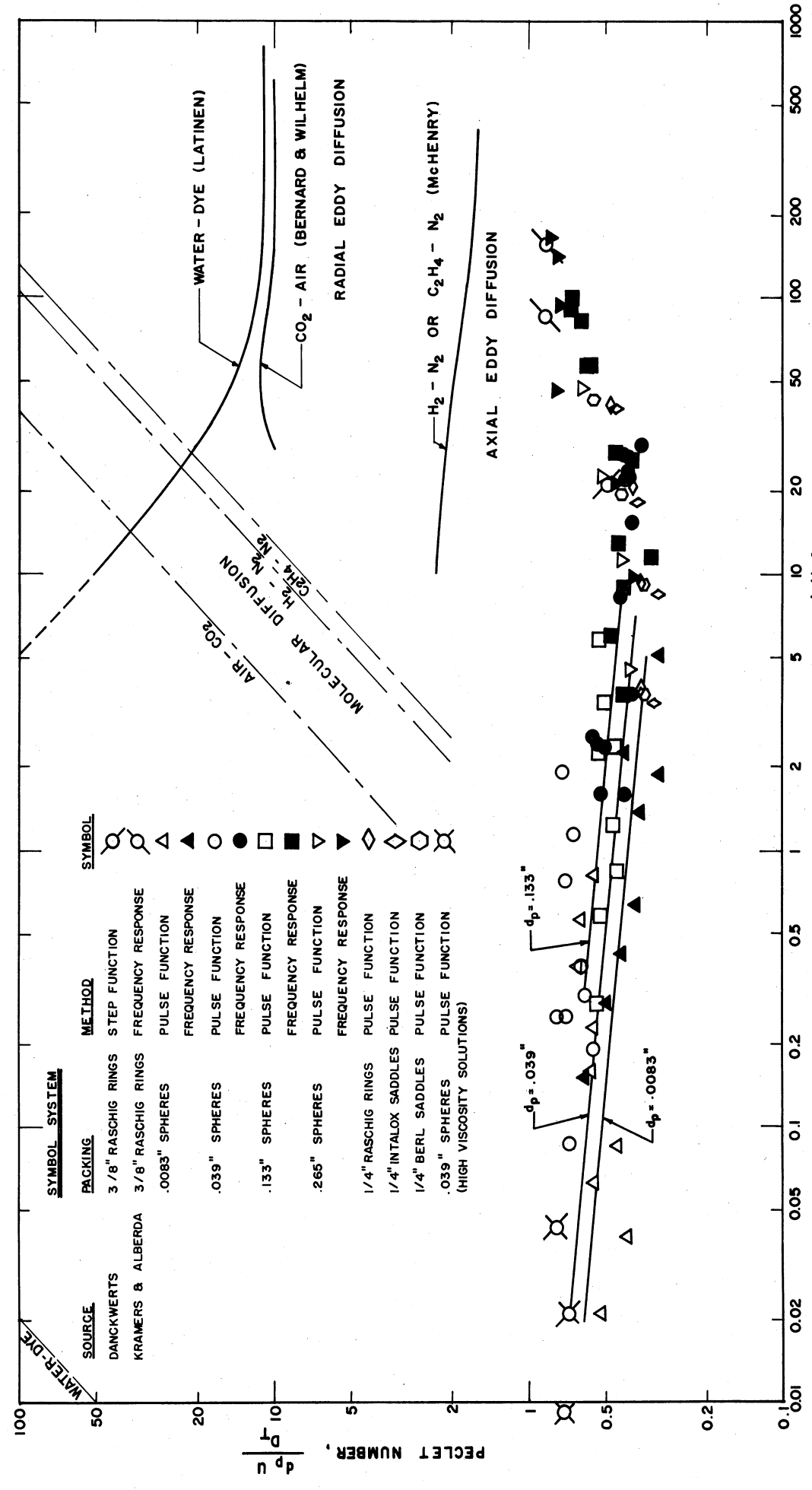

FIG. 26 PECLET NUMBER VS. REYNOLDS NUMBER CORRELATION

where d_p is the particle diameter, u is the interstitial velocity, and D_L is the effective axial diffusivity. The abscissa is Reynolds number, $d_p v_o \rho/\mu$, where v_o is the superficial velocity based on the empty column cross section, ρ is density, and μ is viscosity.

The effect of Reynolds number can be observed by the trend of the plotted data. The data for spherical particles covers a wide range of Reynolds number, 0.01-170, and indicates a general decrease in Peclet number, 0.60-0.80 at Reynolds number 0.01 to 0.32-0.42 at Reynolds number 10.0. A break in the trend occurs at Reynolds number 10.0, as the Peclet number increases gradually to a value of 0.7-0.9 at Reynolds number 170. The data for Raschig rings, Berl saddles and Intalox saddles covers a range of Reynolds number from 3.5 to 45, and the trend follows that of the spherical particles.

The effect of particle diameter is indicated by the three lines drawn for Reynolds number less than 10. Each line represents the correlation between Peclet number and Reynolds number for a particular particle size based on the previously derived equation for axial diffusivity as a function of particle diameter and interstitial velocity,

$$D_L = (3.25 \pm 0.12)\, d_p u^{(1.09 \pm 0.02)} \qquad (32a)$$

The data obtained from experiments in which the viscosity was varied is also plotted in Figure 26, in the Reynolds number range of .009-.05.

COMPARISON WITH PREVIOUS INVESTIGATIONS

The results of this study of axial mixing in liquids flowing through beds of packed solids are graphically compared in Figure 26

with the results of other investigations concerning the axial and radial mixing of gases and liquids flowing through beds.

Kramers and Alberda[24], using the frequency response method, investigated the longitudinal mixing of water flowing through a column (diameter: 2.9 inches, length: 13.4 inches) packed with 3/8 inch Raschig rings. Harmonic waves were obtained by sinusoidally varying the concentration of an electrolyte in water and measuring the electrical conductivity of the solutions. The Peclet numbers (0.86, 0.86), shown in Figure 26 were calculated from the value of $D_L/u\ d_p$ (1.1 ± 0.1) for the two water velocities investigated (Reynolds numbers: 85 and 155). The data agrees with the results of this research.

Another experiment concerning the longitudinal mixing of water flowing through a bed packed with 3/8 inch Raschig rings has been presented by Danckwerts[11]. The column was 1.9 inches in diameter and 4.6 feet in length. The outlet response curve to an inlet step function disturbance was used to evaluate the mixing occurring within the bed. The value of Peclet number (0.488) for a Reynolds number of 22 calculated from the data of Danckwerts is also shown in Figure 26, and is in agreement with the data.

Measurements on the axial mixing of binary gas mixtures flowing through a random bed of spherical particles have been reported by McHenry[27]. The frequency response technique was employed in which an axial Peclet number was computed as a function of the ratio of the amplitudes of a sinusoidal concentration wave at the inlet and outlet of the bed. The test columns were 1.93 inches in diameter randomly packed with .127 inch spherical particles to a height varying from 1 to 3 feet. For the gas systems H_2 - N_2 and C_2H_4 - N_2 and for Reynolds

numbers between 10 and 400 the mean of 21 determinations of axial Peclet number was 1.88 ± 0.15. The curve shown in Figure 26 summarizes graphically the data of McHenry.

The axial mixing data for the gas systems does not coincide with the results for the liquid systems. Perhaps, if the Reynolds number range were increased beyond 170, the values of axial Peclet numbers for liquid systems would approach those of the gas systems. Agreement between the two systems is not necessary, since the more efficient mixing of the liquid system could possibly be the consequence of more complex interaction in the bed. If axial diffusion is the result of local trapping, by-passing, acceleration and deceleration, then it could be assumed that these processes would be more efficient in liquids than in gases because of the great difference in physical properties.

A comparison of the axial mixing data with data from the literature concerning radial mixing is also made in Figure 26. The point source method was employed to evaluate the extent of radial mixing for both liquid and gas systems.

For liquid runs, Bernard and Latinen[3,26,39] allowed methylene blue solution to diffuse from a point source into water flowing at various velocities through beds of packed solids. Spheres, varying from 1 mm to 5 mm in diameter, were used as packing in a 2 inch diameter column. Gaseous experiments[7] were performed with carbon dioxide diffusing across an air stream flowing through an 8 inch diameter pipe packed with 3/8 inch spheres. Fluid samples were taken at various heights and various radial increments; samples of the average effluent were also taken. Hence, concentration profiles were obtained at various

heights and from these experimental data values of u/D_T were calculated. Curves for the two systems are presented in Figure 26. The data for gas systems indicate the radial Peclet number is approximately 10 for Reynolds numbers between 25 and 600. The results of Latinen's investigation for a liquid system show a constant Peclet number of 11 for Reynolds numbers greater than 150, with an increase in Peclet number below this region. The results of both investigations agree with the statistical "random-walk" approach of Baron[2] who predicted a Peclet number of the order of 11 for fully developed turbulence.

Fahien and Smith[15] extended the study of radial diffusion coefficients in fixed beds through which gases are flowing to include a larger range of pipe and packing sizes and the effect of radial position in the bed. The point source method of introducing carbon dioxide into an air stream was used. Measured point values of the Peclet number were found to increase with radial position due to the increase in void fraction and the influence of the pipe wall, when $d_p/d_t > 0.05$. Average values of the radial Peclet number were approximately 8.5 for Reynolds numbers greater than 40, with a decrease in Peclet number indicated for lower Reynolds numbers.

Radial gaseous mass transfer rates have also been investigated by the point-source method by Plautz and Johnstone[30]. The modified Peclet group was found to be constant at a value of approximately 12 in the region of fully developed turbulence.

The results for radial mixing of the gas and water systems coincide to a greater degree than the data for axial mixing. This closer agreement probably results from the mechanism associated with radial mixing, which assumes that mixing occurs because of the splitting

and side-stepping of fluid packets flowing around the particles in a packed bed.

The curves for molecular diffusion for the three gas systems and the water-dye system are also included in Figure 26. These curves indicate the large increase in mixing occurring because of the eddy diffusion process. At low flow rates, with other effects being negligible, the curves for eddy and molecular diffusion should merge.

EFFECT OF AXIAL DIFFUSIVITY IN CHEMICAL REACTORS

In the performance of a steady-flow fixed bed reactor the mixing occurring between products and reactants reduces the reaction rate. The effect of longitudinal eddy diffusion can be approximated for a first-order, or pseudo-first-order, reaction in which the reaction-velocity constant does not vary and no changes in volume occur. The fraction of reactant which has reacted, x, during passage through a packed column can be approximated for small values of diffusivity as

$$x = 1 - \left(1 + \frac{k^2 D_L z}{u^3}\right) e^{-\frac{kz}{u}} \qquad (33)$$

according to Danckwerts[11]. For no axial diffusion this becomes

$$x = 1 - e^{-\frac{kz}{u}} \qquad (34)$$

which is the solution for piston flow. Thus, the effect of diffusion is to decrease the fractional conversion compared to that for piston flow. However, if the factor, $k^2 D_L z/u^3$, is small the effect of longitudinal diffusion is negligible. Even though the results of this research indicate the axial diffusivity is much greater than previously

assumed, it can be seen that for a pseudo-first-order approximation, only those reactions having relatively high reaction velocity constants, which produce steep concentration gradients, are affected by longitudinal diffusion.

This approximate treatment can only serve as a rough guide for the effect of axial mixing in steady-flow fixed-bed reactors. In reactions of order higher than first, the chance of a given molecule reacting depends on the molecules it encounters during its passage through the reactor, hence the effect of mixing on the reaction cannot be described by the above equations. The more complex the reaction, the greater the effect of the mixing occurring within the reactor should be. Take for example a reaction which results in an increase in the total number of moles of fluid; the resulting concentration gradient becomes steeper, since the reactant is being diluted by products as well as being decomposed, and thus the effect of axial diffusion should become more pronounced.

SUMMARY AND CONCLUSIONS

The present investigation has resulted in the evaluation of axial mixing occurring in liquids flowing through fixed beds of solids. The primary variables considered were particle diameter (0.0083 to 0.265 inches), liquid velocity (interstitial velocity from 0.0008 to 0.3 ft/sec), packing shape, and liquid viscosity. The determination of the extent of axial mixing was carried out in equipment designed and constructed to analyze the response to some form of initial disturbance in a flowing system. The method of tracing this response was colorimetry; hence continuous photometers were designed to determine the concentration of tracer dye in the flowing streams. Two methods were employed to evaluate the extent of axial mixing. A frequency response method, in which the inlet composition varies sinusoidally, was employed for high flow ranges. A comparison of the inlet and outlet periodic waves resulted in the evaluation of axial diffusivity. Experimental difficulties led to the use of a second method for the low flow ranges. In the pulse function method the outlet concentration profile resulting from an inlet concentration pulse was used to evaluate the extent of axial mixing.

The primary conclusions resulting from this investigation can be summarized as follows:

1. A series of experiments resulted in data showing the effect of liquid velocity and particle diameter on axial mixing. The interstitial velocity was varied from 0.0008 ft/sec to 0.3 ft/sec for four sizes of glass spheres having diameters of 0.0083, 0.039, 0.133 and 0.265 inches. The plotted data, shown in Figure 21, is described by

the relationship

$$D_L = (3.25 \pm 0.12)\, d_p u^{(1.09 \pm 0.02)}$$

in the region where the product of particle diameter and interstitial velocity is less than 5.5×10^{-4} ft^2/sec.

2. Four types of packing: spheres, Raschig rings, Berl saddles, and Intalox saddles, were investigated to determine the effect of particle shape on axial mixing. Packings having the same approximate equivalent diameter (0.20 to 0.26 inches) produced approximately the same axial diffusivities indicating, in so far as has been investigated, that the shape of the packing has little effect on the axial mixing.

3. Experiments using propylene glycol and water solutions, having viscosities ranging from 1 to 26 centipoises, indicated no effect of viscosity on axial diffusivity over the range investigated.

4. The axial mixing data are correlated in a plot of modified Peclet number, $d_p u/D_L$, as a function of Reynolds number, $d_p v_o \rho/\mu$, as shown in Figure 26. The trend of plotted data indicates that for Reynolds number increasing from 0.01 to 10, the Peclet number decreases from 0.60-0.80 to 0.32-0.42. The Peclet number then increases gradually to a value of 0.7-0.9 at Reynolds number of 170. The data for Raschig rings, Berl saddles and Intalox saddles covers a range of Reynolds number from 3.5 to 45 and the trend follows that of the spherical particles.

Several variables resulting from the experimental technique were also investigated to show that the evaluation of axial diffusivity was not dependent upon the experimental method employed. These non-dependent variables were the frequency and amplitude of the periodic

function in the frequency response experiments, the length of the packed column and the dye solution used as tracer.

A comparison of the results of this investigation with previous mixing studies is made in Figure 26. The data for axial mixing has a much lower value of Peclet number than that of radial mixing, indicating a greater degree of mixing in the longitudinal direction than in the radial direction. The value of axial Peclet number for the liquid system of the present research is lower than that previously presented for gas systems (approximately 2) but agrees with the previously limited data of Kramers and Alberda, and Danckwerts for axial mixing in liquid systems. The results of this study indicate that axial eddy diffusion in liquids flowing through fixed beds is greater than previously assumed and perhaps should not be neglected in reactor calculations.

APPENDIX I

MATHEMATICAL DERIVATIONS

A. DERIVATION OF DIFFUSION-CONVECTION EQUATION

Consider a cylindrical column packed with finely divided particles through which fluid flows at a mean axial velocity u. Assume concentration gradients exist within the fluid, and that adsorption can take place on the surface of the particles. Let

c = concentration of tracer in fluid stream, moles per unit volume of solution

η = amount of tracer adsorbed on particles, moles per unit volume of bed

D_L = effective axial diffusion coefficient, ft^2/sec

D_R = effective radial diffusion coefficient, ft^2/sec

u = mean axial velocity of fluid through interstices of bed, ft/sec

z = distance variable along bed, longitudinal coordinate

r = radial coordinate

ϵ = porosity, fractional void volume in bed

t = time, sec

The mathematical mechanism for diffusion, both eddy and molecular, can be described by the equation which states that the rate of transfer of diffusing substance through a unit area of section is proportional to the concentration gradient measured normal to the section, i.e.

$$N = -D_L \frac{\partial c}{\partial z} \qquad \text{for axial transfer}$$

and

$$N = -D_R \frac{\partial c}{\partial r} \qquad \text{for radial transfer.}$$

The fundamental diffusion-convection equation can then be derived by making a material balance for an increment of time ∂t for a cylindrical element dr in thickness and dz in height.

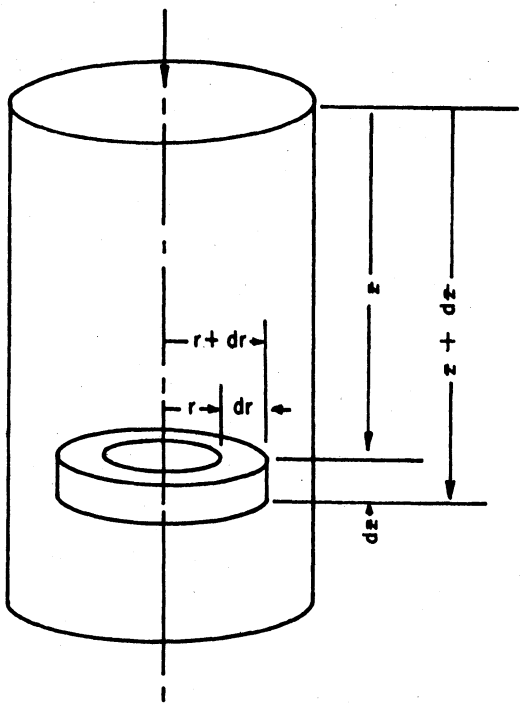

FIGURE 27 - DIFFERENTIAL SEGMENT WITHIN COLUMN

The rate at which the tracer enters the element from the axial direction through the plane perpendicular to the axial direction at distance z is given by

$$(2\pi r dr)\left[-D_L \frac{\partial c}{\partial z} + uc\right]$$

Similarly, the loss of tracer through the plane at distance (z + dz) is equal to

$$(2\pi r dr)\left[-D_L \frac{\partial}{\partial z}\left(c + \frac{\partial c}{\partial z} dz\right) + u\left(c + \frac{\partial c}{\partial z} dz\right)\right]$$

Likewise, the rate of tracer transferred into the element in the radial direction through the cylindrical surface at radius r is given by

$$(2\pi r dz)\left[-D_R \frac{\partial c}{\partial r}\right]$$

while the loss of trancer through the surface at radius (r + dr) can be represented by

$$-D_R \left[(2\pi r dz)\frac{\partial c}{\partial r} + \frac{\partial[(2\pi r dz)\frac{\partial c}{\partial r}]}{\partial r} dr \right]$$

The rate at which the tracer increases in the element is equal to

$$(2\pi r\ dr\ dz)\ \frac{\partial c}{\partial t} + \frac{(2\pi r\ dr\ dz)}{\epsilon}\ \frac{\partial \eta}{\partial t}$$

where the first term represents accumulation in the solution itself, and the second term represents adsorption on the particle surfaces. Summing the above rates and eliminating terms results in the general diffusion-convection equation

$$D_L \frac{\partial^2 c}{\partial z^2} + D_R \left[\frac{\partial^2 c}{\partial r^2} + \frac{1}{r}\frac{\partial c}{\partial r}\right] - u\frac{\partial c}{\partial z} = \frac{\partial c}{\partial t} + \frac{1}{\epsilon}\frac{\partial \eta}{\partial t} \qquad (1)$$

For cases in which the adsorption is negligible the equation reduces to:

$$D_L \frac{\partial^2 c}{\partial z^2} + D_R \left[\frac{\partial^2 c}{\partial r^2} + \frac{1}{r}\frac{\partial c}{\partial r}\right] - u\frac{\partial c}{\partial z} = \frac{\partial c}{\partial t} \qquad (2)$$

In systems in which the effective diffusion is considered to be isotropic, i.e.

$$D_R = D_L = D_T$$

the equation becomes

$$D_T \left[\frac{\partial^2 c}{\partial z^2} + \frac{\partial^2 c}{\partial r^2} + \frac{1}{r}\frac{\partial c}{\partial r}\right] - u\frac{\partial c}{\partial z} = \frac{\partial c}{\partial t} \qquad (3)$$

For the system considered in this research, the concentration gradient was in the axial direction only, i.e.

$$\frac{\partial c}{\partial r} = 0; \quad \frac{\partial^2 c}{\partial r^2} = 0$$

resulting in the equation

$$D_L \frac{\partial^2 c}{\partial z^2} - u\frac{\partial c}{\partial z} = \frac{\partial c}{\partial t}. \qquad (4)$$

B. FREQUENCY RESPONSE TECHNIQUE

1. Solution by Laplace Transform and Inversion Integral[7,6]

The diffusion-convection equation, assuming no radial concentration gradients exist and that effective diffusivity and velocity are independent of position, reduces to

$$D_L \frac{\partial^2 c}{\partial z^2} - u \frac{\partial c}{\partial z} = \frac{\partial c}{\partial t} \qquad (1)$$

in which the standard nomenclature is employed. Two boundary conditions are imposed: first, the inlet concentration is a harmonic function of time

$$c(0,t) = c_m + A(0) \cos \omega t \qquad (2)$$

and second, at a sufficiently long distance down the bed the amplitude approaches zero

$$c(\infty,t) = c_m \qquad (3)$$

or

$$A(z) = 0 \quad \text{for } z \to \infty$$

If in equations (1), (2) and (3) the expression

$$c_1 = c - c_m \qquad (4)$$

is substituted, there results:

$$D_L \frac{\partial^2 c_1}{\partial z^2} - u \frac{\partial c_1}{\partial z} = \frac{\partial c_1}{\partial t} \qquad (1a)$$

$$c_1(o,t) = A(0) \cos \omega t \qquad (2a)$$

$$c_1(\infty,t) = 0 \qquad (3a)$$

With the substitution

$$g = c_1 e^{-\frac{uz}{2D_L} + \frac{u^2 t}{4D_L}} \tag{5}$$

equations (1a), (2a) and (3a) become

$$D_L \frac{\partial^2 g}{\partial z^2} = \frac{\partial g}{\partial t} \tag{6}$$

$$g(0,t) = A(0) e^{\frac{u^2 t}{4 D_L}} \cos \omega t = A(0) e^{at} \cos \omega t \tag{7}$$

where

$$a = \frac{u^2}{4 D_L} \tag{7a}$$

$$g(\infty,t) = 0 \tag{8}$$

and for a column of sufficient length

$$g(z,0) = 0 \qquad \text{for} \qquad z \gg 0 \tag{9}$$

The above partial differential equation and boundary conditions may be solved by applying the Laplace transformation.

Suppose a function $f(t)$ exists for all positive values of the variable t. Then the Laplace transform $\bar{f}(s)$ of $f(t)$ is defined as

$$\bar{f}(s) = \int_0^\infty e^{-st} f(t)\, dt \tag{10}$$

where s is a number sufficiently large to make the integral converge. Applying this principle, equations (6) and (7) become transformed to

$$\frac{d^2 \bar{g}}{d z^2} - \frac{s}{D_L} \bar{g} = 0 \tag{11}$$

and

$$\bar{g}(0,s) = A(0) \frac{s-a}{(s-a)^2 + \omega^2} \tag{12}$$

where $\bar{g}(s)$ is the Laplace transform of $g(t)$. Thus the Laplace transform reduces the partial differential equation (6) to the ordinary differential equation (11). The solution by the method of operators of (11) satisfying (12), and for which $\bar{g}$ remains finite is

$$\bar{g}(z,s) = A(0) \frac{s-a}{(s-a)^2 + \omega^2} e^{-z\sqrt{\frac{s}{D_L}}} \qquad (13)$$

Since the inverse transform of $\bar{g}$ is not apparent, the complex inversion integral of the Laplace transformation is employed. If a complex function $\bar{f}(s)$ is analytic and of the order $O(s^{-k})$ in the half plane $\mathcal{R}(s) \geqslant x_o$, where x_o and k are real constants and $k > 1$, then the inversion integral $L_i^{-1}\left\{\bar{f}(s)\right\}$ along any line $x = \xi$, where $\xi \geqslant x_o$, converges to a function $f(t)$ that is independent of ξ, i.e.

$$f(t) = L_i^{-1}\left\{\bar{f}(s)\right\} = \frac{1}{2\pi i} \lim_{\beta \to \infty} \int_{\xi - i\beta}^{\xi + i\beta} e^{\lambda t} f(\lambda) d\lambda \qquad (14)$$

where the symbol L_i^{-1} represents the transformation of $\bar{f}(s)$ by the inversion integral, and λ is a variable of integration.

Consider the function $\bar{g}(s)$ equation (13), to be complex and having a branch point at $s = 0$, and simple poles at $s = a \pm i\omega$. Define $s = re^{i\theta}$ and

$$\sqrt{s} = \sqrt{r}\ e^{i\frac{\theta}{2}} = \sqrt{r}\ (\cos\tfrac{\theta}{2} + i \sin\tfrac{\theta}{2}) \qquad (15)$$

where $-\pi < \theta < \pi$. With this restriction on θ, the function $\sqrt{s}$ as defined in equation (15) is single valued and analytic at all points in the finite complex plane except on the negative end of the real axis and at the origin. Since $\bar{g}(s)$ is an analytic function of $\sqrt{s}$, $\bar{g}(s)$ is analytic in the same region except for the simple poles at $s = a \pm i\omega$.

The function $\bar{g}(s)$ satisfies the conditions for the integral (14) resulting in the formula

$$g(z,t) = \frac{A(0)}{2\pi i} \int_{\xi-i\infty}^{\xi+i\infty} \frac{(\lambda-a)}{(\lambda-a)^2 + \omega^2} e^{\lambda t - z\sqrt{\frac{\lambda}{D_L}}} d\lambda \qquad (16)$$

This complex integral is evaluated by employing certain principles of complex variables, auxiliary line integrals and theory of residues.

Cauchy's residue theorem states that the counterclockwise integral around a closed curve C within and on which f(s) is analytic except for a finite number of singular points s_1, s_2, ... s_n, inside of C is $2\pi i$ times the sum of the residues of those points, i.e.;

$$\int_C f(s)ds = 2\pi i(K_1 + K_2 + \cdots K_n) \qquad (17)$$

where K_1, K_2,...K_n, denote the residues of the singular points s_1, s_2, ... s_n within the curve.

Hence, the integral (16) can be evaluated by considering the closed curve shown in Figure 28, since the curve so formed lies in a region where the integral is analytic.

By Cauchy's theorem:

$$\frac{1}{2\pi i} \int_{\xi-i\beta}^{\xi+i\beta} \frac{(\lambda-a)}{(\lambda-a)^2 + \omega^2} e^{\lambda t - z\sqrt{\frac{\lambda}{D_L}}} d\lambda =$$

$$= \frac{2\pi i}{2\pi i}\left[K_1 + K_2\right] - \frac{1}{2\pi i}\left[I_{AB} + I_{BC} + I_{CD} + I_{DD'} + I_{D'C'} + I_{C'B'} + I_{B'A'} + I_{A'A}\right] \qquad (18)$$

K_1 and K_2 represent the residues of the poles $a \pm i\omega$, and where I_{AB} denotes the integral over the arc AB, and so on.

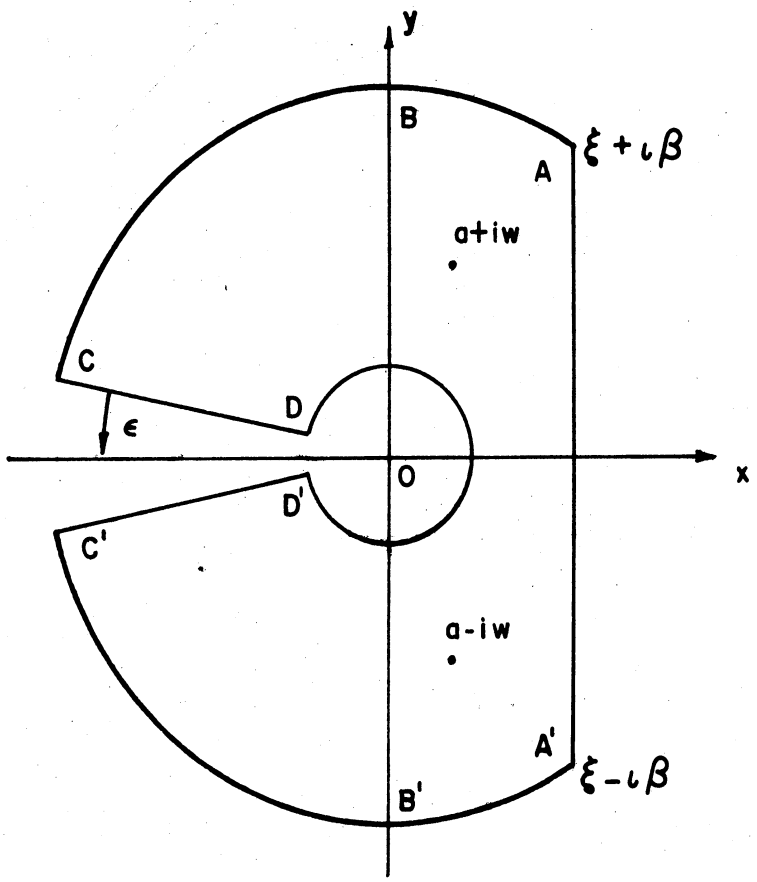

FIGURE 28 - CLOSED CURVE FOR EVALUATION OF COMPLEX INTEGRAL

Let R and r_o denote the radii of the large and small circular arcs; thus $R^2 = \xi^2 + \beta^2$ so that $\beta \to \infty$ when $R \to \infty$. Along the larger arc

$$\lambda = Re^{i\theta} \quad ; \qquad d\lambda = iRe^{i\theta} \quad d\theta$$

while along the smaller arc

$$\lambda = r_o e^{i\theta} \quad ; \quad \sqrt{\lambda} = \sqrt{r_o}\, e^{i\frac{\theta}{2}} \quad ; \quad d\lambda = i\, r_o e^{i\theta} d\theta$$

As $r_o \to 0$ and $R \to \infty$, the left hand member of equation (18), which is independent of r_o, becomes the inversion integral or g(t). For clarity, denote $J_{AC} = \lim_{\epsilon \to 0} I_{AC}$, and so on, for the integrals over the arcs and lines.

Wnen λ is on the arc AB, the real part of the exponent $\lambda t - z\sqrt{\frac{\lambda}{D_L}}$ is not greater than $t\xi$. Hence

$$\left| \frac{(\lambda-a)}{(\lambda-a)^2 + \omega^2} e^{\lambda t - z\sqrt{\frac{\lambda}{D_L}}} d\lambda \right| \leqslant \frac{(R-a)R}{(R-a)^2 - \omega^2} e^{t\lambda} d\theta$$

and, if θ_A is the angle θ at A

$$\left| J_{AB} \right| \leqslant \frac{(R-a)R}{(R-a)^2 - \omega^2} e^{t\xi} \int_{\theta_A}^{\pi/2} d\theta = \frac{(R-a)R}{(R-a)^2 - \omega^2} e^{t\xi} (\pi/2 - \theta_A) \qquad (19)$$

Since $\theta_A \to \pi/2$ as $R \to \infty$, it follows that J_{AB} tends to 0 as $R \to \infty$. Likewise $J_{A'B'}$ vanishes as R tends to infinity.

On the arc BC the real part of the exponent $\lambda t - z\sqrt{\frac{\lambda}{D_L}}$ is less than $tR \cos \theta$, and therefore

$$\left| J_{BC} \right| \leqslant \frac{(R-a)R}{(R-a)^2 - \omega^2} \int_{\pi/2}^{\pi} e^{tR\cos\theta} d\theta$$

Substituting $(\alpha + \pi/2)$ for θ, where $\cos\theta = \cos(\alpha + \pi/2) = -\sin\alpha$, in the above, there results:

$$\left| J_{BC} \right| \leqslant \frac{(R-a)R}{(R-a)^2 - \omega^2} \int_0^{\pi/2} e^{-tR\sin\alpha} \, d\alpha$$

If $0 < \alpha < \pi/2$, then $\frac{2\alpha}{\pi} < \sin\alpha$, and

$$\left|J_{BC}\right| \leqslant \frac{(R-a)R}{(R-a)^2 - \omega^2} \int_0^{\pi/2} e^{-\frac{2tR\alpha}{\pi}} \, d\alpha = \frac{(R-a)R}{\left[(R-a)^2 - \omega^2\right]2tR} e^{-\frac{2tR\alpha}{\pi}} \Bigg]_0^{\pi/2}$$

$$= \frac{(R-a)\pi}{\left[(R-a)^2 - \omega^2\right]2t} \left[e^{-tR} - 1 \right] \qquad (20)$$

Hence, $|J_{BC}|$ vanishes as R becomes infinite, when $t > 0$. Similarly, the limit of $J_{B'C'}$ is zero.

The integral over the small circle can be written

$$J_{DD'} = i \int_{\pi}^{-\pi} \frac{(r_o e^{i\theta} - a) r_o e^{i\theta}}{(r_o e^{i\theta} - a)^2 + \omega^2} e^{r_o e^{i\theta} t - \frac{2\sqrt{r_o}}{D_L^2} e^{\frac{-\theta}{2} i}} d\theta \qquad (21)$$

which vanishes as r_o tends to 0.

On the line CD, $\lambda = r\, e^{i(\pi-\epsilon)}$, $d\lambda = e^{i(\pi-\epsilon)} dr$, and $\sqrt{\lambda} = \sqrt{r}\, e^{\frac{i}{2}(\pi-\epsilon)}$; thus as $\epsilon \to 0$

$$\lim_{\epsilon\to 0} \lambda = \lim_{\epsilon\to 0} r\, e^{i(\pi-\epsilon)} = r\, e^{\pi i} = r(\cos\pi + i\sin\pi) = -r$$

$$\lim_{\epsilon\to 0} \sqrt{\lambda} = \lim_{\epsilon\to 0} \sqrt{r}\, e^{\frac{i(\pi-\epsilon)}{2}} = \sqrt{r}\, e^{\frac{\pi i}{2}} = \sqrt{r}(\cos\pi/2 + i\sin\pi/2) = i\sqrt{r}$$

$$\lim_{\epsilon\to 0} d\lambda = -dr.$$

Similarly on the line D'C', $\lambda = r\, e^{i(-\pi+\epsilon)}$, $d\lambda = e^{i(-\pi+\epsilon)}\, dr$ and $\sqrt{\lambda} = \sqrt{r}\, e^{\frac{i}{2}(-\pi+\epsilon)}$; as $\epsilon \to 0$

$$\lim_{\epsilon\to 0} \lambda = \lim_{\epsilon\to 0} r\, e^{i(-\pi+\epsilon)} = r\, e^{-\pi i} = r[\cos(-\pi) + i \sin(-\pi)] = -r$$

$$\lim_{\epsilon\to 0} \sqrt{\lambda} = \lim_{\epsilon\to 0} \sqrt{r}\, e^{\frac{i}{2}(-\pi+\epsilon)} = \sqrt{r}\, e^{-\frac{\pi i}{2}} = \sqrt{r}\cos(-\pi/2) + i \sin(-\pi/2) = -i\sqrt{r}$$

$$\lim_{\epsilon\to 0} d\lambda = -dr.$$

Therefore

$$J_{CD} + J_{D'C'} = \int_R^{r_o} \frac{(r+a)}{(r+a)^2 + \omega^2}\, e^{-rt - \frac{z}{D_L^2} i\sqrt{r}}\, dr + \int_{r_o}^{R} \frac{(r+a)}{(r+a)^2 + \omega^2}\, e^{-rt + \frac{z}{D_L^2} i\sqrt{r}}\, dr$$

which reduces to

$$J_{CD} + J_{D'C'} = 2i \int_{r_o}^{R} \frac{(r+a)e^{-rt}}{(r+a)^2 + \omega^2}\, \frac{e^{i\frac{z}{D_L^2}\sqrt{r}} - e^{-i\frac{z}{D_L^2}\sqrt{r}}}{2i}\, dr$$

and consequently

$$\lim_{\substack{r_o\to 0 \\ R\to\infty}} (J_{CD} + J_{D'C'}) = 2i \int_0^{\infty} \frac{(r+a)e^{-rt}}{(r+a)^2 + \omega^2}\, \sin\frac{z}{D_L^2}\sqrt{r}\, dr \qquad (22)$$

The residues of the simple poles at $(a \pm i\omega)$ are evaluated as follows. The function $f(\lambda)$ can be represented as the quotient $p(\lambda)/q(\lambda)$ of two analytic functions, i.e.,

$$f(\lambda) = \frac{p(\lambda)}{q(\lambda)} = \frac{(\lambda-a)e^{\lambda t - z\sqrt{\frac{\lambda}{D_L}}}}{(\lambda-a)^2 + \omega^2} \qquad (23)$$

The residue A_{-1} of $f(\lambda)$ at the simple pole λ_o can be represented by definition as

$$A_{-1} = \lim_{\lambda \to \lambda_o} \frac{(\lambda-\lambda_o)\, p(\lambda)}{q(\lambda)} = \frac{p(\lambda)}{q'(\lambda)} \qquad (24)$$

Therefore the residue at $(a + i\omega)$ is

$$K_1 = \frac{1}{2} e^{(a+i\omega)t - z\sqrt{\frac{a+i\omega}{D_L}}} \qquad (24a)$$

and likewise at $(a-i\omega)$ is

$$K_2 = \frac{1}{2} e^{(a-i\omega)t - z\sqrt{\frac{a-i\omega}{D_L}}} \qquad (24b)$$

The sum of the residues is

$$\frac{1}{2} e^{at}\left[e^{i\omega t - z\sqrt{\frac{a+i\omega}{D_L}}} + e^{-i\omega t - z\sqrt{\frac{a-i\omega}{D_L}}} \right] \qquad (25)$$

which on substituting

$$\sqrt{\frac{a}{D_L} \pm \frac{\omega}{D} i} = Y_1 \pm Y_2 i \qquad (26)$$

reduces to

$$e^{at}\, e^{-zY_1} \left[\frac{e^{i(\omega t - zY_2)} + e^{-i(\omega t - zY_2)}}{2} \right] \qquad (27)$$

or

$$e^{at}\, e^{-zY_1} \cos(\omega t - zY_2) \qquad (27a)$$

Remembering that $a = \frac{u^2}{4D_L}$,

$$Y_1 = \frac{u}{2D_L} \sqrt[4]{1 + \left(\frac{4\omega D_L}{u^2}\right)^2} \cos \frac{1}{2}\left[\tan^{-1}\left(\frac{4\omega D_L}{u^2}\right)\right] \qquad (28)$$

and

$$Y_2 = \frac{u}{2D_L} \sqrt[4]{1 + \left(\frac{4\omega D_L}{u^2}\right)^2} \sin \frac{1}{2}\left[\tan \left(\frac{4\omega D_L}{u^2}\right)\right] \qquad (29)$$

To simplify let $\tan\theta = m = \frac{4\omega D_L}{u^2}$ and note that

$$\cos\theta = \frac{1}{\sqrt{1+\tan^2\theta}} = \frac{1}{\sqrt{1+m^2}} = \frac{1}{n}$$

where $n = \sqrt{1+m^2}$

also that

$$\cos\frac{\theta}{2} = \sqrt{\frac{1+\cos\theta}{2}} = \sqrt{\frac{1+\frac{1}{n}}{2}} = \sqrt{\frac{n+1}{2n}}$$

and correspondingly

$$\sin\frac{\theta}{2} = \sqrt{\frac{1-\cos\theta}{2}} = \sqrt{\frac{1-\frac{1}{n}}{2}} = \sqrt{\frac{n-1}{2n}}$$

Now substituting into Y_1 and Y_2

$$Y_1 = \frac{u}{2D_L}\sqrt{n}\sqrt{\frac{n+1}{2n}} = \frac{u}{2D_L}\sqrt{\frac{n+1}{2}} = \frac{u}{2D_L}\sqrt{\frac{\sqrt{1+\left(\frac{4\omega D_L}{u^2}\right)^2}+1}{2}} \tag{28a}$$

$$Y_2 = \frac{u}{2D_L}\sqrt{\frac{\sqrt{1+\left(\frac{4\omega D_L}{u^2}\right)^2}-1}{2}} \tag{29a}$$

Returning to equation (18) and substituting the previous evaluations there results

$$\frac{1}{2\pi i}\int_{\gamma-i\beta}^{\gamma+i\beta}\frac{(\lambda-a)}{(\lambda-a)^2+\omega^2}e^{\lambda t - z\sqrt{\frac{\lambda}{D_L}}}d\lambda = e^{at-zY_1}\cos(\omega t - zY_2)$$

$$-\frac{1}{2\pi i}\left\{2i\int_0^\infty \frac{(r+a)e^{-rt}}{(r+a)^2+\omega^2}\sin\left(\frac{z\sqrt{r}}{D_L^2}\right)dr\right\} \tag{30}$$

Hence, upon eliminating the unsteady state term

$$g(z,t) = A(0)e^{at}e^{-zY_1}\cos(\omega t - zY_2) \tag{31}$$

and substituting into (5) and (4)

$$c(z,t) = c_m + A(0)e^{at}\, e^{-zY_1} \cos(\omega t - zY_2) e^{\frac{uz}{2D} - at} \qquad (32)$$

The final solution is then

$$c(z,t) = c_m + A(0)e^{\frac{uz}{2D} - zY_1} \cos(\omega t - zY_2) \qquad (33)$$

where Y_1 and Y_2 are defined by equations (28a) and (29a).

B. FREQUENCY RESPONSE TECHNIQUE

2. Solution Employing Complex Variables and Principle of Superposition[6,12,24]

The partial differential equation for the diffusion-convection mixing of a liquid flowing through a packed bed has the form

$$D_L \frac{\partial^2 c}{\partial z^2} - u \frac{\partial c}{\partial z} = \frac{\partial c}{\partial t} \tag{1}$$

in which the inlet composition is

$$c(0,t) = c_m + A(0) \cos(\omega t) \tag{2}$$

and is bounded by

$$c(\infty,t) = c_m. \tag{3}$$

The steady-state periodic solution to the above system is assumed to have the form

$$c(z,t) = c_m + A(0)\, e^{-B} \cos(\omega t - \phi) \tag{4}$$

because of the linearity of the system.

Summarized below are several principles of complex variables and the principle of superposition which are employed in the solution.

Complex number $h = p + i\,k$ (5)

$$\theta = \tan^{-1} \frac{k}{p} \tag{6}$$

$$h = |h| (\cos\theta + i \sin\theta) \tag{7}$$

where

$$|h| = \sqrt{p^2 + k^2} \tag{8}$$

Euler's equation states

$$e^{i\xi} = \cos\xi + i \sin\xi \tag{9}$$

and therefore

$$h = |h|e^{i\theta} \tag{10}$$

Principle of superposition states that in a linear system the effect of each action upon a system is as if it alone were present, the effect of a number of actions upon the system being the sum of the individual actions.

As before, let

$$c_1 = c - c_m \tag{11}$$

and obtain

$$D_L \frac{\partial^2 c_1}{\partial z^2} - u \frac{\partial c_1}{\partial z} = \frac{\partial c_1}{\partial t} \tag{1a}$$

$$c_1(0,t) = A(0) \cos(\omega t) \tag{2a}$$

$$c_1(\infty,t) = 0 \tag{3a}$$

$$c_1(z,t) = A(0)\, e^{-B} \cos(\omega t) \tag{4a}$$

Now, consider input to be a complex number; hence, instead of inlet of form (2a) introduce an inlet of same amplitude A(0) but multiplied by the sum of a real cosine term and an imaginary sine term, the angle remaining ωt:

$$c_1(0) = A(0)\, [\cos(\omega t) + i \sin(\omega t)] \tag{12}$$

Hence equation 4a becomes

$$c_1(z) = A(0)\, e^{-B}\, [\cos(\omega t - \phi) + i \sin(\omega t - \phi)] \tag{13}$$

Applying Euler's equation (9), the above becomes

$$c_1(0) = A(0)\, e^{i\omega t} \tag{12a}$$

and

$$c_1(z) = \underline{A(z)}\, e^{i\omega t} \tag{13a}$$

where $\underline{A(z)}$ is the complex amplitude represented by

$$\underline{A(z)} = A(z)\, e^{-i\phi} \tag{14}$$

The use of complex variables now becomes apparent, for when (13a) is substituted into the linear differential equation (1a) containing t as a variable, where c is the independent variable, t drops out. Hence there results

$$\frac{\partial^2 \underline{A(z)}}{\partial z^2} - \frac{u}{D_L}\frac{\partial \underline{A(z)}}{\partial z} - \frac{\underline{A(z)}\, i\omega}{D_L} = 0 \tag{15}$$

with the boundary conditions

$$\underline{A(z)} = A(0) \qquad \text{for } z = 0 \tag{16}$$

and

$$\underline{A(z)} = 0 \qquad \text{for } z = \infty \tag{17}$$

The solution of (15) by method of operators gives

$$\underline{A(z)} = K_1 e^{m_1 z} + K_2 e^{m_2 z} \tag{18}$$

where

$$m_1, m_2 = \frac{u}{2D_L} \pm \sqrt{\frac{u^2}{4D_L^2} + \frac{i\omega}{D_L}} \tag{19}$$

Since the solution is bounded $K_1 = 0$, and applying the boundary conditions (16) and (17), equation (18) becomes

$$\underline{A(z)} = A(0)\, e^{z\left(\frac{u}{2D} - \sqrt{\frac{u^2}{4D_L^2} + \frac{i\omega}{D_L}}\right)} \tag{20}$$

Now substitute (20) into (13a) and (11) giving

$$c(z, t) = c_m + A(0)\, e^{z\left(\frac{u}{2D} - \sqrt{\frac{u^2}{4D_L^2} + \frac{i\omega}{D_L}}\right) + i\omega t} \tag{21}$$

In order to obtain the real solution, the exponent in (21) must be separated into its real and imaginary parts. Application of de Moivre's Theorem to the radical gives

$$\sqrt{\frac{u^2}{4D^2} + \frac{i\omega}{D}} = \sqrt[4]{\left(\frac{u^2}{4D^2}\right)^2 + \frac{\omega^2}{D}} \left[\cos\frac{\alpha}{2} + i\sin\frac{\alpha}{2}\right] \qquad (22)$$

where

$$\alpha = \tan^{-1}\frac{\omega/D_L}{u^2/4D_L^2} = \tan^{-1}\frac{4\omega D_L}{u^2}$$

which reduces to

$$\sqrt{\frac{u^2}{4D_L^2} + \frac{i\omega}{D_L}} = \frac{u}{2D}\sqrt[4]{1 + \left(\frac{4\omega D_L}{u^2}\right)^2}\left[\cos\frac{\alpha}{2} + 1\sin\frac{\alpha}{2}\right] \qquad (22a)$$

This radical, as in the previous solution (Appendix I-B-1) becomes

$$\sqrt{\frac{u^2}{4D_L^2} + \frac{i\,\omega}{D_L}} = Y_1 + Y_2 i \qquad (22b)$$

Now replacing the radical in (21), the solution becomes

$$c(z,t) = c_m + A(0)e^{\left[\frac{uz}{2D} - zY_1 - zY_2 i\right]}e^{[i\omega t]} \qquad (23)$$

Upon application of Euler's equation (9) and the rejection of the imaginary sine terms by the principle of superposition, equation reduces to

$$c(z,t) = c_m + A(0)e^{\frac{uz}{2D_L} - zY_1}\cos(\omega t - zY_2) \qquad (24)$$

where

$$Y_1 = \frac{u}{2D_L}\sqrt{\frac{\sqrt{1 + \left(\frac{4\omega D_L}{u^2}\right)^2} + 1}{2}} \qquad (25)$$

$$Y_2 = \frac{u}{2D_L}\sqrt{\frac{\sqrt{1 + \left(\frac{4\omega D_L}{u^2}\right)^2} \div 1}{2}} \qquad (26)$$

B. FREQUENCY RESPONSE TECHNIQUE

3. Approximate Solution[12,27,41]

An approximate solution may be obtained by referring back to equation 21, Appendix I-B-2, which can be written

$$c(z,t) = c_m + A(0)\, e^{\frac{zu}{2D_L}\left(1 - \sqrt{1+\left(\frac{4\omega D_L}{u^2}\right) i}\right) + i\omega t} \qquad (1)$$

If $\frac{4D_L}{u^2} |i\omega| < 1|$, the radical can be expanded by means of the Binomial Theorem as follows

$$\sqrt{1 + \left(\frac{4\omega D_L}{u^2}\right) i} = 1 + 2b^2 - 10b^4 + 84b^6 - \cdots + i(2b - 4b^3 + 28b^5 - \cdots) \qquad (2)$$

where

$$b = \frac{\omega D_L}{u^2} \quad . \qquad (2a)$$

Substituting this expansion into equation (1) and neglecting terms beginning with

$$10\left(\frac{\omega D_L}{u^2}\right)^4 \qquad (3)$$

the solution becomes

$$c(z,t) = c_m + A(0) e^{\frac{zu}{2D_L}[1 - 2b^2 + 2bi - 4b^3 i] + i\omega t} \qquad (4)$$

which combines to

$$c(z,t) = c_m + A(0) e^{-\frac{z\omega^2 D_L}{u^3}} e^{i(\omega t - \frac{z\omega}{u} + \frac{2z\omega^3 D_L^2}{u^5})} \qquad (5)$$

or

$$c(z,t) = c_m + A(0)\, e^{-\frac{z\omega^2 D_L}{u^3}} \cos\left(\omega t - \frac{z\omega}{u} + \frac{2z\omega^3 D_L^2}{u^5}\right) \qquad (5a)$$

The error in the value of B, where B is approximated by $\frac{z\omega^2 D_L}{u^3}$, is approximately less than the value of the first term neglected. This error can be estimated, for in the expansion of the radical an alternating series results, and the error made in stopping is in absolute value less than the first term neglected. Hence the error in B is

$$\frac{10b^4}{2b^2} = 5\left(\frac{\omega D_L}{u^2}\right)^2 \qquad (6)$$

Should more precision be necessary, the first term neglected in the expansion could be

$$84\left(\frac{\omega D_L}{u^2}\right)^6 \qquad (7)$$

with the solution being

$$c(z,t) = c_m + A(0)e^{-\frac{z\omega^2 D_L}{u^3} + \frac{5z\omega^4 D_L^3}{u^7}} \cos\left(\omega t - \frac{z\omega}{u} + \frac{2z\omega^3 D_L^2}{u^5} - \frac{14z\omega^5 D_L^4}{u^9}\right) \qquad (8)$$

and the error in B becoming

$$\frac{84b^6}{2b^2 - 10b^4} \cong 42\left(\frac{\omega D_L}{u^2}\right)^4 \qquad (9)$$

B. FREQUENCY RESPONSE TECHNIQUE

4. Adoption to Periodic Function[5,22]

In the experiments where the inlet composition wave was not sinusoidal, but periodic, the inlet waves can be represented by the Fourier series:

$$f(\omega t) = \frac{a_o}{2} + a_1 \cos(\omega t) + b_1 \sin(\omega t) + \ldots a_n \cos(n\omega t) + b_n \sin(n\omega t) + \ldots \quad (1)$$

which may also be written

$$f(\omega t) = \frac{a_o}{2} + \sum_{n=1}^{\infty} \left[a_n \cos(n\omega t) + b_n \sin(n\omega t) \right] \quad (1a)$$

where

$$a_n = \frac{1}{\pi} \int_{-\pi}^{\pi} f(\omega t) \cos(n\omega t)\, d(\omega t) \quad (n = 0,1,2\ldots) \quad (1b)$$

$$b_n = \frac{1}{\pi} \int_{-\pi}^{\pi} f(\omega t) \sin(n\omega t)\, d(\omega t) \quad (n = 1,2\ldots) \quad (1c)$$

The Fourier series may also be written as a series of sines or cosines only, hence:

$$f(\omega t) = \frac{a_o}{2} + \sum_{n=1}^{\infty} A_n \cos(n\omega t - \psi_n) \quad (2)$$

where

$$A_n = \sqrt{a_n^2 + b_n^2} \quad (2a)$$

$$\psi_n = \tan^{-1} \frac{b_n}{a_n} \quad (2b)$$

A_n represents the amplitude of the n-th harmonic and the phase angle ψ_n measures the lag of the n-th harmonic with reference to a pure cosine wave of the same frequency. Thus, as the above equations indicate, the periodic function is a combination of simple harmonic waves. The term $\frac{a_o}{2}$ represents the neutral position; the terms, $a_1 \cos(\omega t) + b_1 \sin(\omega t)$, the fundamental wave; and the other terms, $a_n \cos(n\omega t) + b_n \sin(n\omega t)$, the higher harmonics. The outlet concentration wave then also must be represented by a Fourier series in which each harmonic component is dampened and shifted in phase. By the principle of superposition, each harmonic in the outlet corresponds to the outlet expected if the corresponding harmonic in the inlet wave were the only inlet.

The solution to the diffusion-convection equation in which the inlet boundary condition is a periodic wave represented by a Fourier series can be most easily found by the method of complex variables and the principle of superposition. Thus given

$$D_L \frac{\partial^2 c}{\partial z^2} - u \frac{\partial c}{\partial z} = \frac{\partial c}{\partial t} \tag{3}$$

with the boundary conditions

$$c_n(0,t) = A_n(0) \cos (n\omega t - \psi_n) \tag{4}$$

$$c_n(\infty,t) = 0 \tag{5}$$

the assumed solution is

$$c_n(z,t) = A_n(z) \cos (n\omega t - \psi_n - \phi_n) \tag{6}$$

Considering the input and output to be complex, and employing Euler's formula, equations (4) and (6) become

$$c_n(0) = A_n(0) \quad \left[\cos(n\omega t - \psi_n) + i \sin(n\omega t - \psi_n)\right] \tag{4a}$$

$$= A_n(0)\, e^{i(n\omega t - \psi_n)} \tag{4b}$$

and

$$c_n(z) = A_n(z)\, [\cos(n\omega t - \psi_n - \phi_n) + i \sin(n\omega t - \psi_n - \phi_n)] \tag{6a}$$

$$= \underline{A_n(z)}\, e^{i(n\omega t - \psi_n)} \tag{6b}$$

where the complex amplitude

$$\underline{A_n(z)} = A_n(z)\, e^{-i\phi_n} \tag{6c}$$

Subsituting (6b) into (3), and hence removing t

$$\frac{\partial^2 \underline{A_n(z)}}{\partial z^2} - \frac{u}{D_L} \frac{\partial \underline{A_n(z)}}{\partial z} - \frac{\underline{A_n(z)}\; n\, i\, \omega}{D_L} = 0 \tag{7}$$

results in an ordinary differential equation in $\underline{A_n(z)}$ with the boundary conditions

$$\underline{A_n(z)} = A_n(0) \qquad \text{for } z = 0 \tag{8}$$

$$\underline{A_n(z)} = 0 \qquad \text{for } z = \infty \tag{9}$$

Solution of (7) by the method of operators gives

$$\underline{A_n(z)} = A_n(0)\, e^{z\left(\frac{u}{2D_L} - \sqrt{\frac{u^2}{4D_L^2} + \frac{n\, i\, \omega}{D_L}}\right)} \tag{10}$$

which with appropriate substitutions and reductions yields the solution:

$$c_n(z) = A_n(0)\, e^{\frac{zu}{2D_L}\left[1 - \sqrt{1 + \frac{4n\omega D_L}{u^2} i}\right] + i(n\omega t - \psi_n)} \qquad (11)$$

The approximate solution is obtained, if

$$\frac{4nD_L}{u^2} | i\omega | < i, \qquad (12)$$

by expanding the radical by means of the binomial theorem and rejecting insignificant terms. The resulting solution is:

$$c_n(z) = A_n(0)\, e^{-\frac{zn^2\omega^2 D_L}{u^3}}\, e^{i(n\omega t - \psi_n - \frac{nz\omega}{u})} \qquad (13)$$

which on eliminating the imaginary component reduces to:

$$c_n(z) = A_n(0)\, e^{-\frac{zn^2\omega^2 D_L}{u^3}} \cos\left(n\omega t - \psi_n - \frac{nz\omega}{u}\right) \qquad (14)$$

This solution then confirms the earlier statement that each harmonic component is dampened and shifted in phase as if it alone were present. The summation of the harmonic components forms the periodic outlet wave

$$c(z) = \frac{a_o}{2} + \sum_{n=1}^{\infty} A_n(0)\, e^{-\frac{zn^2\omega^2 D_L}{u^3}} \cos\left(n\omega t - \psi_n - \frac{nz\omega}{u}\right) \qquad (15)$$

Therefore, the frequency response experiments in which the inlet composition wave is not sinusoidal, but periodic, can be employed to evaluate the axial diffusivity.

B. FREQUENCY RESPONSE TECHNIQUE

5. Mathematical Approach to Pre-bed [22]

Consider a packed column through which fluid flows with a mean axial velocity u. Assume that the fluid consists of alternate and equal volumes of clear solution and tracer solution. If no mixing occurred, piston-type flow would result and an interface between two solutions would move down the column with velocity u. Denote this imaginary boundary plane as z = 0 and use it as the origin of a frame of reference moving down the column with uniform velocity u. However, as the liquids flow through the column mixing occurs according to the equation

$$D_L \frac{\partial^2 c}{\partial z^2} = \frac{\partial c}{\partial t} \qquad (1)$$

where c now represents the mean concentration of tracer at a plane z at time t, and D_L is the axial mixing coefficient.

The introduced alternate and equal volumes of clear and tracer solutions produce and approximate "square-wave" as shown in Figure 29 which can be represented by a Fourier series having the form

$$f(z) = \frac{a_o}{2} + \sum_{n=1}^{\infty} \left[a_n \cos\left(\frac{n\pi z}{L}\right) + b_n \sin\left(\frac{n\pi z}{L}\right) \right] \qquad (2)$$

where

$$a_n = \frac{1}{L} \int_{-L}^{L} f(z) \cos\left(\frac{n\pi z}{L}\right) dz \qquad (2a)$$

$$b_n = \int_{-L}^{L} f(z) \sin\left(\frac{n\pi z}{L}\right) dz \qquad (2b)$$

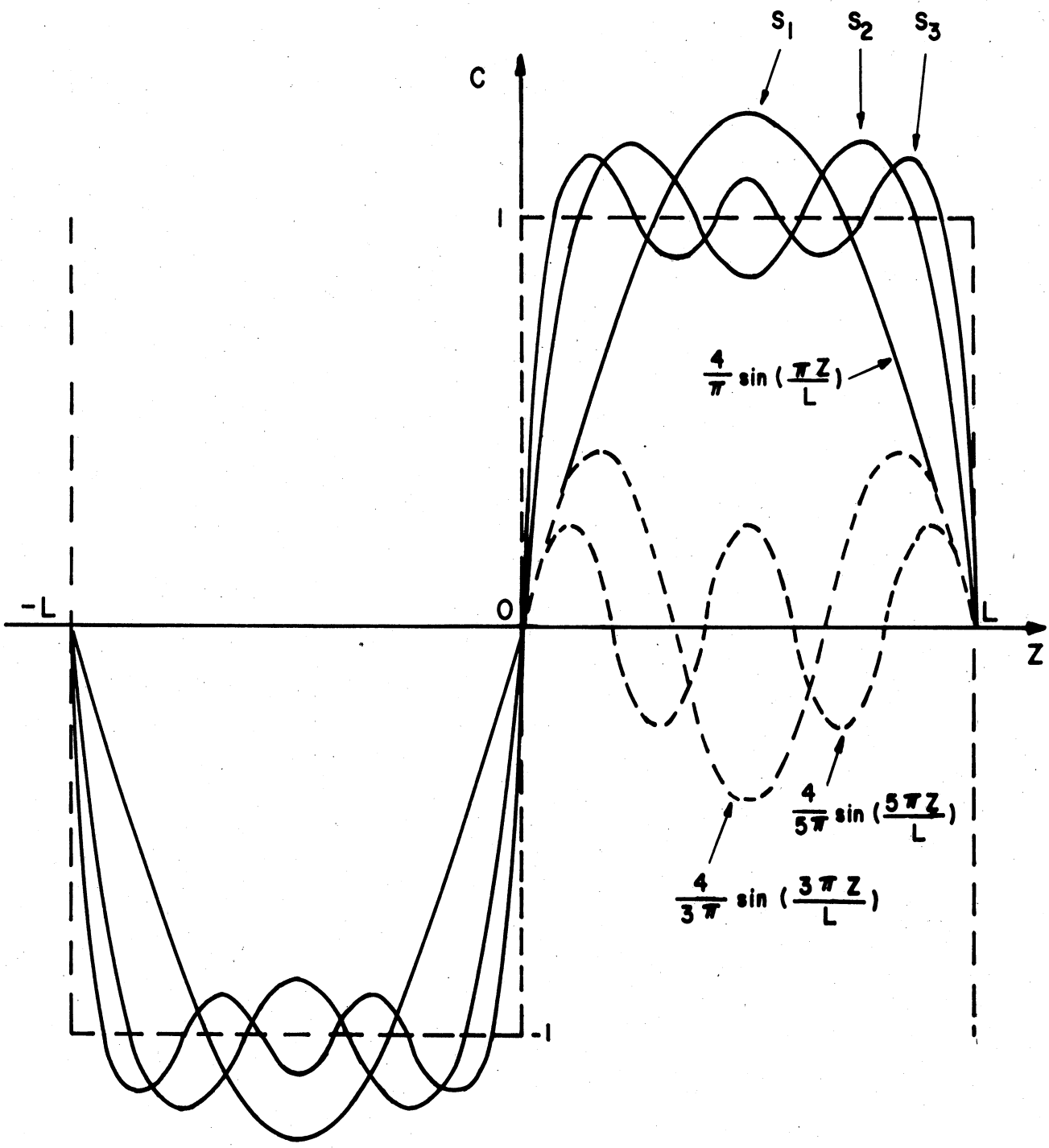

FIGURE 29 - APPROXIMATION OF "SQUARE-WAVE" BY FOURIER SERIES

The function for the square wave is

$$f(z) = -1 \qquad -L \leq z < 0$$
$$f(z) = 1 \qquad 0 \leq z \leq L \tag{3}$$

hence

$$a_n = -\frac{1}{L}\int_{-L}^{0}\cos\left(\frac{n\pi z}{L}\right)dz + \frac{1}{L}\int_{0}^{L}\cos\left(\frac{n\pi z}{L}\right)dz = 0$$
$$\text{for } n = 0,1,2\ldots \tag{4}$$

$$b_n = -\frac{1}{L}\int_{-L}^{0}\sin\left(\frac{n\pi z}{L}\right)dz + \frac{1}{L}\int_{0}^{L}\sin\left(\frac{n\pi z}{L}\right)dz = \begin{cases} 0 \text{ for } n = 0,2,4\ldots \\ \frac{4}{n\pi} \text{ for } n = 1,3,5\ldots \end{cases} \tag{5}$$

The Fourier series resulting, for $0 < |z| < L$, is

$$c_o = \frac{4}{\pi}\sum_{n=1}^{\infty}\frac{\sin\left[\frac{(2n-1)\pi z}{L}\right]}{(2n-1)} = \frac{4}{\pi}\sin\frac{\pi z}{L} + \frac{4}{3\pi}\sin\frac{3\pi z}{L} + \cdots \tag{6}$$

The solution to equation (1) has the form

$$c = \sum_{m=1}^{\infty}\left[A_m \sin(\lambda_m z) + B_m \cos(\lambda_m z)\right] e^{-\lambda_m^2 D_L t} \tag{7}$$

which upon application of the inlet boundary condition becomes

$$c = \sum_{n=1}^{\infty}\frac{4}{(2n-1)\pi}\sin\left[\frac{(2n-1)\pi z}{L}\right] e^{-\left[\frac{(2n-1)\pi}{L}\right]^2 D_L t} \tag{8}$$

or

$$c = \frac{4}{\pi}\sin\left(\frac{\pi z}{L}\right) e^{-\frac{\pi^2 D_L t}{L^2}} + \frac{4}{3\pi}\sin\left(\frac{3\pi z}{L}\right) e^{-\frac{9\pi^2 D_L t}{L^2}} + \frac{4}{5\pi}\sin\left(\frac{5\pi z}{L}\right) e^{-\frac{25\pi^2 D_L t}{L}} + \cdots \tag{8a}$$

which is a Fourier series modified by the exponential terms.

Now if experimental conditions are chosen so that the factor, $\frac{\pi^2 D_L t}{L^2}$, is in the range

$$0.5 < \frac{\pi^2 D_L t}{L^2} < 2$$

the second and succeeding terms become negligible, producing a wave which approaches a true sinusoidal function.

Run 28 is typical of the experimental waves introduced into the test section from the pre-bed filtering system. The experimental conditions which existed are:

Pre-bed: height		1.6 ft
particles		3 mm spheres
Flow rate:	u =	.07 ft/sec
Diffusivity:	D_L =	.002 ft^2/sec
Wave period		24 sec/cycle

Hence

$$t = \frac{1.6 \text{ ft}}{.07 \text{ ft/sec}} = 22.9 \text{ sec}$$

$$L = \frac{(.07 \text{ ft/sec})(24 \text{ sec/cycle})}{2} = .84 \text{ ft/cycle}$$

$$\frac{\pi^2 D_L t}{L^2} = \frac{(3.14)^2 (.002 \text{ ft}^2/\text{sec})(22.9 \text{ sec})}{(.84 \text{ ft/cycle})^2} = .66$$

Therefore

$$c = \frac{4}{\pi} e^{-.66} \sin \frac{\pi z}{L} + \frac{4}{3\pi} e^{-5.96} \sin \frac{3\pi z}{L} + \frac{4}{5\pi} e^{-16.6} \sin \frac{5\pi z}{L} \qquad (9)$$

or

$$c = .657 \sin \frac{\pi z}{L} + .0\dot{0}1 \sin \frac{3\pi z}{L} + \cdots \qquad (10)$$

The predicted outlet from the pre-bed, as calculated by the above equation, is compared with the experimental periodic wave in Figure 5.

C. STEP FUNCTION TECHNIQUE[7,11,25]

Consider now the partial-differential equation for the diffusion-convection flow of liquid through a packed bed

$$D_L \frac{\partial^2 c}{\partial z^2} - u \frac{\partial c}{\partial z} = \frac{\partial c}{\partial t} + \frac{1}{\epsilon} \frac{\partial \eta}{\partial t} \qquad (1)$$

in which the last term represents the adsorption of tracer on the particles. The additional relations

$$\left.\begin{aligned} c(z,0) &= 1 \qquad z > 0 \\ c(z,0) &= 0 \qquad z < 0 \end{aligned}\right\} \text{ Step function} \qquad (2)$$

$$c(0,t) = 0 \qquad t > 0 \qquad (3)$$

describe, respectively, the initial condition of the bed and the inlet fluid.

The assumption, concerning the mechanism of adsorption, that equilibruim is established at each point in the bed gives the relationship

$$\eta = k_1 c + k_2 \qquad (4)$$

which upon differentiation gives

$$\frac{\partial \eta}{\partial t} = k_1 \frac{\partial c}{\partial t} \qquad (5)$$

With the substitution of (5), equation (1) becomes

$$D_L \frac{\partial^2 c}{\partial z^2} - u \frac{\partial c}{\partial z} = \gamma \frac{\partial c}{\partial t} \qquad (6)$$

where

$$\gamma = 1 + \frac{k_1}{\epsilon} \; . \qquad (7)$$

For experiments in which the adsorption effect is negligible, $\gamma = 1$. The substitution of

$$c = g\, e^{\left[\frac{uz}{2D_L} - \frac{u^2 t}{4\gamma D_L}\right]} \tag{8}$$

into equation (6) and the boundary conditions (2) and (3) results in

$$\frac{D_L}{\gamma} \frac{\partial^2 g}{\partial z^2} = \frac{\partial g}{\partial t} \tag{9}$$

and

$$\begin{aligned} g(z,0) &= e^{-\frac{uz}{2D_L}} \qquad z > 0 \\ g(z,0) &= 0 \qquad\qquad\quad z < 0 \end{aligned} \tag{10}$$

$$g(0,t) = 0 \qquad t > 0 \tag{11}$$

The system of equations may be split into two problems. Separate variables by assuming solution to be of form

$$g = Z\, T \tag{12}$$

which when substituted in (9) gives

$$\frac{D_L}{\gamma} Z'' T = ZT' \tag{13}$$

or

$$\frac{Z''}{Z} = \frac{\gamma}{D_L} \frac{T'}{T} \tag{13a}$$

where the primes represent first or second derivatives. Since function on left can vary only with z and the one on right only with t, they must both equal a constant $-\alpha^2$; that is

$$\frac{Z''}{Z} = \frac{\gamma}{D} \frac{T'}{T} = -\alpha^2 \tag{14}$$

which results in two separate differential problems.

The solution of the first of the differential equations (14)

$$Z'' + \alpha^2 Z = 0 \tag{15}$$

that satisfies boundary condition

$$Z(0) = 0 \tag{16}$$

is

$$Z = C_1 \sin \alpha z. \tag{17}$$

The solution of the second of equations (14)

$$T^1 + \alpha^2 \frac{D_L}{\gamma} T = 0 \tag{18}$$

is then

$$T = C_2 e^{-\alpha^2 \frac{D_L}{\gamma} t} \tag{19}$$

Hence the solutions of equations (9) and (10) of the form $g = ZT$ are

$$C_n e^{-\alpha^2 \frac{D_L}{\gamma} t} \cdot \sin \alpha z \ . \tag{20}$$

Since the function is not periodic, and condition (11) must be satisfied for all values of z, the Fourier integral is employed to obtain the solution.[5] Multiply (20) by $(2/\pi)\, f(z') \sin \alpha z'$ and integrate with respect to the parameters α and z', which are independent of z and t, getting the function

$$g(z,t) = \frac{2}{\pi} \int_0^\infty e^{-\alpha^2 \frac{D_L}{\gamma} t} \sin \alpha z \, d\alpha \int_0^\infty f(z') \sin \alpha z' dz' \tag{21}$$

When $t = 0$, the integral on the right becomes the Fourier sine integral of $f(z)$

$$g(z,0) = f(z) = \frac{2}{\pi} \int_0^\infty \sin \alpha z \, d\alpha \int_0^\infty f(z') \sin \alpha z' dz' \tag{22}$$

Therefore, since f(z) satisfies conditions of Fourier integral theorem, solution is given by (21).

Applying the relationship

$$2 \sin \alpha z \sin \alpha z' = \cos [\alpha(z' - z)] - \cos [\alpha(z' + z)] \qquad (23)$$

and inverting the order of integration of (22) there results

$$g(z,t) = \frac{1}{\pi} \int_0^\infty \int_0^\infty e^{-\alpha^2 \frac{D_L}{\gamma} t} f(z') \left\{ \cos[\alpha(z' - z)] - \cos[\alpha(z' + z)] \right\} dz' \, d\alpha \qquad (24)$$

Using the integration formulas

$$\int_0^\infty e^{-\alpha^2 \frac{D_L}{\gamma} t} \cos[\alpha(z' - z)] \, d\alpha = \frac{\sqrt{\pi\gamma}}{2\sqrt{D_L t}} e^{-\left[\frac{\gamma(z-z')^2}{4D_L t}\right]} \qquad (25)$$

$$\int_0^\infty e^{-\alpha^2 \frac{D_L}{\gamma} t} \cos[\alpha(z' + z)] \, d\alpha = \frac{\sqrt{\pi\gamma}}{2\sqrt{D_L t}} e^{-\left[\frac{\gamma(z+z')^2}{4D_L t}\right]} \qquad (26)$$

equation (24) becomes

$$g(z,t) = \frac{\sqrt{\gamma}}{2\sqrt{\pi D_L t}} \int_0^\infty f(z') \left\{ e^{-\left[\frac{\gamma(z-z')^2}{4D_L t}\right]} - e^{-\left[\frac{\gamma(z+z')^2}{4D_L t}\right]} \right\} dz' \qquad (27)$$

Since $f(z') = e^{-\frac{uz'}{2D_L}}$, equation (27) expands to

$$g(z,t) = \frac{\sqrt{\gamma}}{2\sqrt{\pi D_L t}} \left\{ \int_0^\infty e^{-\frac{uz'}{2D_L} - \frac{\gamma(z-z')^2}{4D_L t}} dz' - \int_0^\infty e^{-\frac{uz'}{2D_L} - \frac{\gamma(z+z')^2}{4D_L t}} dz' \right\} \qquad (28)$$

Expanding the exponent and removing the constants of integration from the first integral, there results

$$e^{\frac{u^2t}{4D_L\gamma} - \frac{uz}{2D_L}} \int_0^\infty e^{-\frac{\gamma}{4D_Lt}(z' + \frac{ut}{\gamma} - z)^2} dz' \qquad (29)$$

Now let

$$\lambda = \frac{(z' + \frac{ut}{\gamma} - z)}{\sqrt{\frac{4D_Lt}{\gamma}}} \quad ; \quad d\lambda = \frac{dz'}{\sqrt{\frac{4D_Lt}{\gamma}}} \qquad (30)$$

and at

$$z' = 0 , \qquad \lambda = \frac{\frac{ut}{\gamma} - z}{\sqrt{\frac{4D_Lt}{\gamma}}}$$

$$z' = \infty , \qquad \lambda = \infty$$

Substituting (30) into equation (29) there results

$$\sqrt{\frac{\pi D_Lt}{\gamma}}\, e^{\frac{u^2t}{4D_L\gamma} - \frac{uz}{2D_L}} \frac{2}{\sqrt{\pi}} \int_{\left[\frac{\frac{ut}{\gamma} - z}{\sqrt{4D_Lt/\gamma}}\right]}^\infty e^{-\lambda^2} d\lambda \qquad (31)$$

For purposes of simplification let

$$S = \frac{D_L}{uz} \quad ; \quad R = \frac{ut}{z} \qquad (32),(33)$$

The complimentary error function is defined as

$$\operatorname{erfc}(x) = \frac{2}{\sqrt{\pi}} \int_x^\infty e^{-\lambda^2} d\lambda \qquad (34)$$

hence (31), with the substitution of (32) and (33), reduces to

$$\sqrt{\frac{\pi D_L t}{\gamma}}\; e^{\frac{u^2 t}{4D_L\gamma} - \frac{uz}{2D_L}}\; \operatorname{erfc}\left[\frac{R-\gamma}{\sqrt{4RS\gamma}}\right] \qquad (35)$$

In a like manner the second integral of (28) becomes

$$\sqrt{\frac{\pi D_L t}{\gamma}}\; e^{\frac{u^2 t}{4D_L\gamma} + \frac{uz}{2D_L}}\; \operatorname{erfc}\left[\frac{R+\gamma}{\sqrt{4RS\gamma}}\right] \qquad (36)$$

Substituting (35) and (36) in (28) an then returning to equation (7) the solution is

$$c(z,t) = \frac{1}{2}\left\{ e^{\left[\frac{u^2 t}{4D_L\gamma} - \frac{uz}{2D_L}\right]} \operatorname{erfc}\left[\frac{R-\gamma}{\sqrt{4RS\gamma}}\right] - e^{\left[\frac{u^2 t}{4D_L\gamma} + \frac{uz}{2D_L}\right]} \operatorname{erfc}\left[\frac{R+\gamma}{\sqrt{4RS\gamma}}\right] e^{\left[\frac{uz}{2D_L} - \frac{u^2 t}{4D_L\gamma}\right]} \right\} \qquad (37)$$

which reduces to

$$c(z,t) = \frac{1}{2}\left\{ \operatorname{erfc}\left[\frac{R-\gamma}{\sqrt{4RS\gamma}}\right] - e^{\frac{1}{S}} \operatorname{erfc}\left[\frac{R+\gamma}{\sqrt{4RS\gamma}}\right] \right\} \qquad (38)$$

the equation for the exit concentration profile for a step function inlet.

The slope of the concentration profile at the concentration midpoint which occurs at $R = \gamma$, can be determined by differentiating (38) with respect to R, and setting $R = \gamma$. Hence

$$\frac{dc}{dR} = \frac{1}{4\sqrt{\pi}}\left\{ \frac{R+\gamma}{\sqrt{R^3 S\gamma}}\, e^{-\left[\frac{R-\gamma}{\sqrt{4RS\gamma}}\right]^2} - \frac{R-\gamma}{\sqrt{R^3 S\gamma}}\, e^{\left[\frac{1}{S} - \left(\frac{R+\gamma}{\sqrt{4RS\gamma}}\right)^2\right]} \right\} \qquad (39)$$

and when $R = \gamma$

$$\left(\frac{dc}{dR}\right)_{R = \gamma} = \sqrt{\frac{1}{4\pi R^2 S}} \qquad (40)$$

D. PULSE FUNCTION TECHNIQUE

The pulse function technique is based on the fact that the response of a linear system to a unit impulse is the derivative of the response of the system to a unit step function. Wylie[41] presents proof of this for an analogous electrical system. Danckwerts[11] and Yagi and Miyauchi[42] also derive equivalent hypothesis for flow through reactors.

To obtain a physical interpretation of the pulse function technique it is necessary to refer to the foregoing method of Appendix I-C. In the step function technique, the concentration profiles or distribution functions for residence times were described by plots of F vs R as shown in Figure 18, where F is the fraction of tracer in the exit stream at time t,

$$F(t) = \frac{c(t)}{c(0)} \qquad (1)$$

and R is the residence time. As time t, or R in Figure 18, becomes infinite the fraction of tracer material approaches 1.0; i.e.,

$$\lim_{t \to \infty} F(t) = 1.0 \qquad (2)$$

Now define a new function

$$E(t) = \frac{d\,F(t)}{d\,t} \qquad (3)$$

so that E(t) is the rate of change of the fraction of tracer material in the exit stream. As a result, where "primes" refer to variables of integration:

$$F(t) = \int_0^t E(t')\,d\,t' \qquad (4)$$

and hence upon substituting (3) in (1) there results

$$\lim_{t\to\infty} F(t) = \lim_{t\to\infty} \int_0^t E(t')\, d\, t' = 1 \qquad (5)$$

The instantaneous rate at which the tracer material leaves the column is $\nu F(t)$ and the amount leaving in the interval 0 to t is

$$\nu \int_0^t F(t")\, d\, t" \qquad (6)$$

or

$$\nu \int_0^t \int_0^t E(t')\, d\, t'\, d\, t" \qquad (7)$$

where ν is the volumetric flow rate, ft^3/sec.

Suppose now that we suddenly inject a quantity Q of tracer material, moles tracer, into the flowing stream at time 0. If the concentration is large and the period of injection very small, the product becomes unity; i.e., in the limit an arbitrarily large concentration acting for an infinitesimal time produces a unit impulse. Now let c(t), moles tracer/ft^3 liquid, be the concentration of tracer in the exit stream at time t. Then $\nu c(t)$, moles tracer/hr, is the instantaneous rate at which the tracer leaves the bed, and

$$\nu \int_0^t c(t")\, dt" \qquad (8)$$

is the quantity of tracer (moles of tracer) leaving the bed in time 0 to t.

At time ∞ all the tracer will have left the column, and since the total amount that entered was defined as Q, the equation results;

$$Q = \nu \int_0^\infty c(t")\, dt" \qquad (9)$$

and also the fraction of tracer which had entered at time 0 and had left by time t can be defined by

$$\int_0^t \frac{\nu}{Q}\, c(t")\, dt" \tag{10}$$

Assume now that the tracer, as in the step function treatment, had been fed at the rate ν. During the time interval 0 to t the amount of all the material having left the bed is

$$\int_0^t \nu\, dt \tag{11}$$

Now consider the tracer as having entered during a series of small time increments, i.e., in a series of unit pulses, during time 0 to t. It has been shown that the fraction of tracer which has left the column at time t after entry can be represented by equation (10). Hence, the amount of tracer that has left the bed during time 0 to t is

$$\int_0^t \left[\int_0^t \frac{\nu}{Q}\, c(t")\, dt" \right] \nu dt' = \nu \int_0^t \frac{\nu}{Q} \int_0^t c(t")\, dt"\, dt' \tag{12}$$

But previously this quantity of tracer leaving in time 0 to t was given by equation (7), hence

$$\nu \int_0^t \frac{\nu}{Q} \int_0^t c(t")\, dt"\, dt' = \nu \int_0^t \int_0^t E(t")\, dt"\, dt' \tag{13}$$

Therefore

$$\frac{\nu\, c(t)}{Q} = E(t) = \frac{d\, F(t)}{d\, t} \tag{14}$$

which shows that the distribution function of the pulse is the derivative of the step function distribution.

From equation (5) there also follows

$$\lim_{t\to\infty} \int_0^t \frac{V\, c(t')}{Q}\, dt' = 1 \qquad (15)$$

which means the area under the distribution curve of the pulse function is equal to unity.

The formula for the concentration profile of the pulse function is then found by differentiating equation (39) of Appendix I-C which can be written in the form

$$c(z,t) = 1/2 \left\{ 1 - \operatorname{erf} \frac{R-\gamma}{\sqrt{4\,RS\gamma}} - e^{\frac{1}{S}} \left[1 - \operatorname{erf} \sqrt{\frac{R+\gamma}{4RS\gamma}} \right] \right\} \qquad (16)$$

Since[7]

$$\frac{d\ \operatorname{erf} x}{dx} = \frac{d}{dx}\left(\frac{2}{\sqrt{\pi}} \int_0^x e^{-\lambda^2}\, d\lambda \right) = \frac{2}{\sqrt{\pi}} e^{-x^2} \qquad (17)$$

the derivative of c(z,t) with respect to R becomes

$$\frac{d\ c(z,t)}{dR} = \frac{1}{2} \left\{ -\frac{2}{\sqrt{\pi}} e^{-\left[\frac{R-\gamma}{\sqrt{4RS\gamma}}\right]^2} \frac{\partial \left[\frac{R-\gamma}{\sqrt{4RS\gamma}}\right]}{\partial R} \right.$$
$$\left. \oplus \frac{2}{\sqrt{\pi}} e^{\frac{1}{S}} e^{-\left[\frac{R+\gamma}{\sqrt{4RS\gamma}}\right]^2} \frac{\partial \left[\frac{R+\gamma}{\sqrt{4RS\gamma}}\right]}{\partial R} \right\} \qquad (18)$$

where

$$\frac{\partial \left[\frac{R-\gamma}{\sqrt{4RS\gamma}}\right]}{\partial R} = \frac{1}{4} \left\{ \sqrt{\frac{1}{RS\gamma}} + \sqrt{\frac{\gamma}{R^3 S}} \right\} = \frac{R+\gamma}{\sqrt{R^3 S\gamma}} \qquad (19)$$

$$\frac{\partial\left[\frac{R+\gamma}{\sqrt{4RS\gamma}}\right]}{\partial R} = \frac{1}{4}\left\{\sqrt{\frac{1}{RS\gamma}} + \sqrt{\frac{\gamma}{R^3S}}\right\} = \frac{R-\gamma}{\sqrt{R^3S\gamma}} \qquad (20)$$

Since the dimensionless ratio, R, may be defined as

$$R = \frac{\nu t}{V} \qquad (21)$$

where V represents the void volume of the bed, equation (14) may be written

$$\frac{d\,F(t)}{dR} = \frac{\nu}{V}\,\frac{d\,F(t)}{dt} = \frac{\nu\,c(t)}{Q} \qquad (14a)$$

or

$$\frac{V\,c(t)}{Q} = \frac{d\,F(t)}{dR} \qquad (22)$$

Hence the pulse function distribution, $\frac{V\,c(t)}{Q}$, becomes

$$\frac{V\,c(t)}{Q} = \frac{1}{4\sqrt{\pi}}\left\{\frac{R+\gamma}{\sqrt{R^3S\gamma}}\,e^{-\left[\frac{R-\gamma}{\sqrt{4RS\gamma}}\right]^2} - \frac{R-\gamma}{\sqrt{R^3S\gamma}}\,e^{\left[\frac{1}{S} - \left(\frac{R+\gamma}{\sqrt{4RS\gamma}}\right)^2\right]}\right\} \qquad (23)$$

The maximum concentration of the pulse function occurs at $R = \gamma$, hence the equation for the peak point is

$$\left(\frac{V\,c(t)}{Q}\right)_{R=\gamma} = \frac{1}{2R\sqrt{\pi S}} \qquad (24)$$

APPENDIX II

SAMPLE CALCULATIONS

A. FREQUENCY RESPONSE TECHNIQUE - SINUSOIDAL WAVE

Experimental Data

Run 28

Column properties:

Height:	3.0 ft
Particle diameter:	3 mm spheres
	d_p = .133 in.
Porosity determination:	
Volume water added to packed column:	190.73 ml
Height of water displacement:	27.37 cm

Pre-bed properties:

Height:	1.5 ft
Particle diameter:	3 mm spheres

Liquid flow rate:

Rotometer III	.250

Chart speed: 960 in./hr

Period of sinusoidal wave: 24 seconds

Liquid temperature: 21.5°C

Photometer calibration:

	Inlet	Outlet	Conc.
Clear solution	9.01 mv	9.00 mv	0
Dye solution	1.27 mv	1.23 mv	1

Sinusoidal waves: Minimum and maximum readings in millivolts taken from recorder charts of inlet and outlet waves to determine amplitude ratio are presented below:

	Inlet		Outlet	
	Minimum	Maximum	Minimum	Maximum
1	1.61	6.89	2.67	4.07
2	1.61	6.88	2.58	4.06
3	1.61	6.84	2.57	4.03
4	1.61	6.84	2.54	4.02
5	1.61	6.84	2.55	4.01
6	1.61	6.84	2.54	4.03
7	1.61	6.91	2.60	4.07
8	1.61	6.80	2.57	4.00
9	1.61	6.79	2.53	3.97
10	1.61	6.85	2.54	4.02
Avg.	1.61	6.85	2.57	4.03

Calculated Data

Packing height:

The true packing height was determined as follows:

Gasket	.0 ft	0.1 in.
Column	3.0	0.0
Gasket	.0	0.1
Spacer packing	.0	0.25
	3.0 ft	.45 in. = 3.0375 ft

Porosity:

The porosity was determined prior to each set of runs by adding a known amount of water to the packed column and measuring the change in water levels.

$$\epsilon = \frac{(190.73 \text{ ml})}{(929 \text{ cm}^2/\text{ft}^2)(.02182 \text{ ft}^2)(27.37 \text{ cm})} = .344$$

Flow rates:

The true flow rate was obtained from the calibration chart in Appendix III-A. The superficial velocity through the unpacked column and the actual mean linear velocity in the packed column were calculated from known bed properties.

Flow rate: 0.235 gpm

Superficial velocity:

$$v_o = \frac{(.235 \text{ gal/min})(.1337 \text{ ft}^3/\text{gal})}{(60 \text{ sec/min})(.02182 \text{ ft}^2)} = .0240 \text{ ft/sec}$$

Interstitial velocity:

$$u = \frac{v_o}{\epsilon} = \frac{.0240 \text{ ft/sec}}{.344} = .0698 \text{ ft/sec}$$

Frequency:

The frequency was determined directly from the period, τ, as follows:

$$\omega = \frac{2\pi}{\tau} = \frac{2\pi \text{ radians}}{24 \text{ secs}} = .262 \text{ radians/sec}$$

Liquid properties:

The density was that of water and was obtained from Table 45, p. 175, Perry, J. H., "Chemical Engineers' Handbook". The viscosity, almost identical to that of water, was obtained from an experimentally determined

chart of viscosity versus temperature, Figure 32, Appendix III-C.

$$\rho = .998 \text{ gms/cc}$$

$$\mu = .972 \text{ cp}$$

Amplitude Ratio

The methods used to calibrate the photometers have been described in the section titled Evaluation of Data, page 52.

Inlet amplitude:

Inlet calibration:

$$c = \frac{\log A - \log y}{-m}$$

At $y = 9.01$, $c = 0$
$y = 1.27$, $c = 1$

Hence $A = 9.01$; $\log A = .9547$
$m = \log 1.27 - \log 9.01 = .1038 - .9547$
$= -.8509$

$$c = \frac{.9547 - \log y}{.8509}$$

Minimum and maximum:

$$c_{min} = \frac{.9547 - \log 1.61}{.8509} = \frac{.9547 - .2068}{.8509} = .879$$

$$c_{max} = \frac{.9547 - \log 6.85}{.8509} = \frac{.9547 - .8357}{.8509} = .140$$

Hence

$$A_i = .879 - .140 = .739$$

Outlet amplitude:

Outlet calibration: (follows same procedure as above)

$A = 9.00$; $\log A = .9542$
$m = \log 1.23 - \log 9.00 = .0899 - .9542$
$= -.8643$

$$c = \frac{.9542 - \log y}{.8643}$$

Minimum and maximum:

$$c_{min} = \frac{.9542 - \log 2.57}{.8643} = \frac{.9542 - .4099}{.8643} = .630$$

$$c_{max} = \frac{.9542 - \log 4.03}{.8643} = \frac{.9542 - .6053}{.8643} = .404$$

Hence

$$A_e = .630 - .404 = .226$$

Therefore the amplitude ratio is:

$$\frac{A_i}{A_e} = \frac{.739}{.226} = 3.27$$

and

$$\ln \frac{A_i}{A_e} = 1.1848$$

Calculation of D_L

The error in B resulting from the use of equation (12) is too large, hence equation (13) is employed.

$$\ln \frac{A_i}{A_e} = \frac{z\omega^2 D_L}{u^3} - \frac{5z\omega^4 D_L^3}{u^7}$$

$$1.185 = \frac{(3.038)(.262)^2 D_L}{(.0698)^3} - \frac{5(3.038)(.262)^4 D_L^3}{(.0698)^7}$$

$$1.185 = 612\, D_L - 8.83 \times 10^6\, D_L^3$$

By trial and error

$$D_L = .00207 \text{ ft}^2/\text{sec}$$

Calculation of modified Peclet number

$$Pe' = \frac{d_p\, u}{D_L} = \frac{(.133)(.0698)}{(12)(.00207)} = .374$$

Calculation of modified Reynolds number

$$Re' = \frac{d_p\, v_o\, \rho}{\mu} .$$

$$= \frac{(.133 \text{ ft})(.0240 \text{ ft/sec})(.998 \times 62.4 \text{ lb/ft}^3)}{(12)(.972 \times 6.72 \times 10^{-4} \text{ ft lb/sec})} = 25.4$$

B. FREQUENCY RESPONSE TECHNIQUE - NON-SINUSOIDAL WAVE

Experimental Data

Run 6

Column properties:

Height:	3.0 ft
Particle diameter:	1 mm spheres
	d_p = .039 in.
Porosity determination:	
Volume of water added to packed column:	176.51 ml
Height of water displacement:	25.63 cm

Pre-bed properties:

Height:	1.5 ft
Particle diameter:	25/30 mesh spheres

Liquid flow rate:	
Rotometer II	.0748
Chart speed:	240 in./hr
Period of non-sinusoidal wave:	74 seconds
Liquid temperature:	21.5°C

Photometer calibration:

	Inlet	Outlet	Conc.
Clear solution	9.00 mv	9.00 mv	0
Dye solution	1.14 mv	1.16 mv	1

Periodic waves: The recorder values given in millivolts of the inlet and outlet periodic waves at intervals of one-twelfth of a period are presented in Tables XII and XIII.

TABLE XII. CONCENTRATION VALUES FOR INLET PERIODIC WAVE, RUN 6

Radians		0 or 2π	$\pi/6$ (min)	$\pi/3$	$\pi/2$	$2\pi/3$	$5\pi/6$	π	$7\pi/6$ (max)	$4\pi/3$	$3\pi/2$	$5\pi/3$	$11\pi/6$
MILLIVOLTS	1	1.78	1.69	2.01	3.22	4.41	5.19	5.81	6.06	5.00	3.22	2.38	2.00
	2	1.78	1.69	2.02	3.22	4.49	5.31	5.84	6.09	5.01	3.22	2.37	2.00
	3	1.79	1.69	2.00	3.22	4.37	5.18	5.78	6.10	5.03	3.22	2.36	2.02
	4	1.81	1.72	2.02	3.22	4.42	5.23	5.84	6.09	5.00	3.22	2.38	2.01
	5	1.81	1.71	2.02	3.22	4.42	5.28	5.89	6.13	4.94	3.22	2.40	2.02
	6	1.83	1.72	2.01	3.22	4.41	5.21	5.84	6.12	5.02	3.22	2.39	2.01
	7	1.79	1.71	2.03	3.22	4.40	5.20	5.78	6.08	4.98	3.22	2.41	2.02
	8	1.80	1.72	2.02	3.22	4.46	5.21	5.79	6.05	4.98	3.22	2.39	2.01
	9	1.81	1.71	2.02	3.22	4.43	5.20	5.80	6.08	4.98	3.22	2.41	2.02
	10	1.82	1.72	2.04	3.22	4.40	5.22	5.80	6.08	5.03	3.22	2.39	2.01
	Avg.	1.80	1.71	2.02	3.22	4.42	5.22	5.82	6.09	5.00	3.22	2.39	2.01
Conc.		C_0 .781	C_1 .808	C_2 .726	C_3 .500	C_4 .347	C_5 .266	C_6 .214	C_7 .192	C_8 .288	C_9 .500	C_{10} .645	C_{11} .728

TABLE XIII. CONCENTRATION VALUES FOR OUTLET PERIODIC WAVE, RUN P6

Radians		0 or 2π	$\pi/6$	$\pi/3$	$\pi/2$	$2\pi/3$	$5\pi/6$	π	$7\pi/6$	$4\pi/3$	$3\pi/2$	$5\pi/3$	$11\pi/6$	Min. ($\pi/24$)	Max.
MILLIVOLTS	1	1.95	2.00	2.40	3.20	4.09	4.82	5.14	4.94	4.17	3.20	2.49	2.11	1.95	5.15
	2	1.97	2.00	2.41	3.20	4.09	4.82	5.14	4.95	4.18	3.20	2.49	2.11	1.97	5.15
	3	1.97	2.00	2.42	3.20	4.10	4.81	5.13	4.97	4.21	3.20	2.50	2.13	1.96	5.15
	4	2.00	2.03	2.42	3.20	4.10	4.83	5.17	4.99	4.17	3.20	2.50	2.14	1.99	5.18
	5	1.98	2.00	2.39	3.20	4.10	4.83	5.16	4.95	4.17	3.20	2.51	2.13	1.97	5.16
	6	1.99	2.02	2.42	3.20	4.12	4.86	5.15	4.97	4.20	3.20	2.51	2.13	1.99	5.16
	7	1.99	2.03	2.47	3.20	4.11	4.82	5.14	4.96	4.18	3.20	2.51	2.13	1.98	5.15
	8	2.00	2.03	2.42	3.20	4.11	4.83	5.15	4.98	4.18	3.20	2.50	2.13	2.00	5.16
	9	2.00	2.02	2.39	3.20	4.11	4.84	5.16	4.97	4.19	3.20	2.50	2.14	1.99	5.17
	10	2.00	2.03	2.41	3.20	4.11	4.84	5.16	4.98	4.20	3.20	2.51	2.13	2.00	5.17
	Avg.	1.99	2.02	2.42	3.20	4.11	4.83	5.15	4.97	4.19	3.20	2.50	2.13	1.98	5.16
Conc.		.732	.725	.637	.500	.378	.298	.267	.285	.368	.500	.619	.698	.734	.266

Calculated Data

Calculations described in the previous section of the appendix are only summarized in this section.

Packing height:

Gasket	.0 ft	0.1 in.
Column	3.0	0.0
Gasket	.0	0.1
	3.0 ft	0.2 in. = 3.010 ft

Porosity, ϵ:

$$\epsilon = \frac{(176.51)}{(929)(.02182)(25.63)} = .340$$

Flow rates:

Flow rate: .0744 gpm

Superficial velocity:

$$v_o = \frac{(.0744)(.1337)}{(60)(.02182)} = .00760 \text{ ft/sec}$$

Interstitial velocity:

$$u = \frac{.00760}{.340} = .0224 \text{ ft/sec}$$

Frequency of periodic wave:

$$\omega = \frac{2\pi}{74} = .0850 \text{ rad/sec}$$

Liquid properties:

$$\rho = .998 \text{ gms/cc}$$

$$\mu = .972 \text{ cp}$$

Photometer calibration:

Inlet:

$$\log 9.00 = .9542$$

$$m = \log 1.14 - \log 9.00$$
$$= .0569 - .9542 = -.8973$$

Hence

$$c = \frac{.9542 - \log y}{.8973}$$

Outlet:

$$\log 9.00 = .9542$$

$$m = \log 1.16 - \log 9.00$$
$$= .0645 - .9542 = -.8898$$

Hence

$$c = \frac{.9542 - \log y}{.8898}$$

Inlet periodic concentration values:

The values of the inlet concentration wave at intervals of one-twelfth of a period were obtained by averaging a series of ten periodic inlet waves as shown in Table XII. The recorder values given in millivolts were converted to concentration units by the above equation for the inlet photometer calibration. The minimum and maximum values of the outlet waves are presented in Table XIII.

Harmonic analysis of periodic inlet wave

A 12-ordinate numerical scheme of harmonic analysis was used to determine the coefficients of the Fourier series having the form

$$c = \frac{a_o}{2} + a_1 \cos\theta + b_1 \sin\theta + a_2 \cos 2\theta + b_2 \sin 2\theta + \ldots .$$

The derivation of the method and the layout employed in the calculations is presented in Wylie[41].

Assume that the period of the concentration wave is 2π, so that the interval between the concentration ordinate is $\Delta z = \pi/6$. Applying the trapezoidal rule to the definitions of a_n and b_n there results

$$a_n = \frac{1}{\pi}\left[\Delta z \left(\frac{c_o \cos(nz_o)}{2} + c_1 \cos(nz_1) + \ldots c_{11} \cos(nz_{11}) + \frac{c_{12} \cos(nz_{12})}{2}\right)\right]$$

$$b_n = \frac{1}{\pi}\left[\Delta z \left(\frac{c_o \sin(nz_o)}{2} + c_1 \sin(nz_1) + \ldots c_{11} \sin(nz_{11}) + \frac{c_{12} \sin(nz_{12})}{2}\right)\right]$$

where

$$\Delta z = \frac{\pi}{6} \ , \ z_k = \frac{k\pi}{6} \ , \text{ and } c_k = f(\frac{k\pi}{6})$$

Because of the periodicity of the wave $c_o = c_{12}$. Also

$$\cos(nz_o) = \cos 0 = 1$$

$$\cos(nz_{12}) = \cos 2\pi = 1 \ ;$$

hence the first and last terms in the series for a_n are identical and can be combined. Moreover,

$$\sin(nz_o) = \sin 0 = 0$$

$$\sin(nz_{12}) = \sin 2\pi = 0$$

and thus the first and last terms in series for b_n are zero. The sums can be further simplified by noting that

$$\cos \frac{n(12 - k)\ \pi}{6} = \cos \frac{nk\pi}{6}$$

and

$$\sin \frac{n(12 - k)\pi}{6} = -\sin \frac{nk\pi}{6}$$

which shows that cosine terms in the first series are symmetrical about the term $c_o \sin(n\pi)$ and that the sine factors in the second series are negatively symmetrical about the term $c_6 \sin(n\pi)$. Hence the series become

$$a_n = \frac{1}{6} \left[c_o + (c_1 + c_{11}) \cos \frac{n\pi}{6} + \ . \ . \ .(c_5 + c_7) \cos \frac{5n\pi}{6} + c_6 \cos(n\pi) \right]$$

$$b_n = \frac{1}{6}\left[(c_1 - c_{11}) \sin\frac{n\pi}{6} + \ldots (c_5 - c_7) \sin\frac{5n\pi}{6}\right]$$

The tabular form for this process for forming the sums and differences of the given ordinates is as follows:

	c_o .781	c_1 .807 c_{11} .728	c_2 .726 c_{10} .645	c_3 .500 c_9 .500	c_4 .347 c_8 .288	c_5 .266 c_7 .193	c_6 .214
Sum	s_o .781	s_1 1.535	s_2 1.372	s_3 1.000	s_4 .635	s_5 .459	s_6 .214
Diff		d_1 .080	d_2 .081	d_3 0.000	d_4 .059	d_5 .073	

In terms of s's and d's, the series becomes

$$a_n = \frac{1}{6}\left[s_o + s_1 \cos\frac{n\pi}{6} + \ldots + s_5 \cos\frac{5n\pi}{6} + s_6 \cos(n\pi)\right]$$

$$b_n = \frac{1}{6}\left[d_1 \sin\frac{n\pi}{6} + \ldots + d_5 \sin\frac{5n\pi}{6}\right]$$

If n is an even number the cosine factors in a_n are symmetrical about the middle term $s_3 \cos(n\pi/2)$ and the sine factors in b_n are negatively symmetrical about the middle term, $d_3 \sin(n\pi/2)$. Therefore

$$\left.\begin{aligned} a_n &= \frac{1}{6}\left[(s_o + s_6) + (s_1 + s_6)\cos\frac{n\pi}{6} + (s_2 + s_4)\cos\frac{n\pi}{3} + s_3 \cos\frac{n\pi}{2}\right] \\ b_n &= \frac{1}{6}\left[(d_1 - d_5)\sin\frac{n\pi}{6} + (d_2 - d_4)\sin\frac{n\pi}{3} + d_3 \sin\frac{n\pi}{2}\right] \end{aligned}\right\} \text{ n even}$$

Also if n is odd, the cosine terms in a_n are negatively symmetrical and the sine terms in b_n are symmetrical. Hence

$$\left.\begin{aligned} a_n &= \frac{1}{6}\left[(s_o - s_6) + (s_1 - s_5)\cos\frac{n\pi}{6} + (s_2 - s_4)\cos\frac{n\pi}{3} \right. \\ &\qquad \left. + s_3 \cos\frac{n\pi}{2}\right] \\ b_n &= \frac{1}{6}\left[(d_1 + d_5)\sin\frac{n\pi}{6} + (d_2 + d_4)\sin\frac{n\pi}{3} + d_3 \sin\frac{n\pi}{2}\right] \end{aligned}\right\} \text{ n odd}$$

The above processes can be organized in the following tabular forms:

	s_o .781	s_1 1.535	s_2 1.372	s_3 1.000
	s_6 .214	s_5 .459	s_4 .635	
Sums	e_o .995	e_1 1.994	e_2 2.007	e_3 1.000
Differences	f_o .567	f_1 1.076	f_2 .737	

	d_1 .080	d_2 .081	d_3 .000
	d_5 .073	d_4 .059	
Sums	g_1 .153	g_2 .140	g_3 .000
Differences	h_1 .007	h_2 .022	

Substituting these quantities and the appropriate trignometric forms in the series for a_n and b_n, there results

$$a_o = \frac{1}{6}\left[(e_o + e_3) + (e_1 + e_2)\right] = \frac{1}{6}\left[j_1 + j_2\right]$$

$$a_2 = \frac{1}{6}\left[(e_o - e_3) + 1/2(e_1 - e_2)\right] = \frac{1}{6}\left[k_1 + 1/2\, k_2\right]$$

$$= \frac{1}{6}\left[k_1 + k_2{}^*\right]$$

$$a_4 = \frac{1}{6}\left[(e_o + e_3) - 1/2(e_1 + e_2) \right] = \frac{1}{6}\left[j_1 - 1/2\ j_2 \right]$$

$$= \frac{1}{6}\left[j_1 - j_2^* \right]$$

$$a_6 = \frac{1}{6}\left[(e_o - e_3) - (e_1 - e_2) \right] = \frac{1}{6}\left[k_1 - k_2 \right]$$

$$b_2 = \frac{1}{6}\left[\frac{\sqrt{3}}{2} (h_1 + h_2) \right] = \frac{1}{6}\left[h_1^* + h_2^* \right]$$

$$b_4 = \frac{1}{6}\left[\frac{\sqrt{3}}{2} (h_1 - h_2) \right] = \frac{1}{6}\left[h_1^* - h_2^* \right]$$

$$b_6 = 0$$

$$a_1 = -\frac{1}{6}\left[(f_o + 1/2\ f_2) + \frac{\sqrt{3}}{2} f_1 \right] = \frac{1}{6}\left[(f_o + f_2^*) + f_1^* \right]$$

$$= \frac{1}{6}\left[p + f_1^* \right]$$

$$a_3 = \frac{1}{6}\left[f_o - f_2 \right]$$

$$a_5 = \frac{1}{6}\left[(f_o + 1/2\ f_2) - \frac{\sqrt{3}}{2} f_1 \right] = \frac{1}{6}\left[p - f_1^* \right]$$

$$b_1 = \frac{1}{6}\left[(1/2\ g_1 + g_3) + \frac{\sqrt{3}}{2} g_2 \right] = \frac{1}{6}\left[(g_1^* + g_3) + g_2^* \right]$$

$$= \frac{1}{6}\left[q + g_2^* \right]$$

$$b_3 = \frac{1}{6}(g_1 - g_3)$$

$$b_5 = \frac{1}{6}\left[(1/2\, g_1 + g_3) - \frac{\sqrt{3}}{2} g_2\right] = \frac{1}{6}\left[q - g_2^*\right]$$

Hence, determining the values of j's and k's as follows

	e_o .995	e_1 1.994
	e_3 1.000	e_2 2.007
Sums	j_1 1.995	j_2 4.001
Differences	k_1 - .005	k_2 - .013

and the values of j*'s, k*'s, and h*'s

$$j_2^* = .5j_2 = 2.000 \qquad h_1^* = .866h_1 = .006$$
$$k_2^* = .5k_2 = -.006 \qquad h_2^* = .866h_2 = .019$$

the tabular form for the calculation of a_o, a_2, a_4, a_6, b_2 and b_4 results

	j_1 1.995 j_2 4.001	k_1 -.005 k_2^* -.006	j_1 1.995 j_2^* 2.000	k_1 -.005 k_2 -.013	h_1^* .006 h_2^* .019
Sum	$6a_o = 5.996$	$6a_2 = -.011$			$6b_2 = .025$
Diff			$6a_4 = -.005$	$6a_6 = .008$	$6b_4 = -.013$

Likewise, determining the values of f*'s, g*'s, p and q

$$f_2^* = .5f_2 = .367 \qquad f_1^* = .866f_1 = .933$$
$$g_1^* = .5g_1 = .076 \qquad g_2^* = .866g_2 = .121$$

$$p = f_o + f_2^* = .567 + .367 = .934$$

$$q = g_1^* + g_3 = .076 + .000 = .076$$

there results the tabular form for the calculation of a_1, a_3, a_5, b_1, b_3, and b_5

	p .934	f_o .567	q .076	g_1 .153
	f_1* .933	f_2 .737	g_2* .121	g_3 .000
Sum	$6a_1 = 1.867$		$6b_1 = .197$	
Diff	$6a_5 = .001$	$6a_3 = .170$	$6b_5 = -.045$	$6b_3 = .153$

The Fourier series representing the inlet periodic wave, with the coefficients as determined above but omitting negligible terms is then:

$$c = .500 + .311 \cos \omega\theta + .028 \cos 3\omega\theta + .033 \sin \omega\theta + .025 \sin 3\omega\theta - .008 \sin 5\omega\theta$$

The corresponding Fourier series for the outlet wave is then:

$$c = .500 + 311e^{-B} \cos \delta + .028e^{-9B} \cos 3\delta + .033e^{-B} \sin \delta + .025e^{-9B} \sin 3\delta - .008e^{-25B} \sin 5\delta$$

Calculation of B

The maximum concentration, c_{max}, and the corresponding angle, δ, were averaged for ten outlet waves and found to be:

$$c_{max} = .734 \quad \text{at} \quad \delta = \frac{\pi}{24}$$

Substituting this point into the above Fourier series for the outlet wave

$$.734 = .500 + .311e^{-B} \cos \pi/24 + .028\, e^{-9B} \cos \pi/8 + .033e^{-B} \sin \pi/24 + .025\, e^{-9B} \sin \pi/8 - .008\, e^{-25B} \sin 5\pi/24$$

and solving by trial and error procedure for B, there results

$$B = .2841$$

Using this value of B, the outlet wave can be calculated from the Fourier series representing the exit wave and compared with the experimental data. Figure 17 is a comparison of the calculated and experimental outlet waves for Run 6.

Calculation of D_L

The axial diffusivity was then calculated from the formula

$$B = \frac{z\,\omega^2\,D_L}{u^3}$$

or

$$D_L = \frac{(.0224 \text{ ft/sec})^3\,(.2841)}{(.0850 \text{ rad/sec})^2\,(3.01 \text{ ft})} = .000147 \text{ ft}^2/\text{sec}$$

Calculation of modified Peclet number

$$Pe' = \frac{(.039)\,(.0224)}{(12)\,(.000147)} = .496$$

Calculation of modified Reynolds number

$$Re' = \frac{d_p\,v_o\,\rho}{\mu} = \frac{(.039)(.00760)(62.4 \times .998)}{(12)(6.72 \times .972 \times 10^{-4})} = 2.36$$

Comparison of methods of evaluation

Assuming wave was sinusoidal:

Inlet amplitude = $A_i = .808 - .192 = .616$

Outlet amplitude = $A_e = .734 - .266 = .468$

$$\frac{A_i}{A_e} = \frac{.616}{.468} = 1.320$$

$$\ln \frac{A_i}{A_e} = .278 = B = \frac{z\,\omega^2\,D_L}{u^3}$$

$$\text{or } D_L = \frac{(.0224)^3\,(.278)}{(.0850)^2\,(3.01)} = .000144 \text{ ft}^2/\text{sec}$$

Hence the error in this value of axial diffusivity, obtained by assuming the periodic function to be sinusoidal, is well within the experimental error.

C. PULSE FUNCTION TECHNIQUE

Experimental Data

Run P6

Column properties:

Height of packing:	3.11 ft
Particle diameter:	1 mm spheres
	d_p = .039 in.
Porosity determination:	
Volume water added to packed column:	88.35 ml
Height of water displacement:	12.81 cm

Liquid flow rate:	
Rotometer II	.030
Liquid temperature:	29.5°C
Chart speed:	240 in./hr
Pulse length:	on-off flick of switch
Photometer calibration:	
Clear solution	9.00 mv

Pulse concentration profile: The millivolt readings of three pulse waves taken from recorder charts at intervals of six seconds (60 seconds for pulse tails) are presented in Table XIV.

Calculated Data

Calculations described in the previous sections of the appendix are only summarized in this section.

Porosity:

$$\epsilon = \frac{(88.35)}{(929)\ (.02182)\ (12.81)} = .340$$

Flow rates:

Flow rate (corrected): .0303 gpm

Superficial velocity:

$$v_o = \frac{(.0303)(.1337)}{(60)(.02182)} = .00309 \text{ ft/sec}$$

TABLE XIV. PULSE CONCENTRATION PROFILES - RUN P6

Time After Injection of Pulse sec	Pulse C Recorder Reading mv	Pulse C Conc gm/li x 10^2	Pulse D Recorder Reading mv	Pulse D Conc gm/li x 10^2	Pulse F Recorder Reading mv	Pulse F Conc gm/li x 10^2
276	9.00	0	9.00	0	9.00	0
282	9.00	0	8.94	0019	8.94	0019
288	8.94	0019	8.79	0069	8.82	0059
294	8.83	0056	8.56	0146	8.63	0122
300	8.65	0116	8.22	0265	8.36	0214
306	8.32	0229	7.75	0436	8.02	0336
312	8.10	0307	7.14	0676	7.62	0486
318	7.75	0436	6.37	1007	7.18	0659
324	7.36	0587	5.42	1479	6.66	0879
330	6.79	0822	4.35	2120	6.05	1158
336	5.99	1187	3.20	3016	5.10	1656
342	5.04	1690	2.09	4258	4.00	2364
348	4.29	2160	1.38	5468	3.09	3117
354	3.94	2408*	1.06	6238	2.54	3689
360	4.00	2364	1.02	6350*	2.43	3818*
366	4.48	2033	1.26	5734	2.70	3511
372	5.33	1527	1.96	4445	3.44	2804
378	6.31	1034	3.17	3043	4.57	1976
384	7.19	0655	4.63	1938	5.79	1286
390	7.81	0413	6.02	1172	6.85	0797
396	8.19	0275	7.06	0709	7.61	0490
402	8.90	0201	7.68	0463	8.09	0311
408	8.53	0156	7.95	0362	8.33	0225
414	8.60	0132	8.12	0300	8.44	0187
420	8.64	0119	8.24	0258	8.49	0170
426	8.68	0105	8.30	0236	8.53	0156
432	8.71	0096	8.34	0222	8.57	0142
438	8.73	0089	8.38	0207	8.60	0132
444	8.76	0079	8.41	0198	8.62	0126
450	8.78	0072	8.45	0183	8.64	0120
	Σ (conc.)	1.9367×10^{-2}		5.1017×10^{-2}		3.1018×10^{-2}
	$\Delta R = \frac{6 \text{ sec}}{341.6 \text{ sec}} = .01756$					
480	8.86	0046	8.60	0132	8.74	0085
540	8.92	0026	8.79	0069	8.88	0039
600	8.98	0006	8.89	0036	8.97	0010
660	9.00	0	8.95	0016	8.99	0003
720	9.00	0	8.99	0003	9.00	0
780	9.00	0	9.00	0	9.00	0
	Σ (conc.)	$.0078 \times 10^{-2}$		$.0256 \times 10^{-2}$		$.0137 \times 10^{2}$
	$\Delta R = \frac{60 \text{ sec}}{341.6 \text{ sec}} = .1756$					

*Note: Maximum value of pulse waves

Pulse	C	D	F	Avg.
Time, seconds	356.4	357.7	358.5	---
Recorder reading, mv	3.93	1.01	2.42	---
R	1.043	1.047	1.050	1.047
Concentration, gms/li x 10^2	.2416	.6379	.3830	.421

Interstitial velocity:

$$u = \frac{(.00309)}{(.340)} = .00910 \text{ ft/sec}$$

Liquid properties:

.996 gms/cc

.812 cp

Dimensionless ratio, R:
Time for R = 1

$$\frac{3.11 \text{ ft}}{.00910 \text{ ft/sec}} = 341.6 \text{ seconds}$$

Wave Concentration Profile

The millivolt readings taken from the recorder traces of the pulse waves are converted to concentration units of gms/li by the photometer calibration formula

$$c = \frac{.9542 - \log y}{148.92}$$

where y is the millivolt reading. The concentrations of the pulse waves are also presented in Table XIV.

The area under the pulse profiles is obtained by numerical integration as follows:

$$\text{Area} = \int_0^\infty c\,dR = (\Sigma c)(\Delta R)$$

Hence

$$10^2[(\Delta R)(\Sigma c)]_{\text{Pulse C}} = (.01756)(1.937)+(.1756)(.0078) = .03539 \text{ gm/li}$$

$$10^2[(\Delta R)(\Sigma c)]_{\text{Pulse D}} = (.01756)(5.102)+(.1756)(.0256) = .09402 \text{ gm/li}$$

$$10^2[(\Delta R)(\Sigma c)]_{\text{Pulse F}} = (.01756)(3.102)+(.1756)(.0137)$$

$$= .05689 \text{ gm/li}$$

and average area = $.0621 \times 10^{-2}$ gm/li

The area under a concentration profile for a unit pulse is equal to one, when the ordinate is in terms of the dimensionless concentration ratio, Vc/Q; hence by multiplying each of the concentration points of a pulse wave by the reciprocal of the area calculated for that pulse wave, a concentration profile with Vc/Q as ordinate is obtained. Hence the peak points for each pulse are obtained as follows:

$$\left(\frac{Vc}{Q}\right)_{\substack{R = 1.043 \\ \text{Pulse C}}} = \frac{.2416 \times 10^{-2}}{.03539 \times 10^{-2}} = 6.8274$$

$$\left(\frac{Vc}{Q}\right)_{\substack{R = 1.047 \\ \text{Pulse D}}} = \frac{.6379 \times 10^{-2}}{.09402 \times 10^{-2}} = 6.7820$$

$$\left(\frac{Vc}{Q}\right)_{\substack{R = 1.050 \\ \text{Pulse F}}} = \frac{.3830 \times 10^{-2}}{.05689 \times 10^{-2}} = 6.7326$$

The average $(Vc/Q)_{max}$ of the three pulse waves is 6.7807 at an average R of 1.047.

Calculation of D_L

The value of D_L is found by substituting the experimental values in the formula

$$\left(\frac{Vc}{Q}\right)_{max} = \frac{1}{2R\sqrt{\pi S}} \qquad \text{where } R = R_{\left(\frac{Vc}{Q}\right)_{max}}$$

or

$$\sqrt{S} = \frac{1}{2R\sqrt{\pi}\left(\frac{Vc}{Q}\right)_{max}} = \frac{1}{(2)(1.772)(1.0464)(6.7807)} = .03976$$

$$S = .001581 = \frac{D_L}{zu}$$

$$D_L = Szu = (.001581)(3.11 \text{ ft})(.00910 \text{ ft/sec})$$

$$= .0000447 \text{ ft}^2/\text{sec}$$

Reynolds number:

$$Re = \frac{d_p v_o \rho}{\mu} = \frac{(.039)(.00309)(.996 \times 62.4)}{(12)(6.72 \times .812 \times 10^{-4})} = 1.15$$

Peclet number:

$$Pe = \frac{d_p u}{D_L} = \frac{(.039)(.00910)}{(12)(.0000447)} = .661$$

APPENDIX III

CALIBRATION DATA

A. Flowmeter Calibration Curves - Figure 30

B. Photometer Calibration Curve - Figure 31

C. Solution Viscosity vs. Temperature - Figure 32

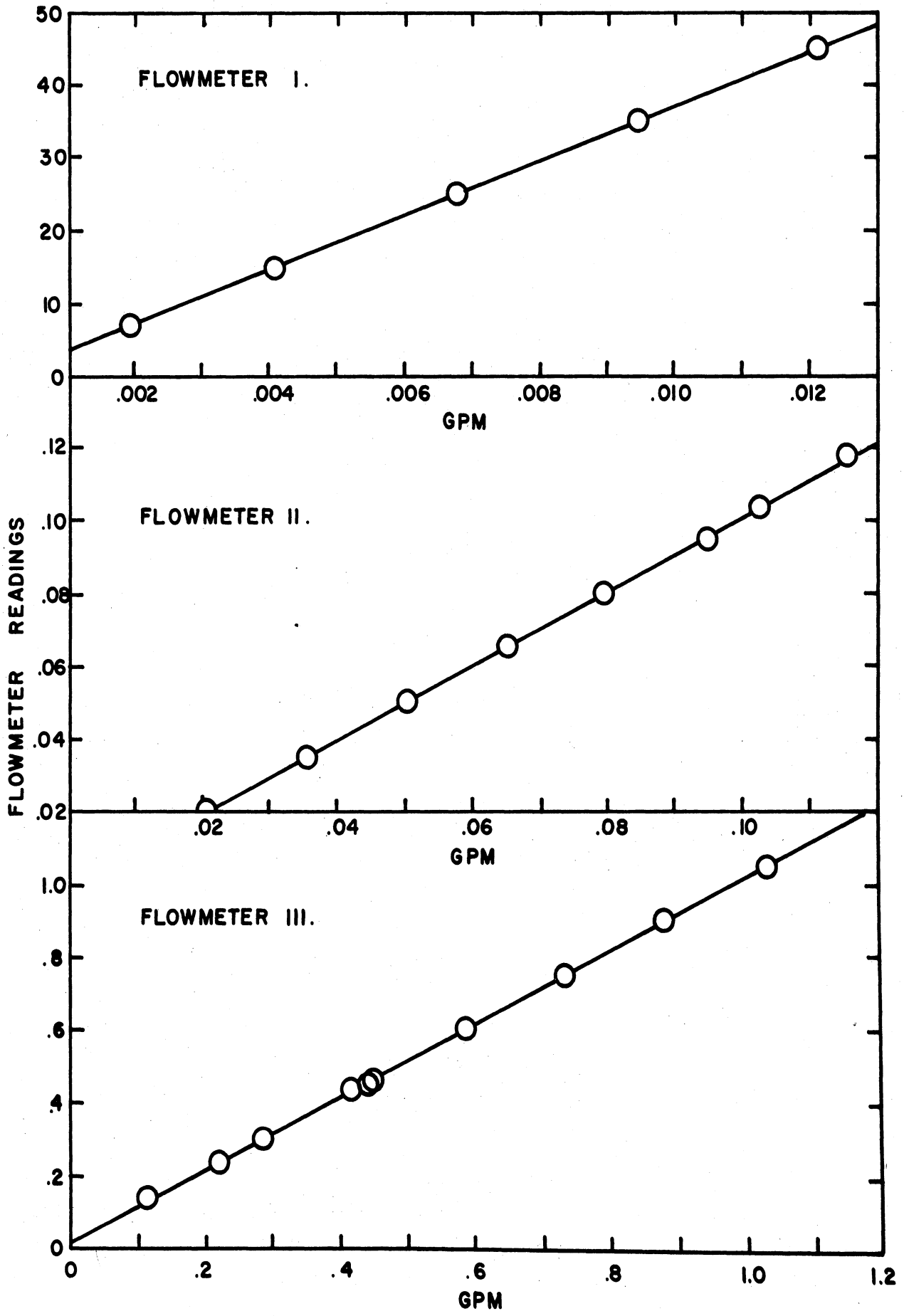

FIGURE 30 - FLOWMETER CALIBRATION CURVES

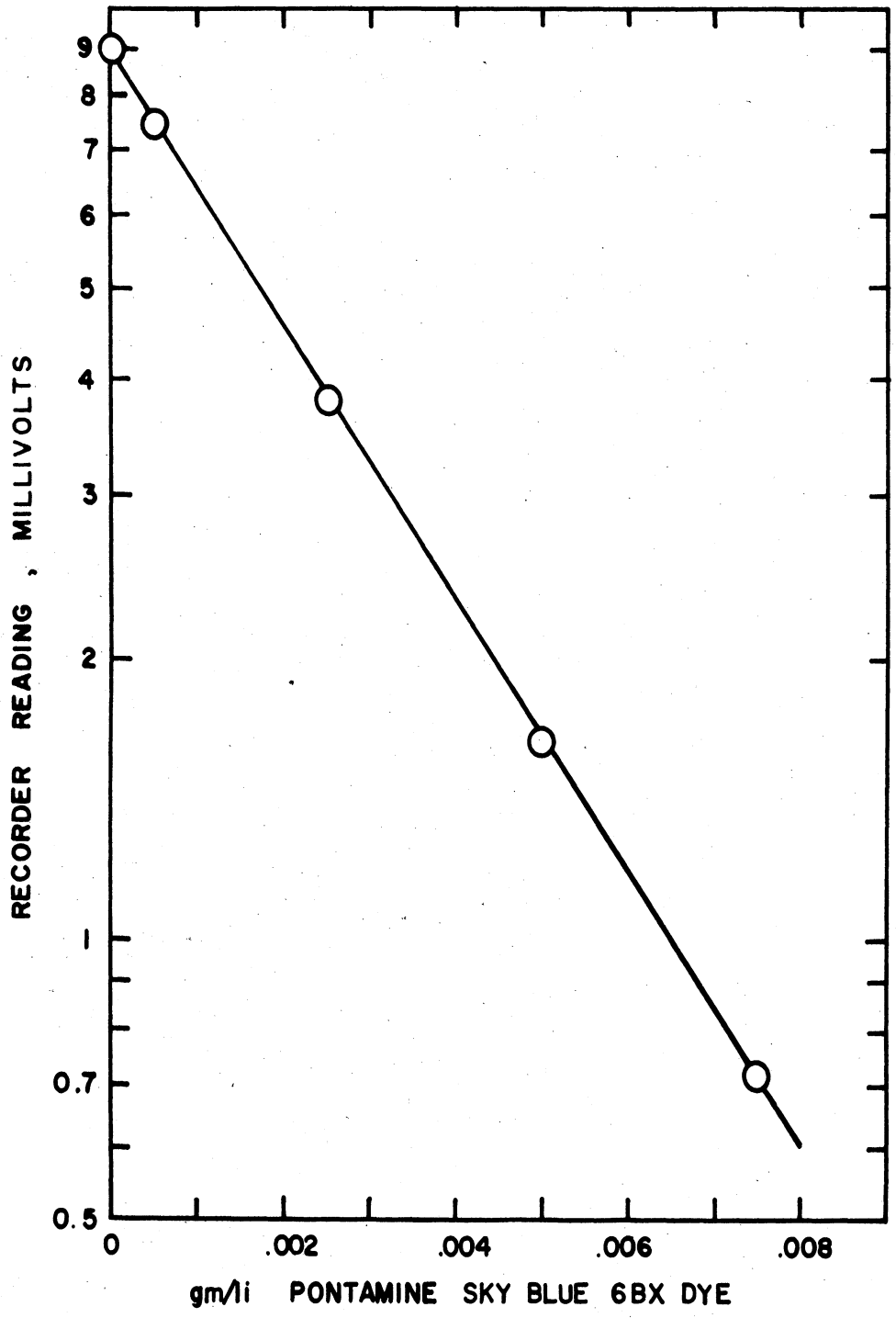

FIGURE 31 - PHOTOMETER CALIBRATION CURVES - INLET AND OUTLET - PONTAMINE SKY BLUE 6BX DYE IN DISTILLED WATER BUFFERED WITH $KHC_8H_4O_4$ (0.001 MOLAR)

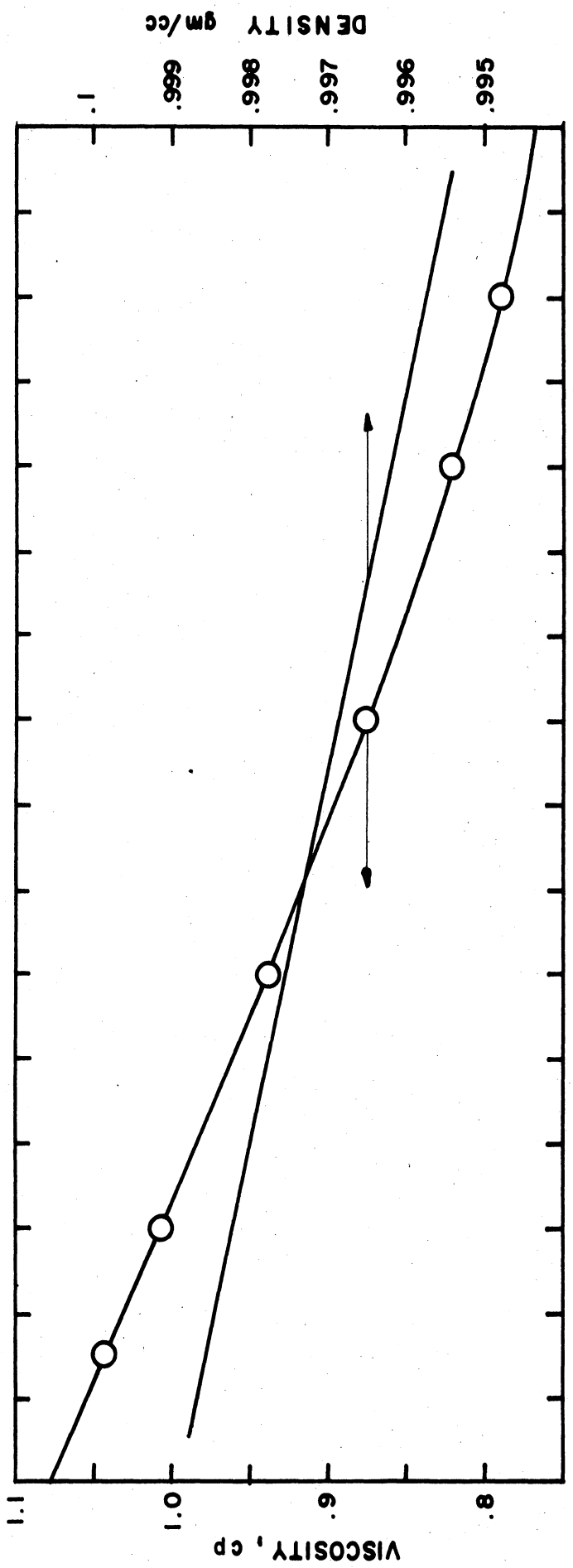

FIGURE 32 - SOLUTION VISCOSITY VS TEMPERATURE

NOMENCLATURE

a = constant, slope

a_n = coefficients of cosine terms of Fourier series

A = constant of photometer calibration (log A = intercept)

A_e = outlet amplitude

A_i = inlet amplitude

$A(0)$ = amplitude of inlet concentration waves

$A(z)$ = amplitude of concentration wave at z

$A_n(0)$ = amplitude of n-th harmonic in periodic wave

b = constant, slope

b_n = coefficients of sine terms of Fourier series

B = function representative of the decrease in amplitude of outlet wave

c = concentration of tracer in solution, moles/unit volume or gms/unit volume

c_m = mean composition about which concentration oscillates in frequency response experiments

c_n = concentration values employed in numerical harmonic analysis

c_o = initial concentration of solution admitted to bed

C = constant, (log C = intercept)

C_1 = constant, (log C_1 = intercept)

$-\frac{\partial c}{\partial y}$ = concentration gradient, moles/ft^3/ft

d_p = particle diameter, inches

d_t = tube or column diameter, in. or ft

D_L = effective axial diffusivity (in longitudinal direction), ft^2/sec

D_R = effective radial diffusivity, ft^2/sec

D_T = total effective diffusivity, ft^2/sec

D_v = molecular diffusivity, $ft^2/$ sec

I = intensity of emergent light beam

I_o = intensity of incident light beam

k = reaction-velocity constant

k_n = adsorption velocity constant, sec^{-1}

K = absorption coefficient

m = constant of photometer calibration, slope

n = number of harmonic

N = mass transfer rate, moles/sec-ft^2

Pe = Peclet number; radial, $d_p u/D_R$ or axial, $d_p u/D_L$

Q = quantity of tracer injected in pulse function experiments, moles

r = radial coordinate in cylindrical coordinate system

R = dimensionless time ratio, ut/z

Re = Reynolds number, $d_p\ v_o\ \rho/\mu$

S = dimensionless diffusivity ratio, D_L/zu

t = time, secs

u = mean linear velocity (interstitial velocity), ft/sec

v_o = superficial velocity based on empty column, ft/sec

V = void volume of bed, ft^3

x = fraction of reactant which has reacted during passage through a reactor

y = recorder reading, millivolts

z = longitudinal coordinate in cylindrical coordinate system

Other Symbols:

γ = function of adsorption velocity constant, equivalent to $1 + \frac{k_1}{\epsilon}$

δ = angle of periodic wave, equivalent to $(\omega t - \varphi)$

δ_E = mixing diffusivity, ft^2/sec

ϵ = fraction void or porosity of packed bed

η = amount of tracer adsorbed on particle surface, moles/unit volume of bed

μ = viscosity of solution, cp

ν = volumetric flow rate, ft^3/sec

ρ = density of solution, gms/cc

τ = period of periodic function, secs

φ = function representative of the phase shift of outlet wave

ψ_n = phase lag of n-th harmonic in periodic wave

ω = angular frequency of periodic wave, rad/sec

∞ = infinity

∂ = partial derivative

BIBLIOGRAPHY

1. Ando, N., Jour. Chem. Soc. Japan, 64, 1192 (1943).

2. Baron, T., Chem. Eng. Prog., 48, 118 (1952).

3. Bernard, R. A., and Wilhelm, R. H., Chem. Eng. Prog., 46, 233 (1950).

4. Brown, G. G., et al., Unit Operations, Wiley and Sons, Inc., New York, 1950.

5. Churchill, R. V., Fourier Series and Boundary Value Problems, McGraw-Hill Book Company, Inc., New York, 1941.

6. Churchill, R. V., Introduction to Complex Variables and Applications, McGraw-Hill Book Company, Inc., New York, 1948.

7. Churchill, R. V., Modern Operational Mathematics in Engineering, McGraw-Hill Book Company, Inc., New York, 1944.

8. Cooper, S. S., Anal. Chem., 19, 254 (1947).

9. Crank, J., Mathematics of Diffusion, Oxford University Press, London, 1956.

10. Crosier, H. E., "The Washing of Porous Media and Conduits," Ph.D. Thesis in Chemical Engineering, University of Michigan, 1949.

11. Danckwerts, P. V., Chem. Eng. Science, 2, 1 (1953).

12. Deisler, P. F., and Wilhelm, R. H., Ind. Eng. Chem., 45, 1219 (1953).

13. Dryden, H. L., Ind. Eng. Chem., 31, 416 (1939).

14. Ergun, S., Ind. Eng. Chem., 48, 2036 (1956).

15. Fahien, R. W., and Smith, J. M., A.I.Ch.E. Journal, 1, 28 (1955).

16. Ferrell, J. K., Richardson, F. M., and Beatty, K. O., Ind. Eng. Chem., 47, 29 (1955).

17. Gilliland, E. R., Mason, E. A., and Oliver, R. C., Ind. Eng. Chem., 45, 1177 (1953).

18. Gilliland, E. R., and Mason, E. A., Ind. Eng. Chem., 44, 218 (1952).

19. Hill, W. R., Electronics in Engineering, McGraw-Hill Book Company, Inc., New York, 1949.

20. Hirai, E., Chem. Eng. (Japan), 18, 528 (1954).

21. Hulbert, H. M., Ind. Eng. Chem., 36, 1012 (1944).

22. Kaplan, W., Advanced Calculus, Addison-Wesley Press, Inc., Cambridge, 1952.

23. Karkalits, O. C., "The Mixing of Dissimilar Liquids by Successive Flow Through Pipes," Ph.D. Thesis in Chemical Engineering, University of Michigan, 1949.

24. Kramers, H., and Alberda, G., Chem. Eng. Science, 2, 173 (1953).

25. Lapidus, L., and Amundson, N. R., Jour. Phys. Chem., 56, 984 (1952).

26. Latinen, G. A., "Mechanisms of Fluid-Phase Mixing in Fixed and Fluidized Beds of Uniformly Sized Spherical Particles," Ph.D. Thesis in Chemical Engineering, Princeton University, 1951.

27. McHenry, L. W., "Axial Mixing of Binary Gas Mixtures Flowing in a Random Bed of Spheres," Ph.D. Thesis in Chemical Engineering, Princeton University, 1956.

28. Mellon, M. G., Colorimetry for Chemists, Smith Chemical Company, Columbus, 1945.

29. Perry, J. H., Chemical Engineers' Handbook, McGraw-Hill Book Company, Inc., New York, 1950.

30. Plautz, D. A., and Johnstone, H. F., A.I.Ch.E. Journal, 1, 193 (1955).

31. Prausnitz, M., "Liquid-Phase Turbulent Mixing Properties," Ph.D. Thesis in Chemical Engineering, Princeton University, 1955.

32. Raseman, C. J., "Evaluation of Ion Exchange Kinetics Using Radioactive Tracer Techniques with Sinusoidal Variation of the Concentration," Ph.D. Thesis in Chemical Engineering, Cornell University, 1951.

33. R.C.A. Tube Handbook HB-3, Radio Corporation of America, Harrison, New Jersey, 1950.

34. Rider, P. R., Modern Statistical Methods, John Wiley and Sons, Inc., New York, 1947.

35. Schwartz, C. E., and Smith, J. M., Ind. Eng. Chem., 45, 1209 (1953).

36. Sherwood, T. K., Trans. Am. Inst. Chem. Engs., 36, 817 (1940).

37. Sommer, A., Photoelectric Tubes, Methuen and Company, Ltd., London, 1951.

38. Thatcher, C. M., "Local Rates of Mass Transfer in a Packed Bed of Spheres," Ph.D. Thesis in Chemical Engineering, University of Michigan, 1954.

39. Wilhelm, R. H., Chem. Eng. Prog., 49, 150 (1953).

40. Withrow, R. B., Shrewsbury, C. L., and Kraybill, H. R., Ind. Eng. Chem., Anal. Ed., 8, 214 (1936).

41. Wylie, C. R., Advanced Engineering Mathematics, McGraw-Hill Book Company, Inc., New York, 1951.

42. Yagi, S., and Miyauchi, T., Chem. Eng. (Japan), 19, 507 (1955).

43. Zworkin, V. K., and Ramberg, E. G., Photoelectricity and Its Application, John Wiley and Sons, Inc., New York, 1949.